Response Properties of Neighboring Neurons in the Auditory Midbrain

by

Chandran V. Seshagiri

B.A. Physics,
Rice University, 1997

SUBMITTED TO THE
HARVARD-MIT DIVISION OF HEALTH SCIENCES AND TECHNOLOGY
IN PARTIAL FULFILLMENT OF THE REQUIREMENTS FOR THE DEGREE OF

DOCTOR OF PHILOSOPHY
IN
HEALTH SCIENCES AND TECHNOLOGY

AT THE
MASSACHUSETTS INSTITUTE OF TECHNOLOGY

JUNE 2006

Signature of Author: _____
Harvard-MIT Division of Health Sciences and Technology
26 May 2006

Certified by: _____
Bertrand Delgutte
Associate Professor of Otology and Laryngology
and Health Sciences and Technology, Harvard Medical School
Thesis Supervisor

Accepted by: _____
Martha L. Gray
Professor of Medical Engineering and Electrical Engineering
Director, Harvard-MIT Division of Health Sciences and Technology

Response Properties of Neighboring Neurons in the Auditory Midbrain

by

Chandran V. Seshagiri

Submitted to the Harvard-MIT Division of Health Sciences and Technology
on 26 May 2006
in Partial Fulfillment of the Requirements for the Degree of
Doctor of Philosophy in Health Sciences and Technology

ABSTRACT

The inferior colliculus, the primary nucleus in the mammalian auditory midbrain, occupies a central position in the ascending auditory pathway. Nearly all ascending neural pathways converge and synapse in the central nucleus of the inferior colliculus (ICC). Further, the anatomical arrangement of axons and neurons in the ICC suggests the existence of functional regions which may play a role in organizing different types of physiological information. To investigate this organization, we characterized the response properties of neighboring neurons in the ICC.

To record reliably from neighboring neurons, we adopted a relatively new electrophysiological technique, *tetrode* recordings. Tetrodes have four closely spaced recording sites (<20μm) which record multi-unit activity from a small number of neighboring neurons. The recorded signals contain action potentials originating from more than one neuron. Based on action potential wave shape differences across the four channels, we can reconstruct the contributions of individual neurons. Applying tetrode recordings to the ICC of anesthetized cats, we successfully reconstructed individual spike trains for 190 neurons at 52 recording sites. To quantify the advantage of tetrodes, we compared our multi-channel recording results with waveform sorting from single-channel electrode recordings. At best, only 32% of the single-units from tetrode sorting were correctly identified using single-channel recordings.

We used tetrode to characterize pure tone responses of neighboring neurons in the ICC in terms of frequency selectivity, level dependence, temporal discharge patterns, and sensitivity to interaural time differences. We find similarities in best frequency and pure-tone threshold among neighboring neurons; however, we find large disparities in bandwidth, level dependence, temporal discharge patterns, and sensitivity to interaural time differences. These results suggest that neighboring neurons in ICC can greatly differ in membrane properties and/or their patterns of synaptic input from different brainstem nuclei and tonotopic regions.

Using tetrode recordings, we investigated how well multi-unit responses represent the response properties of the contributing single-unit responses. We find that multi-unit

responses represent single-unit best frequency, pure-tone threshold and level dependence well, and they represent single-unit bandwidth and interaural phase sensitivity poorly. These results suggest caution must be used not to infer single-unit responses from multi-unit recordings.

Thesis Supervisor: Bertrand Delgutte
Title: Associate Professor of Otology and Laryngology and Health Sciences and Technology, Harvard Medical School

ACKNOWLEDGEMENTS

Nothing worth doing in this life is ever worth doing alone. This thesis is the culmination of many years of work, but it is also the product of strong relationships and wonderful friendships. I would like to thank everyone who has walked with me, helped me, and supported me in this journey:

Bertrand Delgutte, my advisor, for supporting me and this work. I came into his group interested in studying 'neural populations,' though, at the time, I didn't really know what that meant. Through all the years of twisting and winding down the often unclear path of trying to make sense of neural populations, Bertrand was always encouraging and supportive. I am forever grateful to him for allowing me to walk my own path.

My thesis committee for giving me their time and interest. Their suggestions have proved invaluable in developing this thesis. Thank you to Doug Oliver for making many trips from Connecticut to attend committee meetings. I would like to especially thank Jennifer Melcher who was always a great source of encouragement. Her interest and enthusiasm in this project has always been appreciated.

Matthew Wilson, the brains behind the development of the tetrode, graciously opened up his lab to me. Under the guidance of his student, Linus Sun, I was able to learn the intricate art of making tetrodes.

Connie Miller and Leslie Liberman for providing surgical support.

Ishmael Stefanov-Wagner for providing engineering support.

Special thanks to Dianna Sands who makes the world work.

All my colleagues at EPL and in the Speech and Hearing program. This is a great graduate program, largely because of the warm and collegial atmosphere created by the wonderful students.

Don H. Johnson, my research advisor at Rice University, for setting me on this path in the first place. I cannot thank him enough for giving me the opportunity to work with him as a senior in college. His expressive enthusiasm and love for his work is infectious, and the experience of working with him changed my life forever. I cannot adequately express my gratitude to him.

All my friends both in and out of Boston who stood by me, put up with me, and generally kept me sane all these years: Ray, Radha, Brad, Courtney, Jonno, Domenica, Dave O, Irina, Leo, Zach, Tarun, Arpit, Dave (Spin), Edwin, Sarita, Yogi, Theresa, Jonathan and Caroline.

Miles, Trane, Ken, Hamid, Eddie, and Bono for keeping me company on many late nights.

Arjun whose advice and counsel I cherish and rely on.

Akka who has been there through everything. Thank you for being everything all the time.

My parents. Without their support, love, and encouragement, I would never have made it this far.

Ilana, my best friend and constant suppport. She's made my life better in every possible way. What more is there to say?

This work was supported by NIH Grants DC00038 and DC02258

TABLE OF CONTENTS

INTRODUCTION

Traditionally, neurophysiology studies seeking to understand the relationships between the electrical responses of the central nervous system to different stimuli have recorded two types of responses. The first type, evoked potential responses, represents the summed, synchronized activity of large numbers of neurons. The second type, single-unit responses, focuses on the electrical responses of individual neurons. Over the past fifteen years, new technologies have begun to bridge this gap between the responses of single neurons and gross potentials of large numbers of neurons. Many of these advances have enabled recording of individual responses of multiple neurons (Nicolelis, 1999). One of these technologies, the *tetrode* (Wilson and McNaughton, 1993), offers the ability to study directly the responses of multiple neurons contained within a limited spatial area.

Throughout the central nervous system, the cellular architecture of different areas reveals complex anatomical arrangements. From the stereotyped layering of cells and cell types across the entire neocortex, to the complex architecture of the cerebellum, to complex arrangements in the auditory brainstem, the anatomy of the CNS frequently implies a well-defined plan, albeit one that is very complex and hard to understand (Kandel et al., 2000). Therefore, studying the responses of neurons with specific relative spatial arrangements such as either fixed separations or close spatial proximity relative to the overall cell density could illuminate many questions about the processing and organization of physiological information in different systems.

Recording the multi-unit activity of a small number of cells provides a reliable method for recording from multiple neurons that are relatively close together. Because

the extracellular potentials generated by an action potential diminish with distance from the cell (Nunez, 1981), we assume that all neurons contributing to a multi-unit recording lie within some limited spatial area. This boundary is defined by both the electrode properties (Robinson, 1968) as well as the electrical properties of the neurons and the extracellular space (Nunez, 1981). However, if this spatial boundary is very large relative to the cell density, we may expect that the number of cells contributing to the multi-unit activity will get so large that we would no longer be able to discriminate individual action potentials, and we would simply record a gross potential resulting from the summed, synchronized activity of all the cells surrounding the recording site. Therefore, we assume that if we can discriminate action potentials, then the spatial extent over which an electrode can record discriminable action potentials is relatively small compared with the cell density in the area. Based on this assumption, we assume that the neurons contributing to multi-unit activity also lie relatively close together.

As early as the 1970's, researchers began implementing strategies for separating the contributions of individual neurons to multi-unit recordings (Abeles and Goldstein, 1977). These strategies relied on differences in action potential wave shapes to identify distinct groups of action potentials with similar waveform shapes (Lewicki, 1998). To improve the separability of different groups, Wilson and McNaughton (1993) introduced the tetrode, a four channel electrode which introduces additional spatial information about the action potential waveforms to assist in grouping different action potentials.

The four channels of the tetrode are closely spaced (<20μm), so they typically record action potentials from the same group of cells; however, the small differences in spatial location of each recording site results in differences in a given action potential

waveform across the channels. Action potentials with similar relationships of waveform shape across all four channels define groups which likely originate from distinct spatial locations around the tetrode tip, and therefore probably come from different neurons. Because the tetrode allows us to reliably separate multi-unit activity, it offers a chance to study the individual responses of multiple neurons that are relatively close together spatially.

The inferior colliculus (IC), the primary mammalian auditory midbrain nucleus, is an example of a neural center which exhibits a well-defined anatomical architecture, for which there is little understanding of the physiological significance. The central nucleus of the IC (ICC) consists of parallel planes defined by the disc-shaped primary cells of the ICC and the incoming axons which align parallel to the planes defined by the cells to create a laminar structure (Morest and Oliver, 1984; Oliver and Morest, 1984; Oliver and Shneiderman, 1991). Additionally, the laminae of incoming axons from different lower nuclei overlap in some regions, and remain segregated in others (Oliver and Shneiderman, 1991).

This complex arrangement of inputs and cell types shows some evidence of physiological relevance. The planes of cells and axons define iso-frequency regions that define a tonotopic arrangement (Merzenich and Reid, 1974). There are also some reports of organization within iso-frequency laminae by pure tone threshold (Stiebler, 1986), tuning width, and best modulation frequency (Schreiner and Langner, 1988). To investigate more directly the relationship between the anatomical arrangement and physiological properties, we developed techniques for tetrode recordings in the IC.

Before characterizing and comparing the response properties of neurons that are

close together, we first investigated the efficacy of using tetrodes over single-channel multi-unit recordings. Specifically, we looked at how groups of action potentials, clustered and separated with the four channel information of the tetrodes, separate when only one channel of information is used. From the single-channel grouping, we quantify the number of undetected units, misclassified units, and well separated units to determine the error rates relative to the tetrode sorting. If the error rates are low, then we can eschew the added complexity of the extra tetrode channels and simply use single-channel electrodes; if, however, the error rates are high, then we will know that tetrodes not only improve our ability to separate and cluster action potential waveforms, but the added spatial information is necessary to avoid classification errors when sorting multi-unit information.

In the second chapter, we use tetrode recordings to characterize the response properties of neighboring neurons in the central nucleus of the Inferior Colliculus (ICC). We looked at basic responses properties to pure tone stimuli widely used throughout the auditory system to characterize single-unit responses. In particular, we looked at the frequency selectivity as defined by best frequency and the width of the frequency tuning; we looked at both the pure tone threshold and level-dependency; we characterized the temporal discharge patterns elicited by pure tone stimulation; and we looked at the binaural response to interaural timing differences. To compare these properties, we looked at the similarities in each measure between every pair of units recorded from the same site, and we quantified how well related the properties are.

Because the ICC has a well defined tonotopic map (Merzenich and Reid, 1974), we expect neurons within a localized region of space to respond best to similar

frequencies. We have very few expectations regarding how similar other response properties may be between neighboring neurons. We expect that response properties that are similar reflect shared or similar inputs to neighboring neurons. Large differences in response properties may indicate either large differences in the inputs to the neighboring neurons, or it may reflect differences in the processing of these inputs.

Lastly, we investigated the relationship between the unsorted, multi-unit responses, and the isolated single-unit responses. The increased use of fixed arrays of electrodes, where individual recording sites cannot be moved independently to improve single-unit isolation, leads to multi-unit responses becoming more prevalent as a tool describe response properties in a local area. Using the same characterizations we used for comparing single-unit responses, we compared the similarities between the single-unit and multi-unit responses. We expect multi-unit responses t reflect single-unit responses well when the single-unit responses are similar. Large differences may arise when the single-unit responses are poorly correlated.

We believe that this first report of using tetrodes in the auditory midbrain will lay the foundation for future work using tetrodes to investigate the neural coding of various psychophysical phenomena. The ability to record from multiple neurons simultaneously as well as neurons that are physically close together will add new dimensions to studies of neural coding in the auditory brainstem.

Chapter 1: Tetrode Recordings in the Auditory Midbrain

Introduction

Neuroscientists trying to understand neural coding and computation have been recording the electrical potentials of individual neurons for decades. Traditionally, these experiments have focused on recording from a single neuron at a time. However, beginning as early as the 1970s, researchers attempting to better understand the dynamics of large neuronal networks attempted to record from more than one neuron at a time (Moore et al., 1970; Abeles and Goldstein, 1977). Recent advances in computational power, data storage and handling, and micro-electrode technology have made multiple single-unit recordings a routinely viable technique for neurophysiologists.

One of these technologies, the *tetrode* (Wilson and McNaughton, 1993), offers the ability to study directly the responses of multiple neurons contained within a limited spatial area. Because the central nervous system contains many instances of complex anatomical arrangement such as the layered structure of the neocortex, the complex circuitry of the cerebellum, or the laminar structure of the cochlear nucleus (Kandel et al., 2000), the ability to investigate whether responses are grouped in any functional arrangement spatially offers the opportunity to better understand these arrangements.

Using low impedance metal electrodes to record multi-unit activity provides a reliable technique for recording the responses of multiple neurons that are relatively close together. We assume that all cells with observable action potentials are close to the recording site, where close is defined relative to the overall cell density. In general, we

know that the extracellular potentials generated by a neurons diminish with distance from the cell body (Nunez, 1981), so depending on the amplitude of the extracellular action potentials generated by a cell and the overall signal to noise ratio of the electrode and recording system, there is some limit on the spatial separation that can exist between the cell and the recording electrode. If this separation is large relative to the cell density, then we may expect a large number of cells to lie within that spatial limit, and the contribution of such a large number of cells to the multi-unit activity would likely make it very difficult to discriminate individual action potentials. Therefore, if we can discriminate individual action potentials in the multi-unit activity, then we assume that the contributing neurons lie relatively close to the recording site. If all the contributing neurons are close to the recording site, then they are also relatively close to each other. If we can isolate the action potentials that originate from different neurons, then we can reliably record from cells that are relatively close together.

Other than recording multi-unit activity, the other possible approach we can use to recording from multiple neurons in a relatively small space would involve trying to isolate the extracellular activity of each neuron in the area on a separate electrode. This could be achieved in a few different ways. First, serial recordings could be made with a single electrode inserted with a similar penetration and electrode depth. This can be extremely difficult because it is hard to exactly identify where each recording site was, and multiple penetrations into the same location may cause extensive tissue damage in the area, reducing the chances of isolating single-units on successive penetrations. The other alternative is to use multiple electrodes and try and record from the cells simultaneously. If the electrodes can be moved independently, then we could attempt to

insert each electrode into a specific region and try and isolate cells on each channel. The difficulty in this lies in holding all the cells for long enough to acquire useful data. In particular, once a single-unit has been isolated on one electrode, additional time needs to be used to find a single-unit on a second electrode which reduces the time we can hold the first unit. This may not be a serious limitation in brain regions where it is relatively easy to find single-units and where holding times can be long. However, this approach also suffers from the difficulty of identifying the exact recording sites in order to estimate how close the cells were to each other. The last option would be to use an array of electrodes with fixed, close spacing to isolate single-unit activity on two or more channels. This approach suffers from two limitations. First, using many electrodes very closely spaced can inflict a large amount of tissue damage in the region of the insertion. Second, if the incidence of isolating single-unit responses with single channel recordings is low, then once a single-unit is isolated on one of the channels, the likelihood that there will be an isolated single-unit on another channel will be low. For these reasons, we believe that recording multi-unit activity provides the most practical and reliable means for recording the activity of multiple neurons that are relatively close together.

Beginning as early as the 1970's, researchers began implementing strategies for separating the contributions of individual neurons to multi-unit recordings (Abeles and Goldstein, 1977). These strategies relied on differences in action potential waveform shapes to identify distinct groups of action potentials with similar waveform shapes (Lewicki, 1998). These differences in waveform shape can result from differences in the size and shape of different cells or from differences in the relative distance of the cells from the recording site. In regions with very heterogeneous cell populations, the

differences in wave shape may be quite significant and easily sorted. However, if the cell population is homogeneous and show very similar intracellular action potentials, then the greatest differences in the extracellular waveform shape will likely arise from differences in the amplitude which will diminish with relative distance from the recording site. In this case, there can be a large amount of ambiguity in trying to identify the different action potential waveforms. To improve the separability of different units, Wilson and McNaughton (1993) introduced the tetrode, a four channel electrode which introduces additional spatial information about the action potential waveforms to assist in grouping different action potentials.

Tetrodes are four channel electrodes with very closely spaced recording sites ($<20\mu m$). Because the four channels are so closely spaced, tetrodes record multi-unit activity from the same neurons on every recording channel. The relationship of the action potential wave shapes across channels allows reconstruction of the single-unit spike trains contributing to the multi-unit recording.

Tetrode recordings rely on two major assumptions underlying single electrode extracellular electrophysiology: 1) action potential waveforms originating from the same neuron appear similar at a given location in the extracellular space; 2) action potential waveforms originating from a single neuron may differ when recorded from different locations. If the action potentials recorded extracellularly from two separate extracellular locations differ, then action potentials recorded extracellularly from two neurons at a single site may have different waveforms, assuming that the spatial relationship between electrode and neuron is different for the two neurons.

Tetrodes provide four spatially distinct recording sites from which to observe the action potential waveforms. Therefore, even if waveforms from different cells appear identical on a single channel, they may appear different on another channel, providing us with the necessary information to separate action potentials originating from different locations in space. If we only consider changes in the action potential amplitude with distance, then four distinct channels provides the minimum number of observations needed to obtain an unambiguous reconstruction of the individual neurons contributing to the multi-unit activity. In particular we can express the peak-to-peak amplitude of an action potential recorded at a distance r from the cell body as $A_0 f(r)$ where A_0 is a property of the cell and the function $f(r)$ monotonically decreases with increasing r. Since both A_0 and r are unknown, and since r is a function of Cartesian coordinates $x,y,$ and z, we have four unknown variables, so we need four observations to uniquely specify the location of the neuron from which the action potential originated.

We are particular interested in using tetrodes to study the response properties of neurons that are close together in the auditory midbrain. The inferior colliculus (IC), the primary auditory midbrain nucleus, exhibits a complex anatomical architecture. The central nucleus of the IC (ICC), which receives most of the ascending inputs, consists of parallel planes defined by the primary cells of the ICC and the incoming axons which align parallel to the planes defined by the cells to create a laminar structure (Morest and Oliver, 1984; Oliver and Morest, 1984; Oliver and Shneiderman, 1991). The laminae formed by the incoming axons from different lower nuclei overlap in some regions, and remain segregated in others, creating different regions of inputs (Oliver and Shneiderman, 1991). To investigate how this complex arrangement of inputs and cell types reflects in

the responses of local groups of neurons, we implemented tetrode recordings and sorting in the ICC.

We report here on the efficacy of tetrode recordings in the IC. We also investigate the improvements obtained from using tetrodes over single-channel recordings in order to determine whether the complex implementation is necessary to achieve our goals of studying the response of neurons that lie in close proximity to each other.

Methods

Tetrode Fabrication

We use methods similar to previously published reports for fabricating tetrodes (Wilson and McNaughton, 1993; Gray et al., 1995). We begin with a single length of 12μm, insulated Nichrome wire (Kanthal Palm Coast) and fold it in half once, then fold the double strand again over a metal rod, attach a clip with a small, horizontal metal rod to the ends and suspend the wires over a magnetic stirring plate. To wind the four wires together, we use the magnetic stirring plate to rotate the coupled metal rod clipped to the end of the four wires; we wind the wire approximately 4 turns/cm. With the rod still clipped to the wound wire and held static by the magnetic plate, we use a heat gun to melt the insulation and bind the four strands of wire together; the heat was only applied to 2/3 of the strand, leaving one end unfused. Lastly, we cut both ends and separate the unfused wires at the unheated end of the strand.

To mount the tetrode wire, we thread the wire through a 30ga. (0.26mm) stainless steel tube until at least 5mm of the tetrode wire is exposed. The wire is fixed to the tube using cyanoacrylate glue. At the end of the stainless steel tube with the unfused wire exposed, we connect the loose ends of the tetrode wires to a small four-pin connector attached with dental acrylic to the guide tube. The insulation on the loose ends is removed using a small flame and the wires are attached to the pins using conductive silver paint and shrink tubing.

Once the wire is mounted in the stainless steel holder, we make a final cut of the recording tip about 4-5mm from the end of the stainless steel tube and then gold plate the four recording sites to lower the impedance. Specifically, we place the tip in a small bath of gold solution and apply a DC current using a gold cathode in the bath until the impedance at 1kHz is approximately 400-800kΩ. We also test for short circuits among the different tetrode channels that may arise from excessive melting of the insulation when we fused the wires together.

Animal Preparation

The data presented here were collected from the inferior colliculi of 13 anesthetized adult cats. The surgical methods were similar to those described by Litovsky and Delgutte (2002). Briefly, healthy, adult cats received an initial intra-peritoneal injection of diallyl barbituric acid in urethane (75 mg/kg); additional doses were administered as necessary to maintain deep levels of anesthesia. A tracheal canula was inserted to provide a clear passageway for respiration. A rectal thermometer was used to

monitor body temperature which was maintained at 37.2 ^{0}C. Throughout all the experiments we monitored the heart rate; we also monitored respiration rate and expired CO_2 percentage.

Surgically, both pinnae were partially dissected away and the ear canals cut to allow insertion of closed acoustic assemblies. To prevent static pressure building in the middle ear, we drilled a small hole in each bulla and affixed a 30-cm plastic tube. In 10 of the 13 experiments, the posterior surface of the inferior colliculus was exposed via a posterior-fossa craniotomy and aspiration of the overlying cerebellum. In the remaining 3 experiments, the dorsal surface of the inferior colliculus was exposed by a craniotomy anterior to the tentorium and aspiration of the underlying occipital cortex; part of the bony tentorium was removed to allow better visualization of the inferior colliculus.

The animal was placed in a double-walled, electrically shielded, sound proof chamber. To assess the general health of the auditory neural pathway, we measured the click-evoked Auditory Brainstem Response (ABR). The ABR was measured differentially across a vertex screw placed in the skull and a tooth bar used for supporting the animal's head. The signal was amplified 10000x, bandpass filtered (100Hz-10kHz), and 500 responses to a click stimulus were averaged. This was repeated for a series of levels from -70 to -40 dB re1V in 5dB steps.

We measured the ABR level series immediately before and after the aspiration and determined whether there was any noticeable change in the threshold at which the ABR response was just noticeable. The ABR level series was repeated periodically during the experiment to check for any noticeable changes in the threshold. In all

experiments, the ABR threshold never changed more than 5dB, which was considered acceptable.

Data Acquisition

All recordings from the IC were made with tetrodes. Tetrodes were mounted on a remote-controlled, hydraulic microdrive. In the 10 experiments with the posterior-fossa opening, we oriented the tetrodes nearly horizontal in a parasagittal plane parallel to the iso-frequency laminae of the central nucleus of the inferior colliculus (Merzenich and Reid, 1974). In the remaining 3 experiments with dorsal exposure of the inferior colliculus, we oriented electrodes in a nearly dorso-ventral direction in a parasagittal plane and advanced the electrode along the tonotopic axis of the central nucleus of the inferior colliculus. Agar was used to fill the cranial cavity and reduce brainstem pulsation as needed.

We digitally recorded and stored all raw waveforms from our tetrode recordings for off-line data processing and spike sorting. Initially, a Tucker Davis headstage (TDT and pre-amplifier (TDT RA16AC and RA16PA) were used to bandpass filter (1.6Hz – 7.5kHz) and amplify (54dB) each of the four tetrode channels. Custom-built programmable amplifiers further amplified (18dB) the signals which were then digitized (20kHz/channel) and saved to disk.

Offline, prior to applying our detection and classification algorithms, we implemented filters to remove noise from the raw waveforms. First, we bandpass filtered all signals (300-3000Hz). Next, we removed 60Hz and all its harmonics from each

channel by computing the period average of 60Hz over the duration of the entire signal. This provided an estimate of the contribution of a single period of 60Hz and all harmonics. We then subtracted this period estimate from the original signal. Lastly, to remove any gross potentials, we average the signal across every stimulus presentation and subtract the average from our recorded signal.

Stimuli

Acoustic stimuli consisted of pure tones and broadband noise presented either binaurally or monaurally. The stimuli were digitally generated (16 bits, 100kHz) and then converted to analog signals. Custom-built programmable attenuators set the stimulus level at each ear.

The analog output was delivered to closed acoustic assemblies inserted into the cut ends of the ear canals. The assemblies contained an electrodynamic speaker (Realistic 40-1377; Radio Shack, Ft. Worth, TX) and a calibrated probe-tube microphone. To ensure a flat frequency response at the tympanic membrane, we measure the sound pressure at the tympanic membrane as a function of frequency and then synthesize digital filters to equalize the magnitude and phase response of the acoustic system.

Experimental procedure

During the experiment, we visually monitor the waveforms of all four tetrode channels on an oscilloscope. One of the four channels, selected by the experimenter,

feeds into a spike amplifier with a threshold trigger. The output of the spike amplifier drives a loudspeaker for audible monitoring; the output of the threshold trigger feeds into an event timer that records each threshold crossing as an event.

We use a 500ms, 60dB SPL frozen broadband noise burst as a search stimulus and advance the tetrode until we observe clear spiking activity. Once audible spikes are encountered, we select the channel with the largest spikes to feed into the spike amplifier and measure a frequency tuning curve based on the multi-unit activity using an automated tracking procedure (Kiang and Moxon, 1974). If the tuning curve exhibits a relatively narrow tuning, we assume our tetrode is in the central nucleus.

In early experiments, we would begin immediately studying response properties at the site. For the last nine experiments, we implemented an on-line preliminary spike sorting algorithm. For these experiments, we first recorded the neural response to a frozen broadband noise stimulus, applied our detection and sorting algorithm to the recorded response (see below), and observed the clustering of spike waveforms. If the recording showed well isolated clusters, we studied the site in more detail; otherwise, we continued advancing the electrode.

Throughout recording from a single site in the later experiments, we occasionally repeat the broadband noise measurement and check the clustering of spike waveforms to ensure stability of the recording. If a cluster disappeared or a new cluster appeared, we either ceased recording from that location, or we discarded previous measurements and started a new set of measurements.

Tetrode Processing

Spike Detection

Before sorting spike waveform, we have to identify candidate spike times from the four-channel recordings. Single-unit, single electrode recordings usually rely on a simple amplitude threshold for identifying spike times. Typically, the experimenter subjectively decides on an amplitude threshold on-line in order to maximize the detection rate and minimize the false alarm rate.

Figure 1A shows a single-channel, single-unit recording. For these recordings, where all action potentials presumably originate from a single neuron, fine movement of the electrode position can result in large changes in the signal-to-noise ratio (SNR), and experimenters typically adjust the electrode position slightly to maximize the SNR. For this recording, a wide range of thresholds will produce prefect or nearly perfect detection. In contrast, Figure 1B shows four channels from a tetrode, multi-unit recording. Compared with Figure 1A, the variability in the amplitudes of the action potentials is much larger, suggesting the contributions of more than one neuron. Also, the tetrode recordings exhibit a lower overall signal-to-noise ratio than the single-unit recording in Fig. 1A. The lower signal-to-noise ratios means that detection by amplitude thresholding is more sensitive to the threshold levels chosen than the higher SNR single-unit recordings and is less likely to produce near perfect detection.

We extend amplitude thresholding to the four-dimensional tetrode signal. One option would be to identify a threshold level for each of the four channels and identify all

threshold crossings on any channel as a candidate spike time. While this is the common spike detection scheme used with tetrodes (Gray et al., 1995; Lewicki, 1998), this implementation creates ambiguities when a single neural event generates threshold crossings on multiple channels at different time samples. Also, because the noise is usually correlated across the tetrode channels, we can take advantage of the correlated structure of the noise to design an optimal detector.

Every time sample is a 4-D vector giving the amplitude on each of the tetrode channels at that time. Therefore, in four-dimensions, the amplitude threshold involves defining a four-dimensional boundary based on the noise structure such that all points outside the boundary are candidate spike times. If we assume the noise can be modeled as a zero-mean Gaussian with covariance $\mathbf{\Lambda}$, then the boundary is an ellipsoid of equi-probability for the Gaussian. The ellipsoid is defined by the following equation

$$r^2 = \mathbf{X}^T \mathbf{\Lambda}^{-1} \mathbf{X}$$

where $\mathbf{X}$ is the 4-D vector describing the observed sample across all four tetrode channels and $\mathbf{\Lambda}$ is the spatial covariance matrix of the noise. The metric r is called the Mahalanobis distance.

Figure 2 illustrates the detection boundary in two-dimensions. The figure shows a scatter plot of each sample of channel 3 plotted against the corresponding sample on channel 4 for the tetrode recording shown in Figure 1B. The red ellipse shows a detection boundary corresponding to $r = 4$. For a two-dimensional Gaussian noise, this corresponds to a false alarm rate of approximately 0.03%.

To implement our detection algorithm, we first estimate the statistics of the noise across the four channels (see Appendix A for how we estimate the noise). Once we have obtained an estimate of the noise, we compute the noise covariance matrix. Using the noise covariance matrix, we compute the Mahalanobis distance for every sample in our raw waveform. We apply a boundary criterion of $r > 4$. Under our assumption that the noise is Gaussian, a boundary of $r = 4$ will result in a false alarm rate of approximately 0.03% which is similar to thresholding at 3.5σ of the noise level for a single-channel recording where the noise is also Gaussian. This criterion gives a low expectation of false alarms while setting a low enough threshold to identify even small action potentials.

We define an event for every continuous set of samples that exceeds our threshold criterion. For every event, we define an event time as the time sample in the continuous set that has the greatest Mahalanobis distance.

Spike Classification

Once the times of action potential occurrences have been determined using the detection method described above, we extract 15 samples (0.75ms) of the raw waveform centered around these event times from each channel, giving four waveforms for every detected event. Based on the shapes of these waveforms, we seek to group similar events together to associate each group with a unique single neuron. Figure 3 shows a 100ms segment of the raw waveforms seen in Figure 1B with the waveforms across all four channels for three events enlarged. Qualitatively, the waveforms in inset A differ strongly from those in inset B. While the waveforms are similar on channel 3, they differ slightly

on channels 2 and markedly on channels 1 and 4, suggesting that these events arise from different locations in space and consequently from different neurons. The event seen in inset C is more similar to that seen in inset A, and determining whether these come from the same or different neurons is more difficult.

We want to implement an algorithm to group together events with similar waveform profiles. Clustering schemes typically first reduce each N-point waveforms to one or two scalar quantities that represent the waveform features – e.g. peak-to-peak amplitude, temporal width, etc. Waveforms cluster into different groups based on the values of these features. We use principal component analysis (PCA), to 'choose' the most salient features of the waveform (Abeles and Goldstein, 1977).

PRINCIPAL COMPONENT ANALYSIS

Principal component analysis (PCA) defines an orthonormal basis set of vectors that can be linearly combined to exactly reproduce every waveform in our original data set. More importantly, the bases chosen through PCA capture successively less of the variance of the data set with the first principal component containing most of the variance of the dataset. Figure 4 demonstrates the linear reconstruction of a single action potential waveform using PCA. Figure 4A shows the set of waveforms extracted from a single channel (all waveforms are aligned at their maximum amplitude), with one waveform, randomly selected, shown in red. Figure 4B illustrates the reconstruction of this waveform using PCA. The Nth row shows the first N principal component waveforms, the weight applied to those waveforms (in green), and the waveform resulting from the

weighted sum (dashed blue) plotted over the original waveform (red). As we add additional principal components, the resulting waveform increasingly resembles the original waveform until using all fifteen components provides a perfect reconstruction.

While the full set of fifteen principal components is necessary for an exact reproduction, the weighted first principal component is already very similar to the original waveform and additional principal components offer only small adjustments. For this particular data set, the first principal component captures approximately 69% of the variance of the data set. On average, for the entire set of tetrode recordings we have made, the first principal component captured approximately 73% of the variance of the detected waveforms, as compared with 12% of the variance captured by the second component. Since the first principal component captures such a large percentage of the waveforms' variances, we use the weight of the first principle component as a reasonable scalar representation of the fifteen point time waveforms extracted for each action potential.

CLUSTERING

Using the weights of the first principal components to represent each waveform, each neural event is reduced to four values – the four weights of the first principal components from each of the four tetrode channels. Action potentials from a single neuron are assumed to have similar representations in the four-dimensional, first-PC space. Figure 5 illustrates how the principal component weights associated with the recording from Figure 3 cluster to form distinct and separable groups. We have plotted the weight for the first principal components of the waveforms on channel 3 vs. the

weight of the first principal components of the waveforms on channel 4. Four distinct groups are apparent in the two-dimensional space. Across the whole four-dimensional space, we have six two-dimensional projections. Figure 6 shows the result of clustering in all two-dimensional projections. Each identified cluster of spikes is shown in a different color. Events in black do not belong to any cluster. We generally discard the yellow cluster at (0,0) because it comprises false alarms and spikes with very low signal-to-noise ratio.

To cluster the data, we first use manual hand sorting to define templates for each cluster; then we use these templates to sort the entire set of waveforms. The initial manual sorting process involves identifying clusters using the six two-dimensional projections. In some projections, two or more overlapping clusters may appear as a single cluster of points; however, in another projection, they will separate into well defined groups. Therefore, we begin with one of the projections and manually draw ellipses around each distinct, separated cluster of points. In the next projection, each of these clusters will appear either as a single cluster with perhaps some outlying points or as two or more distinct groups. In the former case, we may refine our cluster definition from the previous projection to more tightly define our boundary; in the latter case, we select each of the distinct groups and split the original grouping. We repeat this process for every group and every projection until we obtain a set of points that define each group.

Once we have manually clustered our groups, we use these results to define templates for each group. Specifically, we assume the variability in waveform clusters can be represented by a four-dimensional Gaussian variable, and we compute the mean and covariance matrix of the points in the four-dimensional space for each cluster. From

the estimated means and covariance matrices for each of the N groups, we compute a Mahalanobis distance for every event in the four-dimensional space. Therefore, for every event we have a distance metric from each of the N possible clusters. Each event is assigned to the group that it is closest to. We discard any event that has a Mahalanobis distance $r > 4.5$ relative to the group the event is originally assigned to. On average, 6.4% of the spikes remain unsorted. At some sites the percent of spikes unsorted was as high as 11%.

Once events are clustered, we assume each cluster contains spikes from a distinct neuron, and we reconstruct the corresponding single-unit spike train by associating the event times with each event in the cluster.

Results

The data presented here were recorded from the IC of thirteen cats. Using tetrodes, we recorded and isolated a total of 190 single-units from 52 recording sites (avg. 3.7 units/site). Column 2 of Table 1 gives the overall distribution of the number of units separated at each of the 52 sites using tetrodes. At most sites (31/52; 60%), we reliably separated three or four single-units. At most, we were able to separate eight single-units from one site; however, we were unable to hold all eight for more than approximately five minutes.

Single Channel Spike Sorting vs. Tetrode Spike Sorting

Prior to the development of tetrodes (Wilson and McNaughton, 1993), multi-unit, single-channel recordings were sorted based on the spike waveform variations seen on a single channel (Abeles and Goldstein, 1977; Lewicki, 1998). Generally, these studies applied spike sorting algorithms similar to the algorithm we use with tetrode recordings. In the instances with single-channel recordings, waveforms were clustered by either comparing specific waveform features (e.g. peak-to-peak amplitude, waveform width, max amplitude, min amplitude) or comparing the weights of the first and second principal components for the spike waveforms on the single channel.

To investigate the performance of tetrodes vs. single-channel spike sorting, we compared the overall data yield from the tetrode spike sorting with the efficacy of using one of the four tetrode channels. Separating units from the tetrode recordings followed the methods described above. For the single-channel comparison, we used all the events and corresponding waveforms detected and sorted using tetrodes. For every event, we computed the weights of the first and second principal components of the waveforms from every tetrode channel.

Rather than manually select every cluster again for the single channel cluster plots, we looked at the separability of the clusters defined by tetrode spike sorting in the two-dimensional space of the first two principal component weights. We used the R' measure defined in Appendix B as our measure of cluster separability.

Using the clusters identified from tetrode clustering, we computed the mean and covariance matrix for each of these clusters in the space of the weights of the first and

second principal components. After estimating the distributions for each unit, we computed the R' statistic for every pairwise combination of clusters. If a particular cluster has an R' value > 2.5 relative to every other cluster, we label that group as separable. The R' cutoff of 2.5 corresponds to the boundary that contains approximately 95% of the distribution. Also, empirically we find that clusters with $R' > 2.5$ are visually well-identified.

The third column of table 1 shows the number of single-units that are separable from each recording site using the tetrode channel that yields the best results. Overall, single channel recordings only successfully separate 31.5% (60 of 190) of the units obtained using tetrode recordings. At most sites (27/52; 51.9%) single-channel recordings only reliably yield one single-unit, while at 17% (9/52) of the sites, no single-unit was isolated.

Sorting errors using single-channels

Using single-channels not only reduces number of single-units we can successfully isolate, but it also introduces significant sorting errors relative to using tetrodes. For the 130 units that were not well separated using single-channels, we investigated the possible outcome for each unit if they were sorted in the cluster spaced defined by the weights of the 1st and 2nd principal components. Figure 7 shows the decision tree used to identify different errors using single-channel sorting.

The first problem that can arise is that a unit may not be detected. Using four channels increases our ability to detect spikes because spike with low signal to noise

ratios on one channel may have a better signal to noise ratio on another channel; therefore, using only a single channel may result in missing an entire cluster that was identified using tetrodes. To determine the incidence of missed clusters, we again looked at the separation of tetrode clusters in the single channel sorting space, as defined by the weights of the first and second principal components.

As mentioned previously, from our tetrode sorting, we typically discarded one cluster because it comprised false alarms and very small, non-separable spikes. Using this cluster as a measure of the noise level, we determined that any cluster that was sufficiently close to this 'noise' cluster would not be detected. Again, computing R' between every single-unit cluster and our noise cluster, we determined that all single-unit clusters within $R' = 0.9$ would not be detected using only the single-channel. The boundary $R' = 0.9$, which we chose empirically, contains approximately 33% of the distribution. We find that 15 of the 130 units were unidentified because they would not have been detected. This decreases our overall data yield, but it does not introduce sorting errors.

If a single-unit cluster lies within the region $0.9 < R' < 2.5$ relative to the noise cluster, then enough spikes would be detected to appear as a detected group; however, the overlap with the noise cluster indicates that some spikes will not be detected. We call this a Type I error, and we find that 5 of the 130 single-units would have a significant number of undetected spikes.

Units with $R' > 2.5$ relative to the noise will be cleanly detected. However, if they lie within the region $R' < 2.5$ relative to any other single-unit cluster, they will overlap with that cluster. If the overlap is severe, the two clusters will appear as a single unit; if

the overlap is mild, and we can visually distinguish two overlapping groups, we would discard both clusters because they could not be sorted. We distinguish between severe and mild overlaps based on the distance between the two clusters; based on empirical observation, if $R' < 1.6$, the overlap is severe and the two clusters would appear as a single-unit. We call this a Type II error. 84 of the 130 units were part of a multi-unit cluster that would be classified as a single-unit.

The remaining 26 clusters that were not well isolated lie within the region $1.6 < R' < 2.5$ relative to the nearest cluster. Because the overlap is mild, it would be visually noticeable and both clusters would be discarded. As with the undetected clusters, this reduces our data yield, but does not introduce errors in the usable data.

So, of the 190 units separated using tetrodes, 60 (31%) are well isolated using single-channels. Of the remaining 130 units, 41 (22%) would either be undetected or be discarded while 89 (47%) would be misclassified. These results are listed in Table 2.

Discussion

We have discussed here, our implementation of tetrode recordings in the inferior colliculus. In general, we have applied methods similar to those of other labs for the tetrode manufacturing as well as the processing of tetrode data (Wilson and McNaughton, 1993; Gray et al., 1995; Lewicki, 1998). For spike detection, we have implemented a slightly different algorithm using all four channels jointly rather than thresholding independently on single-channels. Regarding classification, we implemented a principal component based clustering scheme. While others have used neural networks (Ohberg et

al., 1996; Quiroga et al., 2004), independent component analysis (Takahashi et al., 2003), and wavelet techniques for sorting (Hulata et al., 2002; Quiroga et al., 2004), we believe that these methods offer only minimal improvement over principal components for our data. First, we find that the first principal component captures a large amount of the overall variance of the waveforms (73%) compared with (12%) for the second component. Figure 8A shows the distribution of the percent of variance captured by both the 1st and 2nd principal components across every site and every tetrode channel. The two distributions do not overlap, and at over 90% of the sites, the 1st principal component captured 60% or more of the variance. Second, the first principal components for each channel at every recording site are very similar. Figure 8B shows the waveforms of the 1st principal components from every channel and every site plotted together. They are nearly identical. We measured the magnitude of the projection of the principal components onto each other, which is the same as looking at the correlation coefficient because the principal components are normalized to unit energy. Across every channel pair and every site, the mean length of projection is 0.998. This suggests that the action potential waveforms we have sorted are very similar to within a scaling factor. Thus, for our IC recordings, the amplitude of the action potentials seems to be the dominant waveform feature that changes with position.

The dominance of amplitude and common shape of the action potential waveforms may arise from a number of factors. First, the bandpass filtering (300-3000Hz) may strip away features that contain useful information to improve spike sorting. Second, the anatomy of the IC may have a large effect. Because the majority of cells in the central nucleus of the IC are disc-shaped cells and the physical arrangement of cells is similar,

this may contribute to common action potential shapes from most cells which may not be true in other regions of the brain. Also, IC cells typically do not exhibit bursting patterns which can create changes in the spike waveform from an individual neuron.

Efficacy of Tetrodes

The results of our tetrode experiments show the importance of using spatial information, as in tetrodes, for reconstructing single-unit spike trains from multi-unit recordings. First, data yield increases significantly with tetrode recordings in part because of the opportunity to detect spikes across four channels and in part because fewer units remain unseparable. More important than data yield, tetrodes significantly reduce error rates for the reconstruction.

As we have reported, of the 190 units recorded using tetrodes, from the best single-channel, we only recovered 60 single-units. Of the remaining 130 units, two major reasons contribute to the failure to identify these units. First, because we only have one channel to use for our detection scheme, some units fall below the noise floor, and they are never detected. Second, there may be overlap among different clusters. In some cases, the overlap may be significant enough to preclude reliable unit separation, but visually, the overlap may be recognized. In these cases, the overlapping units will be discarded. For these two cases, data yield is lowered; however, all identified single-units are well isolated, and the major result is a reduction in data yield.

The last error we encounter is overlap so complete that two or more overlapping clusters appear to form a single, well-isolated cluster. In this condition, we end up with

spike-trains made up of spike times from two or more units. This poses a serious problem, and within our data set, this type of error dominates our results with 84/190 units falling into this category. With tetrodes, the additional channels resolve the overlap by separating the two groups in a different projection space.

Tetrodes in IC vs. Visual Cortex

Table 1, which shows our results for sorting with tetrodes vs. single channel electrodes, also includes results from the visual cortex, as reported by (Gray et al., 1995). Columns four and five of table 1 give their results for tetrode sorting and single channel PCA sorting respectively. Using tetrodes, they average 5.4 units/site. At the 28 sites they recorded from, they always isolated at least three units and regularly isolated up to seven units per site. They report a maximum of nine units at one site. In general, they have better data yield than we do in the inferior colliculus.

When they apply PCA clustering on single-channels, they are able to isolate 95/151 single units with a yield of 3.4 units/site. Also, using only single channels they were able to isolate up to six units at two sites. By comparison, in the inferior colliculus, our overall yield drops from 3.7 units/site to 1.2 units/site with only one instance yielding three isolated units on a single channel. These results suggest that in the inferior colliculus using tetrodes is even more necessary than indicated by these earlier reports from the visual cortex.

Differences in the respective experimental setups may explain the better performance seen in the visual cortex study. However, anatomical differences between

the visual cortex and the inferior colliculus may also play a role. First differences in cell sizes may contribute to some of the differences. While we do not know what cortical layer Gray et al. (1995) recorded from, somata of cortical pyramidal cells can have diameters as large as 100μm; by contrast, the somata of the largest IC disc-shaped cells have diameters of approximately 30μm (Oliver and Morest, 1984). The larger soma size may result in larger recorded action potentials which would improve SNRs for all units, thereby improving separability. Additionally, the cortex also exhibits greater heterogeneity of cell types across different cortical layers as compared with the extremely homogeneous population of disc-shaped cells seen in the IC. This heterogeneity may give rise to greater differences in action potential wave shapes which would improve separation of clusters. This may also account for the vastly superior performance seen using only single-channel sorting.

Overlapping Spikes

One significant error that can occur in tetrode sorting is when action potentials from different cells overlap. In this case, the individual waveforms are superimposed, resulting in a waveform that is different from the waveforms produced by either cell. If two neurons have highly correlated firing times, we may expect to see a large number of overlapped action potentials. These occurrences would be marked by a high degree of similarity among the waveform shapes, and we might run the risk of having an entirely new cluster of overlapped spikes that we would classify as a single-unit. In the extreme case where the two cells fire identically or nearly identically, this would not be a problem

since the resulting cluster would provide a good representation of the spike trains of the two contributing neurons. More likely, there is not such a tight coupling that all spikes overlap. In this case, the best option for identifying this occurrence is visual inspection of the spike waveforms that form each cluster. Unless the spikes exactly overlap, the superposition of the two waveforms would result in an overlapped waveform that does not resemble the typical single-unit. We routinely visually inspect the waveform groups, and we have never observed groups with waveforms that resemble the superposition of other spikes.

Even if the two units do not exhibit correlated firing, we expect some overlaps due to random chance. If the spikes overlap with random offset, then the resulting waveforms will not create a clustered group, but rather would appear with extremely variable shape. Our sorting routinely ignores spikes that are sufficiently far away from the identified clusters. These may be from the random chance of spikes overlapping. In general, approximately 6.4% of the spikes remain unsorted in our data set. This can range from as little as 1.5% up to 11% across different recording sites.

We estimated the likelihood of overlapping spikes given two neurons with spike rates of 30 spikes/s, which is a typical average firing rate observed in our data. We used a simplified model of random spike firing where we divide time into 0.75ms bins and let the probability of a spike in a given bin be p. For a spike rate of 30 spikes/s, p is 0.0225. Therefore, the probability of two neurons generating a spike in the same bin is 5.06e-4, and the rate of overlap is 0.67 overlaps/s. The resulting percent of spikes that overlap is 2.2%. This is lower than the rates we observe, but this is only for two neurons, and we typically have at least three or four neurons at a given site, so we expect this rate to be

higher with more neurons. Also, this only accounts for the average spike rate. At the onset many neurons exhibit instantaneous firing rates of over 300 spikes/s. Using the same model, the probability of a spike in a 0.75ms bin is now 0.225 and the probability of two neurons generating spikes in the same bin goes up to 0.0506. Therefore, the rate of overlap becomes 67 overlaps/s, and the resulting percent of spikes that overlap is 22%. So, for cells with large onsets, the probability of overlapping spikes during the onset is high.

This problem of overlapping spikes remains a large problem with tetrodes, or any spike sorting of multi-unit activity. However, this is a tradeoff we must accept if we want to be able to study neurons in close proximity to each other.

Conclusions

Sorting multi-unit activity from the IC using single channel recordings is prone to high error rates. Introducing additional spatial information improves our ability to separate single-unit spike trains from multi-unit recordings. Since four channels is a theoretical minimum for achieving reliable reconstruction based on changes in action potential amplitudes, the tetrode offers an ideal tool for acquiring the spatial information needed to sort action potentials from multi-unit recordings.

Recordings from the auditory midbrain using large electrode arrays such as the Michigan multi-channel electrodes (Drake et al., 1988) and the Utah 100-channel arrays (Maynard et al., 1997) may produce multi-unit data on many of the channels if the impedances of the recording sites are low enough. Unless the arrays incorporate tetrode

site configurations, the results presented here suggest that attempting to sort waveforms to reconstruct single-unit spike trains from single channels of these large arrays will likely introduce classification errors. However, using tetrode style configurations can enable successful simultaneous single-unit recording in the IC.

Having established the efficacy of tetrode recording in the auditory midbrain, we can now apply tetrodes to study the similarities among the responses of neurons that lie in close proximity to each other.

Appendix A – Estimating noise covariance

To estimate the noise from our tetrode recordings, we begin by assuming that the noise on each channel is normally distributed and fit a Gaussian to the distribution of recorded amplitudes. The distribution should follow a Gaussian distribution for small amplitudes; samples with higher amplitudes are likely due to action potentials. Panel A in figure A1 shows a histogram of amplitudes from the raw waveforms of a single tetrode channel. The red-line shows a Gaussian curve fit to the central peak of the histogram in the least mean square sense. We discard all samples across all four channels if on any channel, the amplitude exceeds four four standard deviations of the estimated Gaussian. The region shaded in grey in panel A shows the 4σ boundaries. Panel B shows a 250ms segment of a single channel from the original recording, and panel C shows an estimate of the noise waveform from that channel.

Appendix B - Quantifying separation of clusters

To quantify the separation between clustered data points in a two-dimensional space, we define a distance metric, *R'*, which is similar to the *d-prime* measure used to quantify discriminability of two one-dimensional Gaussian distribution. For one-dimensional Gaussian distributions with means μ_1 and μ_2 and variance σ^2, *d-prime* is defined as

$$d' = \frac{\mu_2 - \mu_1}{\sigma^2}$$

This expression gives the distance between the means normalized by the standard deviation of the two distributions. Quantitatively, the d-prime measure relates to the detection and false alarm rates for a detection task involving these two distributions. For our two-dimensional case, we create a measure similar to d-prime. Specifically, our measure is the value of the Mahalanobis distance at a point along the line defined by the means of the two distributions where the Mahalanobis distances from each distribution are the same. Figure B1 shows an illustration of this measure for two distributions.

For any two clusters, we compute the mean and covariance of the data points. If we denote the means and covariances of the two distributions as $\boldsymbol{\mu}_1$ and $\boldsymbol{\mu}_2$ and $\boldsymbol{\Lambda}_1$ and $\boldsymbol{\Lambda}_2$ respectively, we are simply looking for a point $\mathbf{X} = (x,y)$ which satisfies the following

$$R^2 = (\mathbf{X} - \boldsymbol{\mu}_1)^T \boldsymbol{\Lambda}_1^{-1} (\mathbf{X} - \boldsymbol{\mu}_1) = (\mathbf{X} - \boldsymbol{\mu}_2)^T \boldsymbol{\Lambda}_2^{-1} (\mathbf{X} - \boldsymbol{\mu}_2)$$

but with the added constraint that the point (x,y) lies on the line defined by the two points $\boldsymbol{\mu}_1$ and $\boldsymbol{\mu}_2$. Our quantitative measure of separation is simply the value of R, the square root of the Mahalanobis distance at the point **X**. We denote our measure R'.

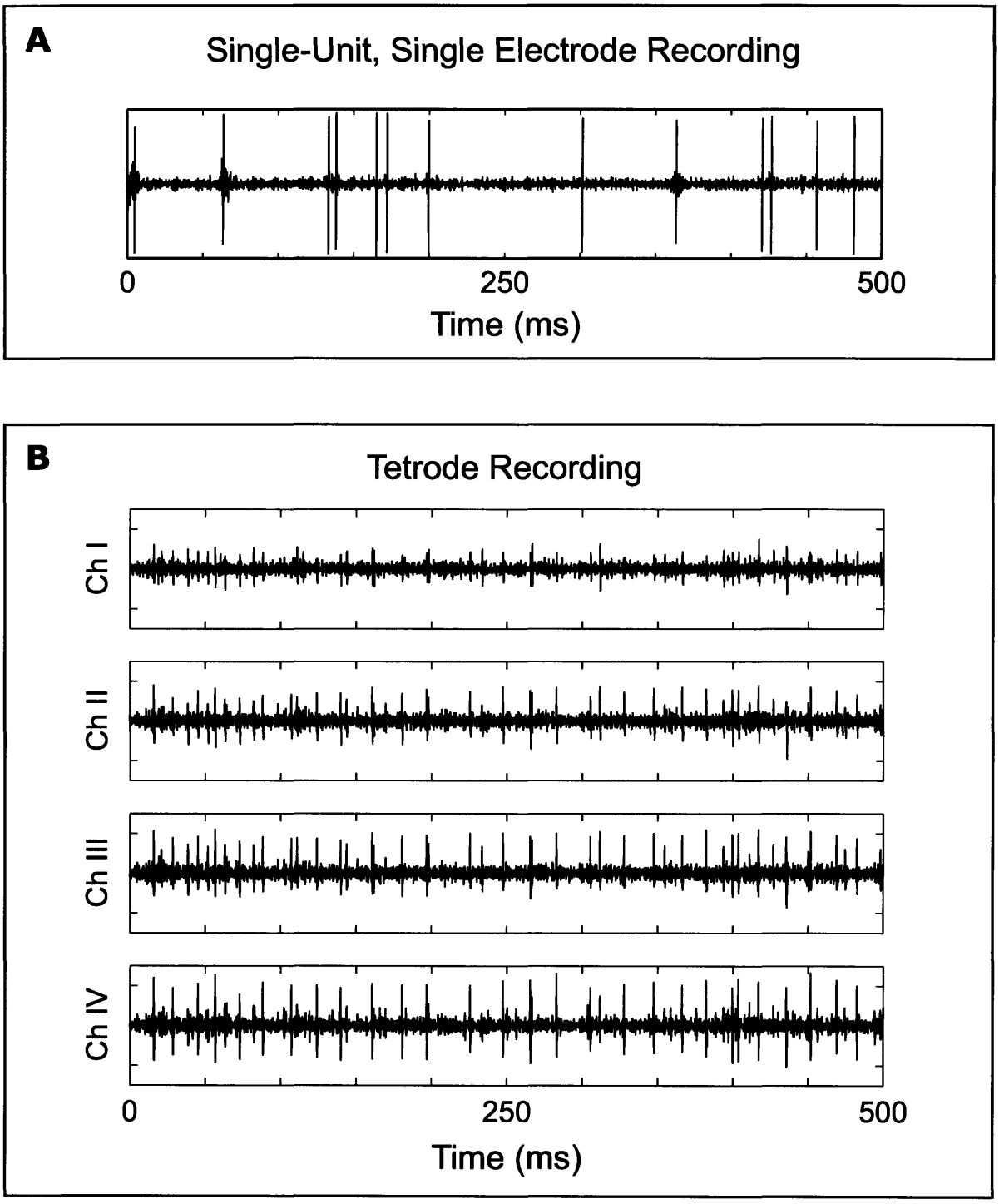

Figure 1 - (A) - Raw waveforms from a single-unit, single electrode recording. Action potentials appear similar with large SNR. (B) - Raw waveforms from four channels of a tetrode recording.Action potentials vary greatly in amplitude and SNR is much lower.

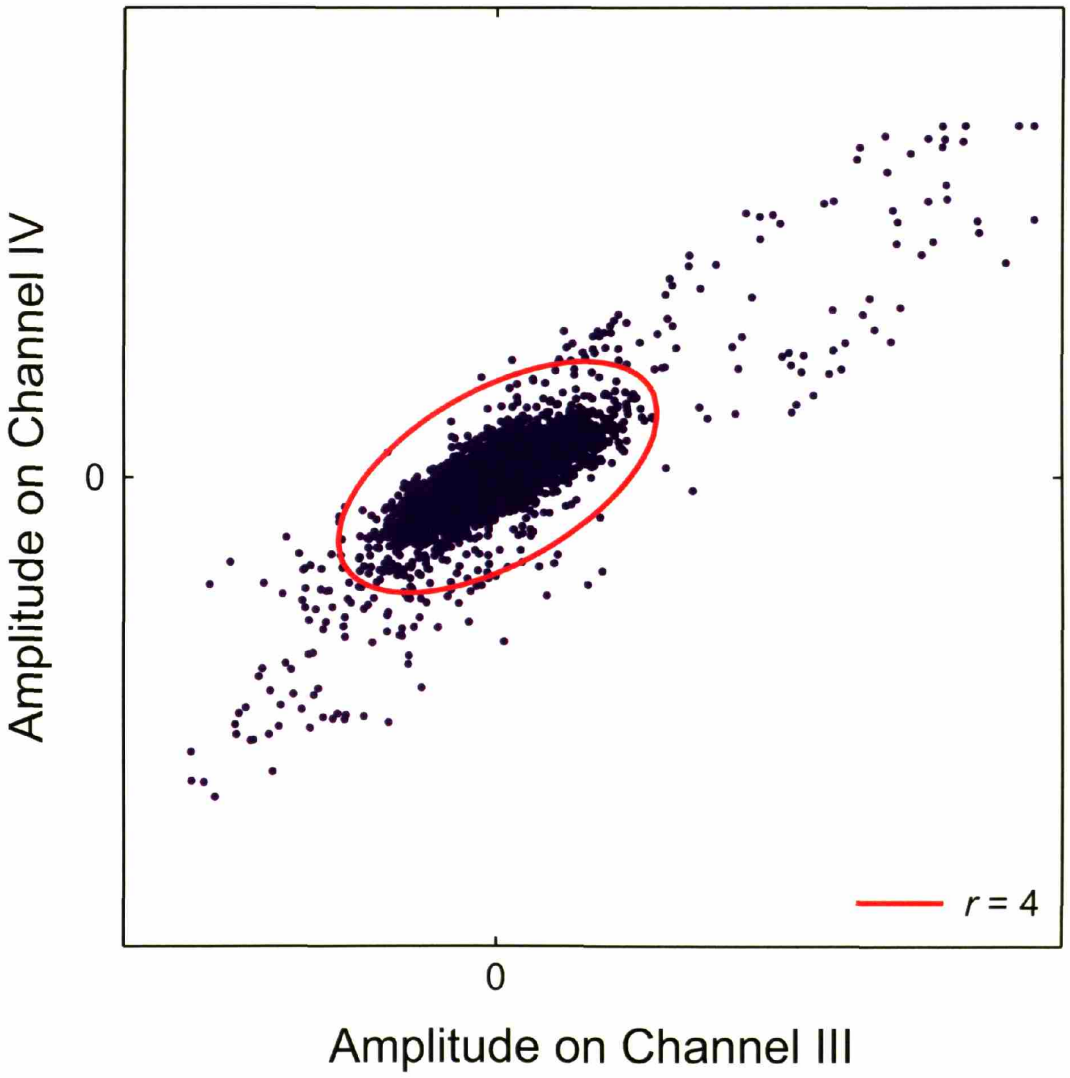

Figure 2 - 2D boundary detection. In this two dimensional case, the optimal detection strategy assuming the noise is Gaussian, is an elliptical boundary. All points outside the boundary are kept and processed.

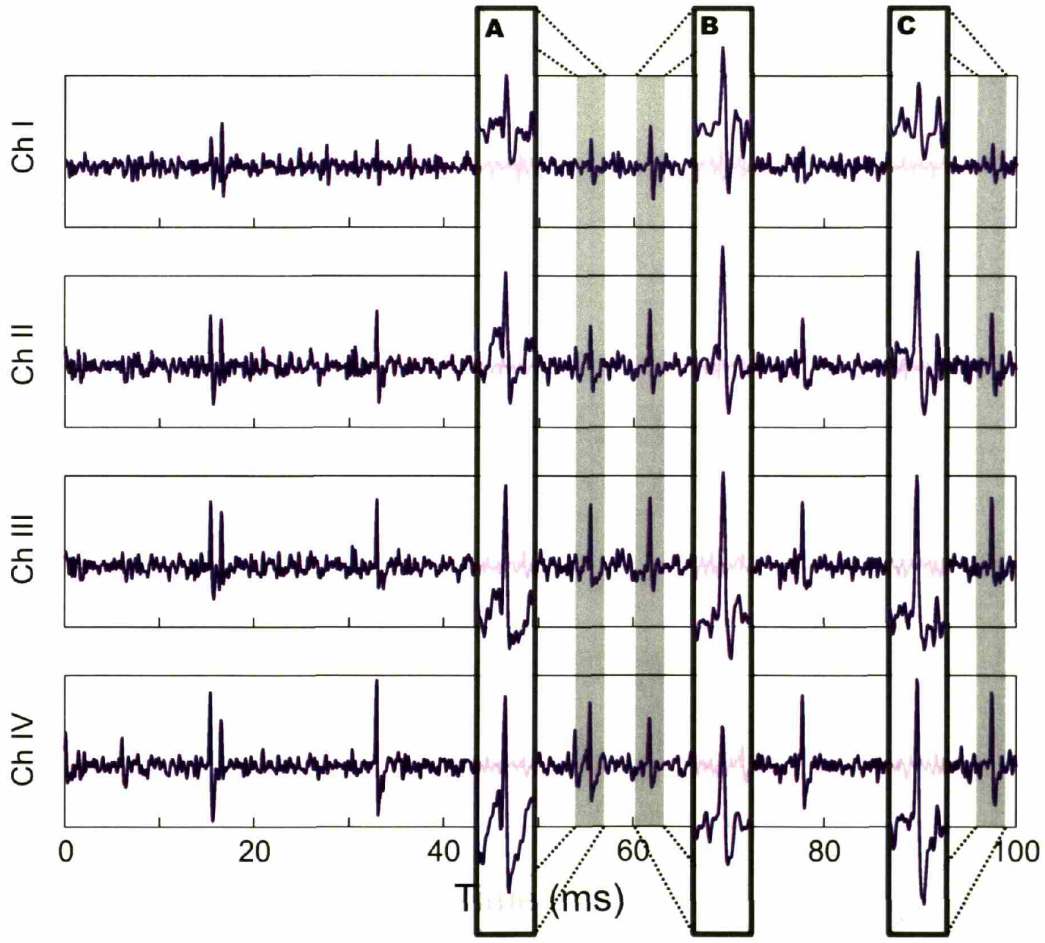

Figure 3 - Spike waveforms across channels from tetrode recordings. This figure shows a 100ms segment of the raw wavefroms recorded on all four channels. (A): One event seen across all four channels. (B): Another event with different waveform profile from A; e.g. amplitude on channel I is bigger while amplitude on channel IV is smaller. (C): This event may be from same source as A.

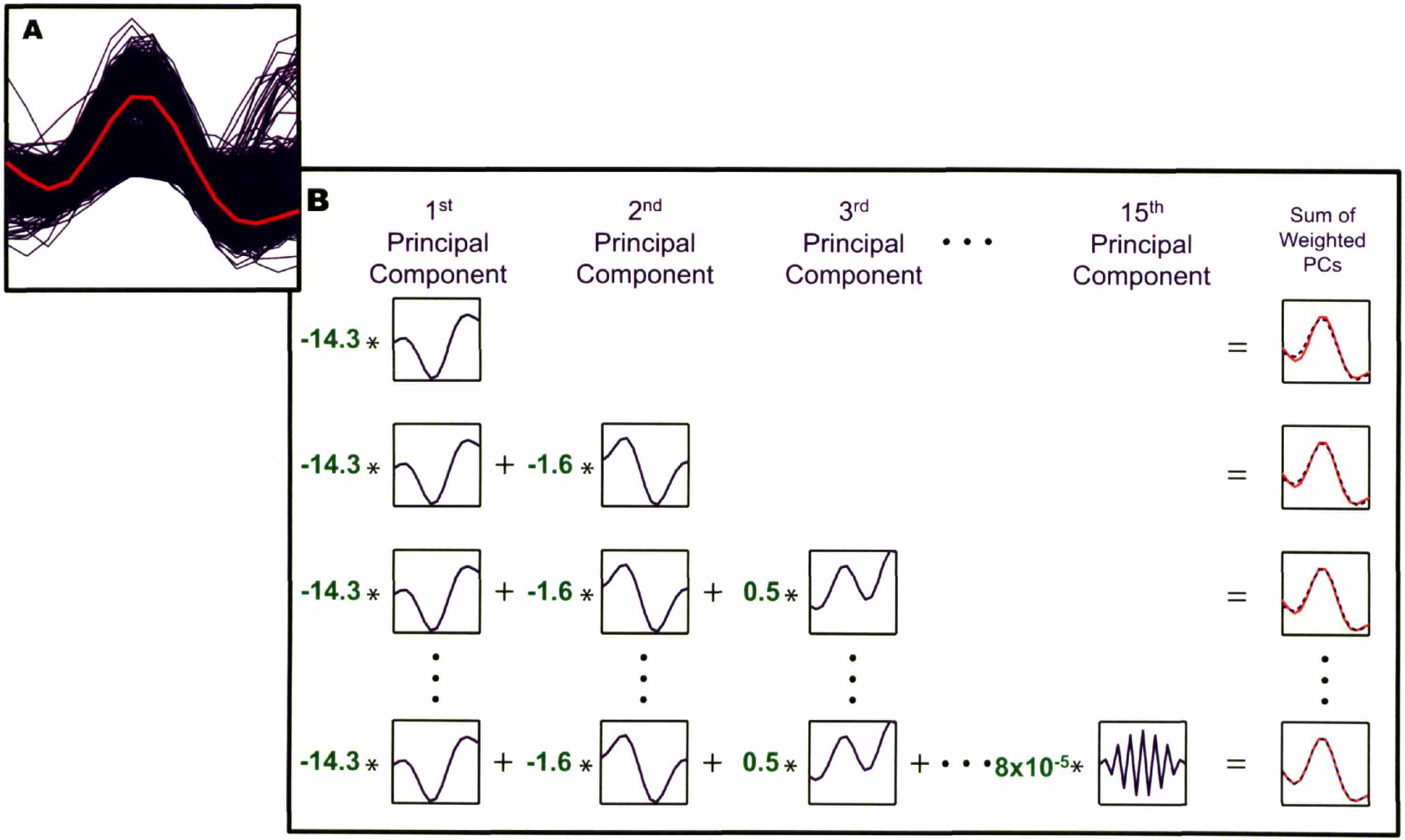

Figure 4 - PCA analysis. Panel A shows a set of waveforms extracted from channel III of the tetrode recording shown in figure 1. One of the waveforms, shown in red, has been randomly selected. Panel B shows the Principal components used to describe the entire wave set, and specifically the reconstruction of the waveform shown in red. With only the 1st principal component, reasonable reconstruction is acheived.

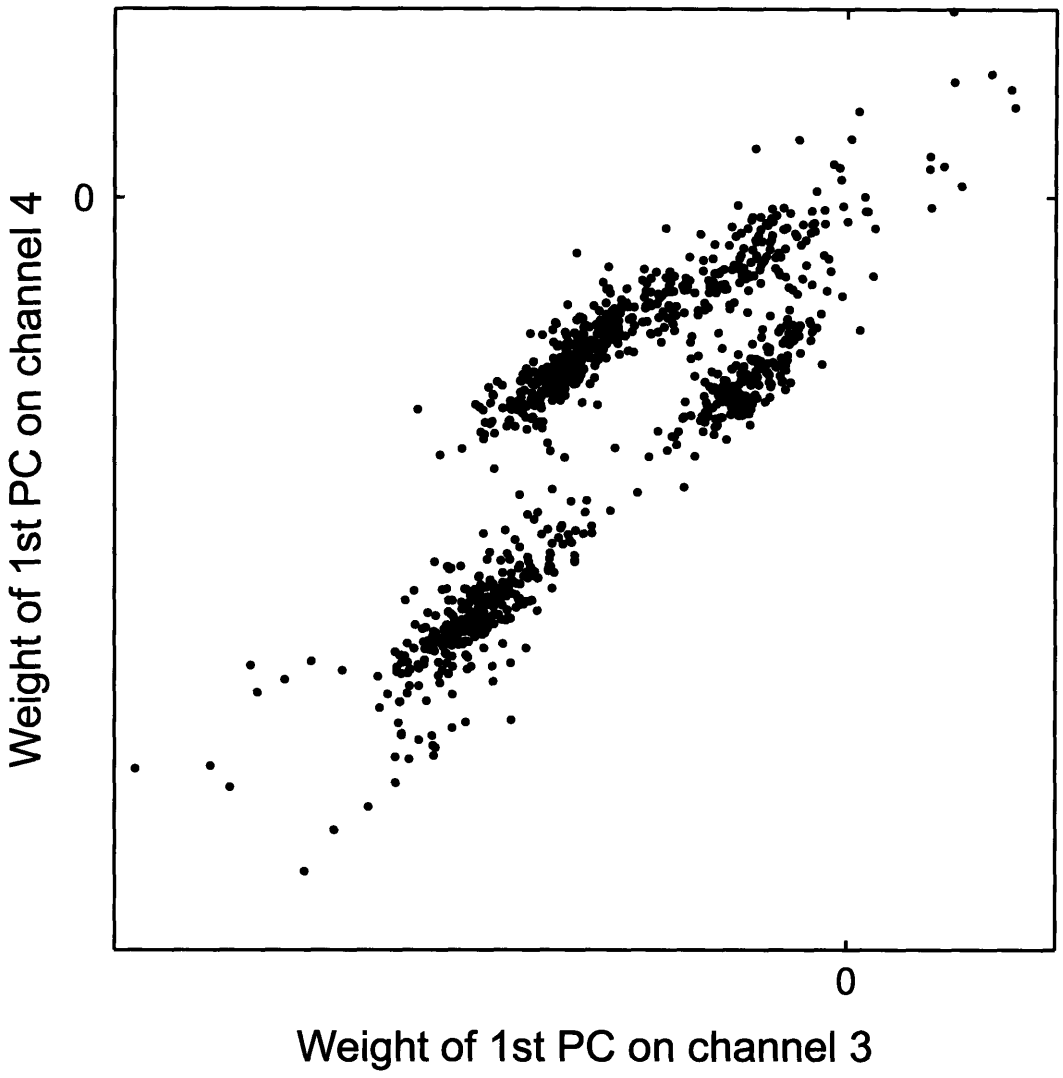

Figure 5 - Clustering in one two-dimensional projection of the four-dimensional Principal Component space. This plot reveals four separated clusters.

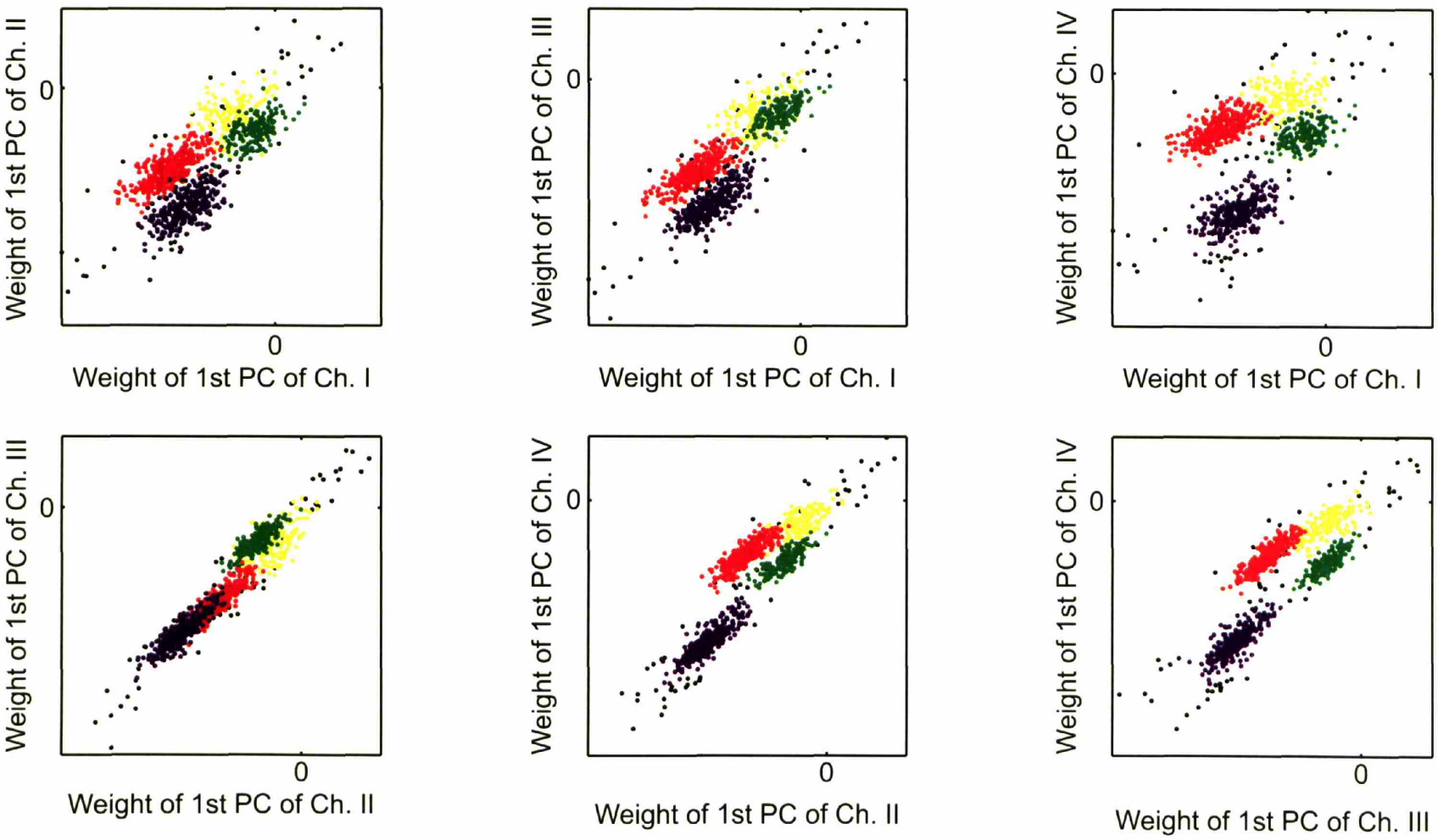

Figure 6 - Each panel shows one two-dimensional projection of the four-dimensional principal component space. Three clusters in blue, red, and green, show three separated clusters that presumably originate from distinct sngle-units. The fourth cluster shown in black likely consists of false detections and low SNR spikes.

	Inferior Colliculus		Visual Cortex	
	Tetrodes	Single Channel	Tetrodes	Single Channel
Total # of sites	52	52	28	28
0 units/site	0	9	0	0
1 unit/site	0	27	0	2
2 units/site	8	15	0	5
3 units/site	19	1	5	7
4 units/site	12	0	4	10
5 units/site	11	0	5	2
6 units/site	1	0	6	2
7 units/site	0	0	6	0
8 units/site	1	0	1	0
9 units/site	0	0	1	0
Total # of units	190	60	151	95
Mean units/site	3.7	1.2	5.4	3.4

Table 1 – Column 2 lists our results using tetrodes to isolate single-units in the IC. Column 3 lists estimates of performance for spike sorting from the best tetrode channel at each site. Number of units misclassified or discarded is presented. Columns 3 and 4 present similar results from the visual cortex (Gray, Maldonado et al. 1995).

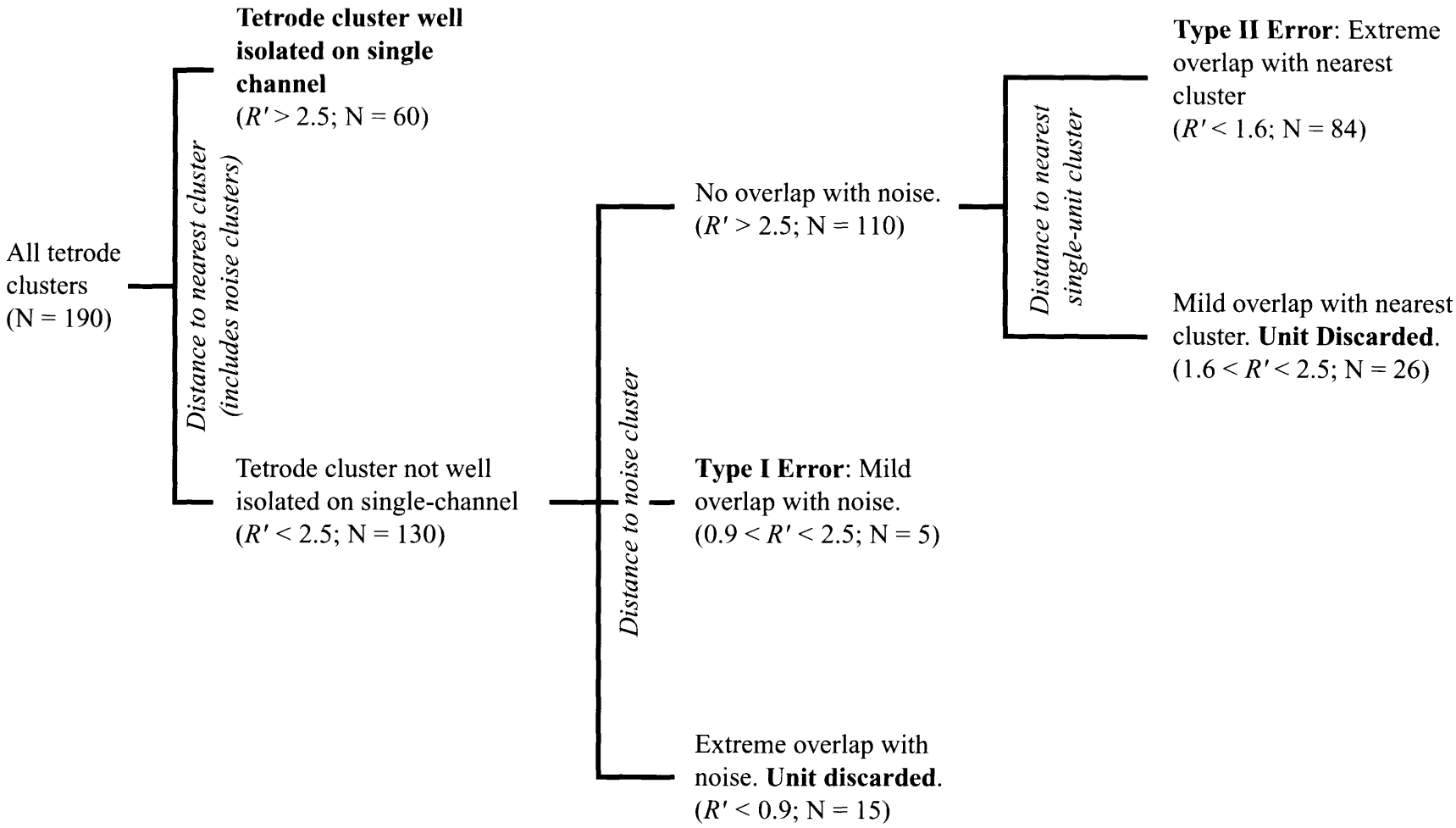

Figure 7. Decision tree for identifying clustering on single-channel based on tetrode classification. In the first branch, we distinguish based on distance to nearest cluster where we have included the noise clusters. In the second branch we classify the clusters that were not well isolated based on their distance to noise cluster. The third branch classifies those clusters that did not overlap with the noise based on how much they overlap with the nearest single-unit cluster

		Inferior Colliculus		Visual Cortex	
		Tetrodes	Single	Tetrodes	Single
Total # of units		190	60	151	95
# Discarded	Undetected	-	15	-	56*
	Multi-Unit	-	26	-	
# Misclassified	Type I	-	5	-	
	Type II	-	84	-	

Table 2. This table lists the different errors encountered using a single channel for sorting vs. the tetrode. The visual cortex results are from Gray et al. (1995). * Note that Gray et al. did not distinguish between misclassified and discarded units. The misclassified number for this study is simply the difference between the number of units with tetrodes vs. a single channel.

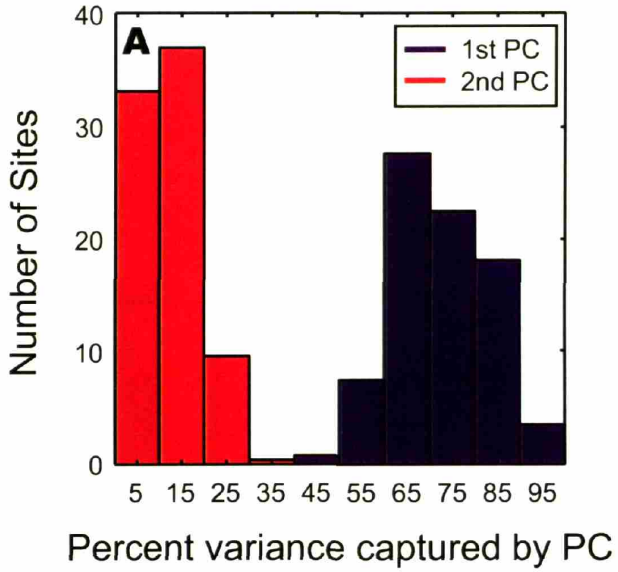

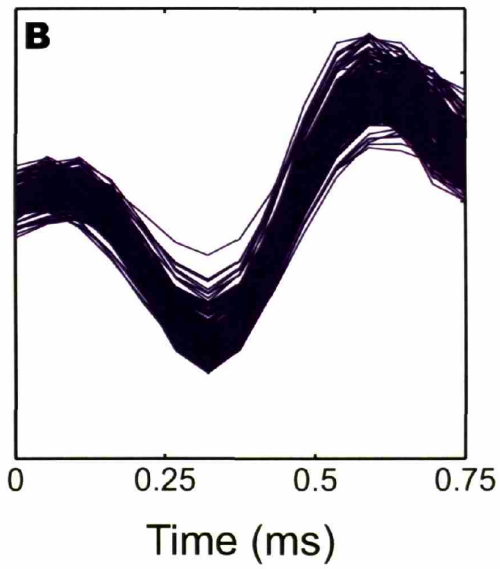

Figure 8 - (A) - Histograms of percentage of variance captured by 1st and 2nd principal components (PC). The 1st PC captures 73% of the variance on average. At 90% of the sites, the 1st PC captures at least 60% of the variance. The second PC only captures 12% of the variance on average. (B) - Principal component waveforms from all channels at every site. The waveforms are very similar

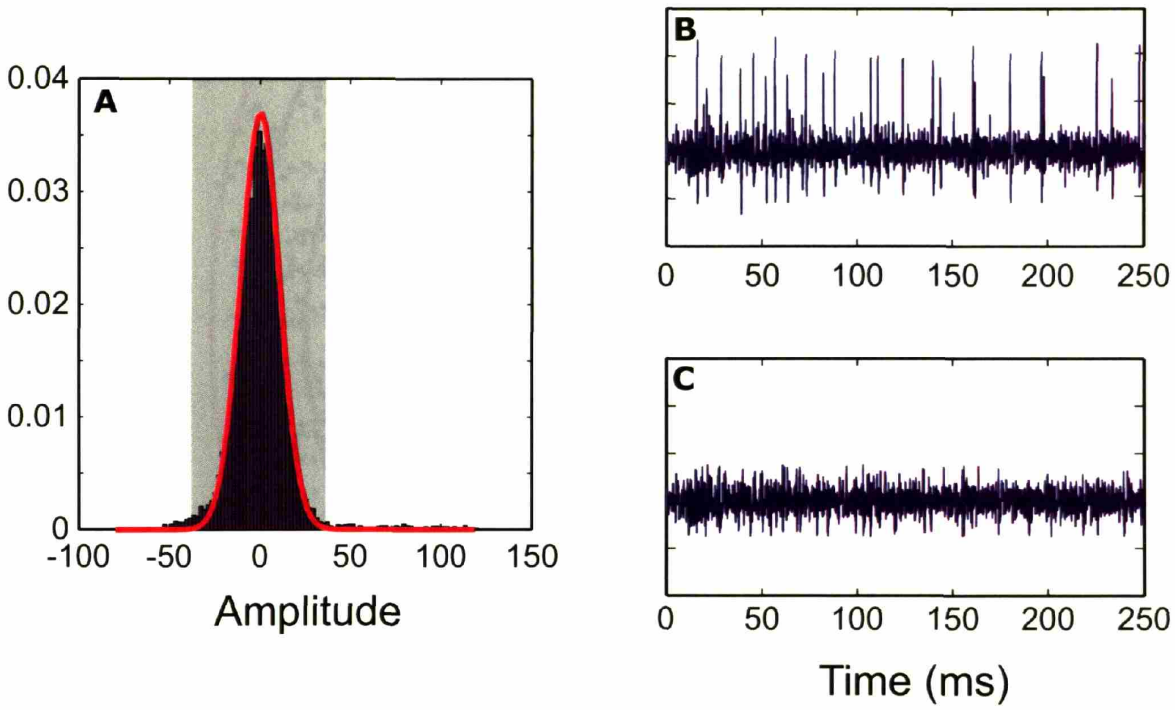

Figure A1- Estimating noise on one channel. (A) - Histogram is distribution of sample amplitudes from raw waveform. The red curve is a Gaussian fit to the central part of the histogram in a least mean squares sense. (B) - The original waveform. (C) - The remaining noise once the action potentials are removed.

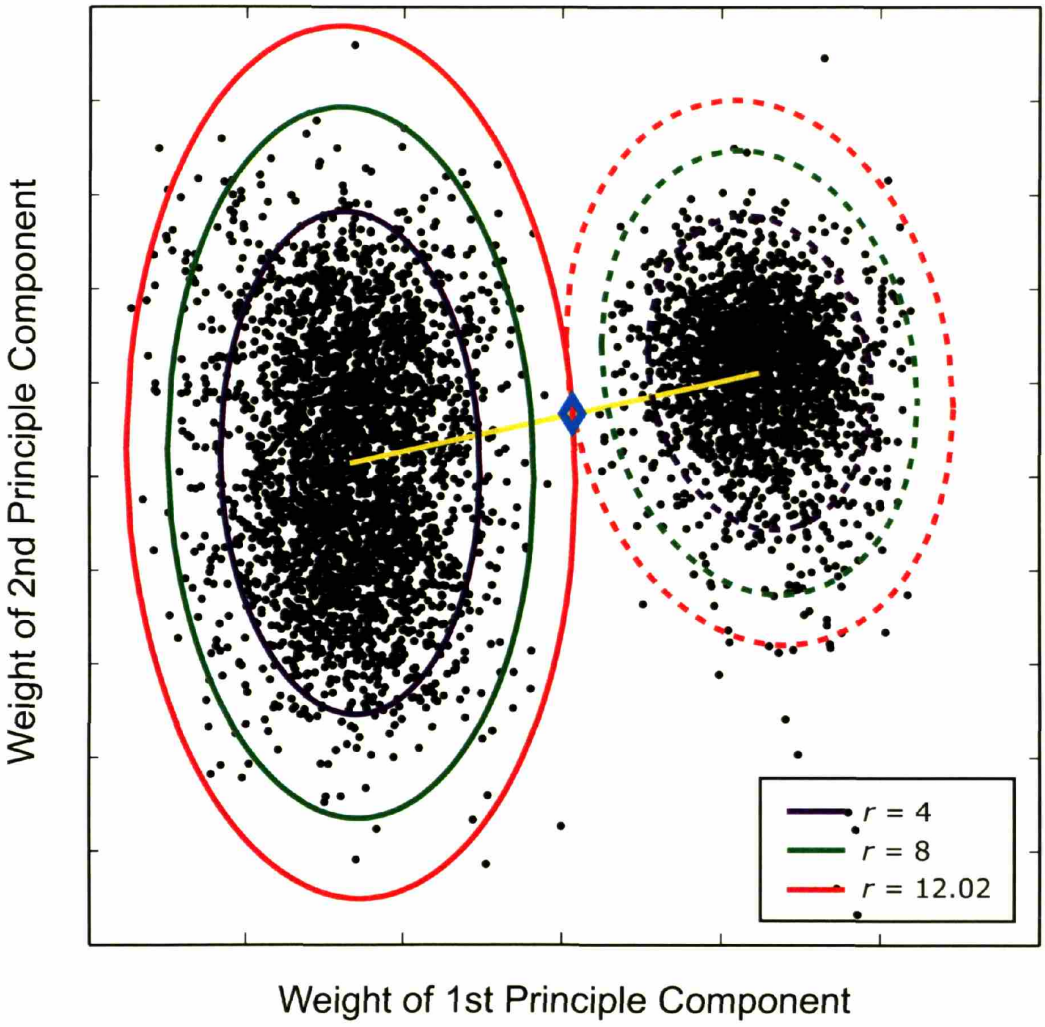

Figure B1. Illustration of calculating *R'*. For the cluster on the left, the solid ellipses show contours of equi-probability defined by the Mahalanobis distace. The cluster on the left shows ellipses (dashed) defining the same Mahalanobis distances. The yellow line shows the line connecting the centers of the two distributions. The green diamond shows the point along the yellow line that is the same Mahalanbobis dstance from both distributions.

Chapter 2: Responses of Neighboring Neurons to Pure Tone Stimulation in the Inferior Colliculus

Introduction

The inferior colliculus (IC), the main auditory nucleus in the mammalian midbrain, occupies a central position in the ascending auditory pathway. Virtually all neural pathways originating from the auditory nerve and continuing on to the auditory cortex synapse in the IC (Adams, 1979; Brunso-Bechtold et al., 1981). Auditory information passes from the cochlea to the cochlear nucleus via the auditory nerve; the information splits into parallel paths that project to separate brainstem nuclei (e.g. medial and lateral superior olivary nuclei, nucleus of the lateral lemniscus). The processed information from these nuclei eventually converges again in the IC before continuing on to the thalamic and cortical areas. By its unique position, the IC may serve an organizational role in collecting and sorting the parallel processed auditory information from the lower nuclei before passing this information to the thalamus and cortex.

The anatomical structure of the central nucleus of the inferior colliculus (ICC), which receives the majority of the ascending inputs (Oliver and Shneiderman, 1991), also suggests an organizational role. At the cellular level, the central nucleus contains only two morphological cell classes (Oliver and Morest, 1984). Disc-shaped cells, characterized by planar dendritic fields, account for approximately 90% of the cells in the central nucleus. The remaining 10% are stellate cells with long, minimally branching dendrites. The disc-shaped cells of the central nucleus align in a co-planar fashion to

create parallel sheets, or laminae; the long dendrites of the stellate cells, on the other hand, span many laminae.

In addition to the organization seen in the cellular anatomy, afferent axons align parallel to the laminae created by the disc-shaped cells. The axons from some of the lower nuclei form distinct bands that partly interleave and partly overlap with bands from other nuclei to form even more complex regions of inputs (Henkel and Spangler, 1983; Shneiderman and Henkel, 1987; Oliver et al., 1997). This complex anatomical arrangement has led Oliver and Shneiderman (1991) and others to hypothesize the existence of different functional regions within the ICC.

Many studies have sought to identify functional maps and organizations of physiological responses in the ICC that correlate with the complex anatomical structure. The strongest evidence of a functional organization is a tonotopic map that is orthogonal to the anatomical laminae (Merzenich and Reid, 1974). Since the laminae correspond to iso-frequency planes, other studies have investigated the existence of maps within a lamina. Within lamina maps have been reported for latency (Langner and Schreiner, 1987), pure tone threshold (Stiebler, 1986), tuning width (Schreiner and Langner, 1988), and best modulation frequency (Schreiner and Langner, 1988). To further investigate the organization of response properties in the ICC, we were interested in characterizing the similarities and differences of responses among neurons in close spatial proximity to each other.

Studies of response maps have typically relied on traditional, serial recording of single-units and histological reconstruction of electrode tracks to identify global organization of physiological responses. They cannot, however, directly investigate local

relationships because they cannot reliably record individual spike trains from several neurons in a localized region of space. As we have discussed in Chapter 1, a new recording technology, the *tetrode* (Wilson and McNaughton, 1993), offers the opportunity to record simultaneously from neurons that are 'close' together. Tetrodes, closely-spaced, four channel electrodes, record multi-unit spiking activity from neurons in the vicinity of the recording site. Using spatial sampling from the four channels, we can reconstruct the single-unit spike trains which contributed to the multi-unit recording because the relationships among the action potential waveforms observed across all four channels should be different for action potentials originating from neurons at different locations in space.

We assume that the individual channels of the tetrode only record from cells that are closer to the recording sites than some maximum limit. As we described in chapter 1, this limit is a property of the electrodes and the cell density in the region. In particular, if the range of the electrodes is large relative to the cell density, then the number of cells contributing to the multi-unit activity will be so large that individual action potentials will not be observed. Therefore, if we can discriminate action potentials, then we assume that these action potentials come from cells that are close to the recording sites relative to the cell density in the region. In the visual cortex, the range of tetrodes has been estimated at approximately 65μm (Gray et al., 1995). Therefore, we assume here that this is an upper bound on the range of the tetrode, so we use the terms close and neighboring to describe neurons that lie within this effective recording radius of the tetrode.

Using physiological characterizations applied widely in studies of the auditory system, we recorded simultaneously from multiple neighboring neurons with our tetrodes

and characterized and compared the response properties of these neurons. If the cells of the ICC are spatially organized by physiological properties, we would expect to see a high degree of similarity among neighboring neurons in that particular response category.

Methods

Animal Preparation

The data presented here were collected from the inferior colliculi of 13 anesthetized adult cats. The surgical methods were previously described in Chapter 1. To assess the general health of the auditory neural pathway, we monitored the click-evoked Auditory Brainstem Response (ABR) as described in Chapter 1.

Data Acquisition

All recordings from the IC were made with tetrodes as described in Chapter 1. Because we were interested in characterizing binaural beat sensitivity, we typically positioned our electrode in low-frequency regions of the ICC. For the posterior approach, this meant inserting the electrode into dorso-lateral regions of the IC; whereas for the dorsal approach, we restricted our penetrations to shallow depths.

Stimuli

Acoustic stimuli used for quantitative analyses consisted of pure tones presented either binaurally or monaurally. The stimuli were digitally generated and delivered via closed acoustic assemblies as described in Chapter 1.

For rate-frequency measurements, we used either 150-ms or 200-ms tone bursts follower by either a 150-ms or 300-ms silent interval between stimuli, respectively. Rate-frequency responses were typically measured in ¼-octave steps centered around the multi-unit tuning curve CF. For rate-level measurements, we used 250-ms tone bursts followed by a 250-ms silent interval. The rate-level measurements were typically measured in 5dB steps. The stimuli for both rate-frequency and rate-level curves were presented 50 times each at each frequency or level.

Binaural beat stimuli had a 2Hz beat frequency; the ipsilateral ear was typically the higher frequency. Typically, the beat stimuli were presented continuously over 75s or 150 cycles of the beat period. Some neurons exhibited noticeable adaption to the continuous stimulus. For these units, we presented a 1.5s beat stimulus followed by a 500-ms silent interval between stimulus presentations. This stimulus, containing three full beat periods, was presented 50 times.

Experimental procedure

The experimental procedure used to identify a stable recording site was described in Chapter 1. Once we have identified a stable recording site with at least two well-

isolated clusters, we first measured rate-frequency responses and rate-level responses.. Typically, we measured the rate-frequency curves at a near threshold level (within 15dB SPL of the multi-unit threshold at CF) and a moderate to high sound level, typically about 20-30 dB above the near threshold level. We also measured the rate-level response at the CF for the multi-unit tuning curve.

If we were in a low-frequency region of the ICC, we also measured the binaural beat response. In early experiments, we only measured the beat response at the multi-unit CF. However, in later experiments, we measured the beat response at multiple frequencies spanning the range of frequencies over which we observed beat sensitivity in the hash response from a single tetrode channel.

Data Analysis

SINGLE-UNIT RECONSTRUCTION

Tetrode recording, processing and single-unit spike train reconstruction are described in detail in Chapter 1. Briefly, from a given recording site, we record the raw waveforms from all four tetrode channels in response to our different stimuli. Off-line, the signals are bandpass filtered (300-3000Hz) and any 60-Hz noise is removed from the recording. We apply the spike detection algorithm described in chapter 1 and identify the times of all detected neural events. For every neural event time, a 0.75 ms sample of the waveforms from each channel is collected. Using the collected waveforms from each channel, we sort the data based on the Principal Component weights for each channel.

Events generated from an individual neuron cluster together in Principal Component space, and are separated to define the spike times for each single-unit in our recording.

Response Properties

Best frequencies and bandwidth at each level were obtained from average rate responses. At each frequency, we count the total number of spikes measured over the duration of the stimulus to obtain the rate-frequency curve. To increase the frequency sampling by a factor of ten, we apply a cubic spline interpolation operation. From the interpolated curve, we typically define the best frequency as the frequency that elicits the maximum number of spikes; in a few cases, the single-unit response is primarily inhibitory, so we define the best-frequency in these cases as the frequency that elicits the fewest spikes.

To characterize the width of tuning, we use the half-bandwidth of the rate-frequency curve. The half-bandwidth is the bandwidth of the rate-frequency curve at a rate halfway between the maximum rate and the spontaneous rate. We use the average spike rate across all frequencies during the silent intervals between stimuli as a measure of spontaneous rate.

From the rate-intensity measurements, we measured the threshold and characterized the monotonicity of the rate-intensity curves. Rate-intensity curves were obtained by counting the total number of spikes during the entire stimulus at each level. We increased our overall sampling of levels by a factor of ten by applying a piecewise cubic interpolation to the measurement of counts vs. level. We defined the rate-level

dependency as non-monotonic if the rate dropped below 2/3 of the maximum rate at a level above that which elicited the maximum rate.

To determine the pure tone threshold, we measured the spontaneous rate for every trial and every level. Then, we computed the standard deviation of the spontaneous rate. We defined the threshold as the level at which the rate-level curve exceeded 2 standard deviations of the spontaneous rate above the mean spontaneous rate. In many cases, the spontaneous rate was zero. In these cases, we defined the threshold as the lowest level that produced at least 5 spikes.

For binaural beat responses, we characterized the mean interaural response by using a vector-averaging approach (Goldberg and Brown, 1969). We convert the spike times to phase angles defined over the binaural beat period and compute a vector average across all spikes to obtain a mean interaural phase difference (IPD). In the cases where we presented non-continuous binaural beat stimuli, we removed the first beat period of each stimulus presentation before computing the mean IPD.

For some sites, we measured binaural beat responses at more than one frequency. For these sites, we investigate the frequency vs. best-IPD relationship among the neighboring neurons. From the frequency-IPD relationship, we can estimate the characteristic delay (CD) and the characteristic phase (CP) (Yin and Kuwada, 1983). If neighboring neurons exhibit similar CDs, we may expect that these units are either coincidence detectors themselves with similar delays in the inputs to the neighboring neurons or they reflect input from a lower region with common delays between the two ears. Looking at the relationship of CP among neighboring neurons may provide some insight into the mechanisms underlying the IPD sensitivity in neighboring neurons.

Briefly, for each unit and each frequency, we computed the mean interaural phase. We only include the mean interaural phase at a particular frequency if the beat period histogram is significantly different ($p < 0.001$) from uniform, as defined by using the Rayleigh test of uniformity (Fisher, 1993). Once we have obtained a set of mean interaural phases at a set of frequencies for a given unit, we fit a weighted regression line to the data points. The slope of the regression line gives the CD and the y-intercept gives the CP. Next, we check the linearity of the data points using the linearity test described by (Yin and Kuwada, 1983) and using a criterion for the linearity test of $p < 0.005$. We ignore those units whose frequency-phase relationships are not linear.

Results

We present data recorded from 44 sites in 13 cats from which we isolated 145 single-units. Our comparisons consider pairs of neighboring neurons, and we have a total database of 193 neighboring neuron pairs (e.g. a site with four units has six pairs – (1,1), (1,2), (1,3), (2,3), (2,4), and (3,4)). From these neuron pairs, we investigate the similarities and differences between the pairs in best frequency, tuning bandwidth, pure tone threshold, level dependence, temporal response patterns, and ITD sensitivity.

Best Frequency

Most reports of frequency tuning in the auditory system measure the characteristic frequency (CF), which is defined as the frequency at which a unit exhibits the lowest

response threshold. The CF is measured from an iso-rate contour as a function of frequency. Because we do not have on-line access to the separated responses of each single-unit in our multi-unit recording, we cannot measure iso-rate responses. Therefore, we measure the Best Frequency (BF) instead. The BF is the frequency that elicits the maximum rate response at a given level. This measure depends on the level of the tones used, so we measure the best frequency at a level close to threshold to get an estimate of the CF. In general, we used the multi-unit threshold at the 'characteristic frequency' obtained from a multi-unit tuning curve. We typically measure the best frequency at 5-10dB above this threshold.

Figure 1 shows the dot raster plots as a function of frequency for three units recorded simultaneously from the same site. These three units exhibit similar best frequencies (green triangles). The BF's are 1892 Hz, 1840 Hz, and 1741 Hz respectively, and span a range of about 0.12 octaves.

From our population of 193 neighboring pairs, we discarded 33 pairs from 11 sites because the rate-frequency curves were measured at levels higher than 15dB above the multi-unit threshold. For the remaining 160 pairs, we create a scatter plot of the BF of one unit against the BF of the other unit in the pair (Figure 2). Note that, because we specifically targeted regions tuned to lower frequencies, the majority of the units have BFs below 3kHz. In general, the BFs of neighboring neurons are similar. The median difference between BFs is 0.16 octaves, and 69% (111/160) of the pairs have BFs within ¼-octave of each other, which corresponds to the typical frequency spacing used in our measurements. The correlation coefficient for the BF comparison is ρ=0.89. If we only

consider the sites where the BFs were below 5kHz, which accounts for most of the data, the correlation drops to ρ=0.79 which corresponds to R^2=0.63.

Bandwidth

To investigate the width of tuning, we measured the half-bandwidth of the rate-frequency curves. The half-bandwidth is the width of the curve measured halfway between the rate at the best frequency and the spontaneous rate. Figure 3 shows the rate-frequency curves for the three units whose dot raster responses are seen in figure 1. For each curve, the horizontal line indicates the point at which we measured the half-bandwidth. Qualitatively, from both the dot raster plots and the rate-frequency curves, the bandwidths are more variable than the BFs. The half-bandwidths are 1862Hz, 912Hz, and 915Hz. As with the best-frequency measurements, the half-bandwidth is typically measured at a level 5-10 dB above the multi-unit threshold.

Figure 4 shows a scatter plot comparing the half-bandwidths between each of the 160 neighboring pairs used for the best frequency comparison. This measure is not very well correlated among neighboring neuron pairs. The correlation coefficient for the half-bandwidth comparison is ρ=0.35 ($p < 0.0001$) which corresponds to R^2=0.13 indicating a very weak relationship between bandwidths of neighboring pairs.

Rate-Level Responses

We characterized the effects of level on the response to a pure tone near the best frequency. Figure 5 shows dot raster plots for four units simultaneously recorded at the same site as a function of level. For these four units, we can make two observations about their rate-level behavior. First, the pure tone thresholds appear similar; second, the dependency of rate on level differs among the units. The latter is more easily seen in figure 6 which shows the corresponding rate-level curves for the four neighboring units. Because the rates were widely different among the units, we have normalized the rate-level curves to their maximum. Figure 6 shows that units 1 and 2 have a non-monotonic behavior; that is, the rate peaks at a particular level above which the rate decreases; in contrast, rate of unit 3 continues to increase with increasing level. Unit 4 appears to decrease in rate above 50dB; however, based on our criterion for monotonicity, we label this response as monotonic because the rate does not fall below 66% of the maximum.

The triangles on the x-axis in figure 6 indicate the thresholds for each of the four single-units. The thresholds span a range of less than 10dB. From our database of units, we have rate-level curves measured for 121 neighboring neuron pairs. Of the 121 neighboring pairs, threshold could not be determined for 13 pairs from two sites because these units already responded at the lowest level tested. Figure 7 shows a scatter plot of the thresholds for the 108 remaining pairs. The dashed lines define the boundaries outside of which the pairs differ in threshold by more than 10dB. Only two pairs differ by more than 10 dB and neither pair exceed a difference of 11dB. The correlation coefficient is

ρ=0.949 corresponding to R^2=0.90. This reveals a very strong relationship between pure tone thresholds of neighboring neuron pairs.

The monotonicity of the level dependency showed no significant relationship. We measured the monotonicity of 120 neighboring pairs. Comparing neighboring neurons, we find that 41 (34%) pairs both have monotonic level dependence, 27 (23%) pairs both have non-monotonic level dependence, and 52 (43%) pairs have one unit with a monotonic level dependency while the other has a non-monotonic dependency. If non-monotonic and monotonic units are distributed by chance with some incidence rate p and $(1-p)$ respectively, then we expect the rate of mixed pairs to be $2*p*(1-p)$. Therefore, if the montonic and non-monotonic units are distributed randomly, the we expect p, the incidence of non-monotonic units to be p=0.31. From our single-unit distribution, we estimate p as 0.43. The 95% confidence interval for this estimate is [0.30,0.57] which contains the expected value for p under the hypothesis that monotonic and non-monotonic units are randomly distributed.

Temporal Response Patterns

Temporal discharge patterns in response to pure tone stimulation at CF provide another common characterization of single-unit responses throughout the auditory system. We classified temporal discharge patterns based on a scheme previously defined for the ICC by LeBeau et al. (1996). In their classification scheme, they defined six different PSTH types: *chopper*, *pauser*, *onset*, *on-sustained*, *on-chopper*, and *sustained*. Any PSTH types that don't fall into these categories were classified as *other*.

Figure 8 illustrates the various PSTH types we used. Chopper responses (Fig. 8A) are characterized by sustained firing throughout the stimulus duration with regular intervals between successive action potentials. The inset in Figure 7A shows the histogram of the first order interspike intervals. The interspike interval histogram shows a clear peak at the preferred chopping rate. Adopting a measure used by Young et al. (1988) in the cochlear nucleus, we designate units whose interspike interval distribution has a coefficient of variation (CV) < 0.35 as chopper units, where the CV is defined as the ratio of the standard deviation of the distribution to the mean of the distribution. Pauser responses (Fig. 8B) exhibit a large onset peak with a significant reduction or cessation of activity for up to 25ms after the onset followed by sustained firing. Onset units (Fig. 8C) exhibit a large peak of no longer than 30ms following the stimulus onset with little or no activity following the onset response. On-sustained responses (Fig. 8D) exhibit a large onset peak followed by sustained firing. On-sustained units are distinguished from pausers by the lack of a gap following the onset. On-chopper responses (Fig. 8E) have a large onset response of no more than 30ms with little or no activity observed in the rest of the stimulus duration. The on-chopper, however, differs from the onset response because it exhibits shows two or more distinct peaks within the onset response. Sustained units (Fig. 8F) respond throughout the duration of the stimulus without any observed onset component.

In some instances, the PSTH changed with level, though the majority of our single-units exhibited a relatively stable PSTH across a wide range of levels. Of 130 single-units for which we measured pure tone responses at multiple levels, we found that 28 (22%) units showed changes in PSTH type with level. Of the 28 units that changed

PSTH type with level, over half (16/28) exhibited a transition from onset response at lower levels to a different PSTH type at higher levels with most of these (13/16) transitioning from onset to pauser response. For the purposes of characterizing the responses with a single descriptor, we chose to use the PSTH measured at a level approximately 25-35dB above threshold. Using this criterion, the most common response type was pauser (42%; 55/130) followed by onset (32%; 41/130). Table 1 shows the distribution of response types for the entire population of 122 single-units for which we have characterized temporal discharge patterns.

Table 2 shows a matrix of pair-wise combinations of response types. Given the prevalence of pauser and onset units, the most common discharge pattern pairs are Pauser/Pauser, Onset/Onset, and Pauser/Onset. To determine whether the paired combinations differed from the expected distribution for randomly distributed unit types, we applied a χ^2 test and tested this contingency table against the null hypothesis that the units are randomly distributed. Since some of the PSTH types had low incidence of occurrence, some of the entries in our contingency table have values fewer than 5 invalidating a χ^2 test. Therefore, we grouped together Onset and Onset-Chopper as one category; Chopper, Onset-Sustained, and Sustained as another group; Pausers remained a separate group. From this grouping, we apply our χ^2 test, and we find that the distribution shows no significant correlation ($p = 0.061$).

Interaural Time/Phase Sensitivity

Many single-unit studies of the inferior colliculus focus on characterizing binaural responses. In particular, considerable attention has been focused on studying the coding of interaural time and phase differences because they are important cues for sound localization. Here, we consider whether sensitivity to interaural phase differences is similar among neighboring neurons.

The top four plots in figure 9 show dot raster responses for four simultaneously recorded neighboring neurons in response to binaural beats at the CF. Each row of the raster indicates 1.5s of the recording and contains three cycles of the binaural beat. Below each raster plot, we have plotted the period histogram for each unit over the 500ms beat period. We see that all four units respond preferentially to a limited range of interaural phase differences (IPD). The mean-IPDs (red triangles) for these units can differ greatly.

We recorded the response to binaural beats at 27 sites in 7 cats yielding a total of 93 single-units and 130 neighboring pairs. For every single-unit, binaural beat response we first determine whether the observed period histogram may arise from a uniform distribution, indicating no beat sensitivity. Specifically, we use the Rayleigh test for uniformity as defined in (Fisher, 1993). The null hypothesis of uniformity is rejected for $p<0.001$. After applying this test, we find that 9 of 93 single-units sites are *not* beat sensitive. These 9 units come from 6 of the 27 recording sites. Therefore, more than 20% of the sites in our sample contained at least one unit that was beat sensitive and one unit that was not.

For the 107 available neighboring pairs of beat sensitive neurons we calculate the mean interaural phase as described by Yin and Kuwada (1983). Figure 10 shows a scatter plot of mean-IPD for unit 1 vs. unit 2 for each neighboring pair. We have adjusted the mean phase of some of the units by adding or subtracting 1 cycle to minimize the difference between the phases of each pair. The dashed lines indicate the boundary beyond which IPDs differ by more than 0.5 cycles. We observe a correlation coefficient of ρ=0.585. However, because phase is a circular variable, the interpretation of correlation coefficient is tricky. In particular, to determine whether the correlation coefficient is significant, we randomly generated sets of 107 data points uniformly distributed between -0.5 and 0.5. As with our data, all points with differences greater than ½-cycle are adjusted by adding or subtracting ½-cycle to maximize the correlation and then compute the correlation coefficient. We repeat this for 100,000 randomly generated data sets to obtain a mean correlation with confidence limits for the null hypothesis of no correlation between neighboring pairs. We find that the 95% confidence interval for the correlation coefficient under the null hypothesis ([0.512,0.675]), contains the correlation we observe.

For most of the recording sites we were only able to measure the binaural beat response at one or two frequencies. However, for 6 sites and 19 single-units we measured the binaural beat response for at least five frequencies around the best frequency. From these measurements, we estimated the Characteristic Delay (CD) and Characteristic Phase (CP) as defined by Yin and Kuwada (1983).

Figure 11 shows the raw data and weighted regression line for six different units. The first four (11A-D) pass our linearity test; the last two (11E-F) do not pass the

linearity test and are discarded. After applying the linearity criterion, we have 14 units and 17 neighboring pairs from 5 sites that are beat sensitive and exhibit a linear phase-frequency relationship.

Figure 12 shows scatter plots for both CD and CP. Error bars indicate 95% confidence intervals of the parameter estimates from the linear regression. The CD shows little sign of any correlation between neighboring neurons (ρ= -0.19; p = 0.43). On the other hand the characteristic phase relationship between neighboring neuron pairs appears quite strong. The correlation coefficient is ρ=0.84. Applying the same test used above with the best-IPD comparison, we find that the 95% confidence interval for the correlation coefficient if the CPs are randomly distributed is [0.41,0.76], so the correlation is significant at the 0.05 level.

Comparison of BF Differences with Other Characterizations

Gray et al. (1995) estimated the effective distance over which a tetrode effectively records at approximately 65μm from the recording site. This means that individual units may be separated by over 100μm. We are interested in investigating whether greater separation leads to greater differences in the range of characterizations we have used. In particular, we are interested in knowing whether there may be physiological differences between units that may occupy different laminae compared with pairs located in the same lamina.

Because the laminar organization of the ICC reflects organization of frequency tuning, we investigated whether units with greater differences in BF showed an overall

greater difference in other response properties. Figure 13 shows the comparison of the difference in BF with both differences in bandwidth (Fig. 13A) and pure tone threshold (Fig. 13B). Neither plot reveals any obvious correlation between large differences in BF and differences in either bandwidth or threshold. In both instances, we see that the five pairs with BF differences greater than 1 octave show a wide spread of bandwidth and threshold differences that span the range of observed differences. For bandwidth and threshold, we measure R^2=0.062 and R^2=0.055 respectively.

We also looked at whether large differences in BF were reflected in the likelihood of two units to have similar rate-level dependency as measured by the monotonicity of the rate-level curves. We looked at the percentage of mixed pairs, that is the number of pairs made up of one monotonic and one non-monotonic response, in the 25% of pairs with the smallest BF difference and the 25% of pairs with the greatest BF difference. The former shows 32% of the pairs are mixed while in the latter, 38% of the pairs are mixed.

We similarly looked at the relationship of PSTHs and BF differences. We found that 43% of the neighboring neuron pairs had different PSTH types. Again, if we look at the 25% of pairs with the smallest BF difference, we find that 48% show differences in neighboring neuron pairs; the 25% of pairs with the greatest BF difference show 38% of pairs have differences in neighboring neuron pairs. Since the trend moves towards fewer differences in PSTH type with larger BF differences, we can rule out the hypothesis that the separation implied by large BF differences results in more differences in PSTH types.

Lastly, we considered whether greater BF differences influence differences in IPD. Figure 13C shows a comparison of BF differences and IPD differences. Again, we see no relationship between the two measures (ρ=0.012).

Discussion

We have presented results comparing pure tone response characteristics of neighboring ICC neuron pairs. Across the different response characteristics that we have investigated, our results suggest varying degrees of similarity and difference between the pairs. Some of these results are consistent with previous studies and expectations about arrangements and response maps in the ICC; however, some of these results suggest a complexity of organization not previously seen. We need to consider these differences and similarities individually.

Best Frequency

In general, neighboring neuron pairs have similar best frequencies. The correlation coefficient is ρ=0.89, though if we ignore the few high frequency units, it drops to ρ=0.79. Five pairs show a difference in BF greater than 1 octave and 9% (15/160) of the pairs differ by more than 0.5 octaves. However, even if we ignore the outliers, there are still pairs that show differences in BF of up to ½-octave.

Some of the variance in the BFs might be explained by the sensitivity of the BF measurement to level. We have tried to keep our rate-frequency measurements as close to the pure tone threshold as possible; however, in some cases, our BF measurements may be at levels as high as 15dB above the pure tone thresholds. Under these conditions, two units who have nearly identical CFs may have slightly different BFs when the rate-frequency curves are measured at levels 10-15dB above threshold. Also, neighboring

neurons may not have identical pure tone thresholds, and the rate-frequency curves are measured at different levels re: threshold for such units.

Other than these measurement considerations, as we have mentioned previously, estimates of the 'range' of tetrode recordings suggest that two units recorded from a single site may differ in spatial location by more than 100μm. The width of the laminae in the ICC is approximately 70-150 μm (Rockel and Jones, 1973; Oliver and Morest, 1984; Malmierca et al., 2005). Therefore, we may encounter units distributed within a single lamina or units from adjacent laminae. First, within a single lamina, it is probable that there exists some small variations in single-unit CFs. (Merzenich and Reid, 1974) show the change of CF with increasing electrode depth in the ICC. From their data, we estimate the relationship between depth and frequency in the 1kHz region at approximately 380μm/octave. This suggests that a single lamina would span between 0.2 and 0.4 octaves. Therefore, we may expect to see differences within a single lamina of as much as 0.4 octaves. If we record from two units in adjacent laminae, we may expect this difference to be even greater.

Lastly, the few pairs we observe with BFs separated by more than ½-octave may include stellate cells. Since stellate cells span many laminae, they may be excited by a wide range of frequencies, and the BF of these cells may be different from neighboring disc-shaped cells. All the pairs with BF differences of more than 1 octave also all have pauser PSTH Types which may suggest that this population contains a similar cell type. This is consistent with the hypothesis that these may be stellate cells. However, because pauser units represent the largest PSTH type in our population and we only have five

instances of neighboring pairs with BF differences over 1 octave, it is likely that this is simply coincidental.

Bandwidth

Half-bandwidths were not very well correlated among neighboring neurons. The weak $R^2 = 0.126$, though statistically significant, indicates that there is very little relationship between the bandwidths of neighboring neurons. In contrast, using single-unit techniques, Schreiner and Langner (1988) have reported the existence of a map of Q_{10} in the ICC. Some differences may result from differences in the use of Q_{10} vs half-bandwidth; however, as we typically tried to keep our rate-frequency measurements within 10dB of threshold, the half-bandwidth should be correlated with Q_{10}. One difference may be that Schreiner and Langner's (1988) data comes from higher frequency regions of the ICC than our data (3-12kHz). Also, the largest bandwidths we observe are approximately 2.5 octaves with over 70% of the bandwidths observed within 1 octave. By contrast, Schreiner and Langner report Q_{10} values as large as 8 octaves. Therefore, it is possible that we only sampled a limited region within a laminae, or that there are large differences in the organization of bandwidth at low frequencies compared with high frequencies.

Threshold

We have shown that the pure tone thresholds of neighboring pairs are highly correlated (ρ=0.949), with most of the pairs showing thresholds within 10dB of each other. The minimal differences seen in the thresholds between neighboring pairs can be attributed to measurement errors. Some of the differences may be due to our calculation of threshold which only relies on the average rate response. There are a few cases where the temporal response shows visually noticeable deviation from spontaneous rate at a level lower than where the average rate response differs from the spontaneous rate. More significantly, the rate-level curves may not have been measured at the exact characteristic frequency for the neuron. As we have observed, BF differences of as much as ½-octave are not uncommon; in these cases, because the rate-level curve is only measured at a single frequency, we may observe some differences even if the pure tone thresholds are identical if one unit is stimulated slightly away from its CF.

Temporal Discharge Patterns

One of the greatest differences observed among neighboring neurons in the ICC is the temporal discharge patterns. Onset and pauser units dominated our sample, and accordingly, the most common pairings between neighboring pairs were onset-onset, onset-pauser, and pauser-pauser. Our overall distribution of temporal discharge patterns is compared in Table 1 with the distribution seen by (Le Beau et al., 1996). The relative orders of frequency for each discharge pattern are similar, though we encounter many

more pauser and onset units. This may arise from species differences – cats as opposed to guinea pigs, differences in regions sampled since we focused on low frequency units, or differences in the anesthesia used.

As we have mentioned, the matrix of discharge pattern pairings shows no significant deviation ($p=0.061$) from the null hypothesis that the different discharge patterns are randomly distributed. The temporal patterns we see may arise from either a reflection of the temporal patterns of the incoming axons, or they may reflect processing occurring at the level of the IC itself. Despite the common morphology of the disc-shaped principal cells, recent studies of slice preparations reveal the existence of multiple physiological classes defined by membrane channel properties (Peruzzi et al., 2000; Sivaramakrishnan and Oliver, 2001). The different classes based on membrane properties may give rise to the different temporal discharge patterns; in particular, the responses seen in the slice preparation may give rise to observed response features such as onset responses, pauser behavior, regular firing patterns, etc. If the different temporal discharge patterns we observe arise in the IC rather than simply reflecting different inputs, then our results would suggest that the different cell classes defined by membrane channel properties are randomly distributed within the IC. This would be in sharp contrast to the Ventral Cochlear Nucleus, where morphology and physiological response types are closely related, and different cell types are grouped together.

Interaural Time Difference Sensitivity

22% (6/27) of the recording sites contained at least one single-unit that was not beat sensitive. In fact, we had a total of 9 non-beat sensitive single-units and 20 pairs containing one beat sensitive unit and one non-beat sensitive unit. This suggests that while there are regions that predominantly contain IPD sensitive units, it is not a hard rule that all cells in a particular region must be IPD sensitive.

Figure 10 shows that mean-IPDs are not strongly correlated between neighboring neurons; the correlation observed (ρ=0.585) is not significant. The lack of correlation of mean-IPD between neighboring neurons is consistent with the lack of any discernable correlation in the characteristic delays seen in our small population of pairs for which we are able to compute CDs. The lack of any statistically significant correlation in CD may partly reflect the small sample size; however, we observe neighboring pairs with CDs separated by as much as 3.5ms.

While the IPD and CD relationships show no relationship between neighboring pairs, we do observe a significant relationship in Characteristic Phase (Figure 11B). One interpretation of the CP is that it reflects the mechanism of binaural processing. In particular, CPs of 0 or 1 reflect peak-type ITD sensitivity which is believed to arise through coincidence detectors which receive excitatory input from both ears as in the Medial Superior Olive (MSO); conversely, CPs of 0.5 reflect trough-type ITD sensitivity which likely arises from neurons who receive an excitatory input from one ear and an inhibitory input from the other ear as in the Lateral Superior Olive (LSO). Neurons which have CPs between 0 and 0.5 may receive convergent inputs from both MSO and LSO that

influence the cell differently at different frequencies (Yin and Kuwada, 1983; McAlpine et al., 1998). It is significant that neighboring neurons show similar characteristic phase, as this may indicate similar or common inputs among neighboring ITD-sensitive neurons.

The MSO and the LSO are the first places where binaural processing occurs in the ascending auditory pathway, and they reflect the processing that gives rise respectively to the peak-like and trough-like ITD sensitivity respectively. The MSO receives excitatory inputs from both ears end is believed to employ coincidence detection as we expect for units with CP of 0 or 1; the LSO, on the other hand receives excitatory input from the ipsilateral ear and inhibitory inputs from the contralateral ear giving rise to trough-like ITD sensitivity which corresponds to a CP of 0.5 Because both nuclei project to the ICC, the correlation in CP we observe may reflect different regions of ITD sensitivity that receive primary inputs from the LSO or MSO exclusively.

In measuring the CD and CP, we discarded units that did not have a linear phase-frequency relationship. Overall, among 19 single-units at 6 sites (24 pairs) where we measured responses to binaural beats at multiple frequencies, we discarded six units (7 pairs) because they did not pass our linearity criteria. This is consistent with previous reports that show that about half of ITD-sensitive units in the IC exhibit a non-linear IPD-frequency relationship when using a criterion level of $p < 0.005$ (Yin and Kuwada, 1983; Kuwada et al., 1987; McAlpine et al., 1998). More significantly, the units that follow a linear phase-frequency relationship do not seem to be spatially segregated from units with more complex behavior.

McApline et al. (1998) have suggested that units with complex phase-frequency relationships may result from convergence of inputs with different CDs. By using a

second tone to suppress the response of an input, they reported being able to linearize some phase-frequency responses, though there were still some units which continued to exhibit a complex phase-frequency relationship. Our results suggest that these multiple inputs do not influence all units in a specific region; we see evidence of complex phase-frequency relations alongside units with linear phase-frequency relationships.

Differences in response with spatial separation

As we have discussed previously, based on estimates of the recording distance of tetrodes (Gray et al., 1995), we may record from units in different laminae. Because units in different laminae would likely have widely different BFs, we investigated whether neighboring neuron pairs were more likely to show differences in response properties if their BFs were more different.

As seen in figure 13, which compares differences in BF against bandwidth differences, threshold differences, and IPD differences, there appears to be very little differences between response similarities between pairs with very similar BFs and those with larger differences in BF. This lack of effect of BF difference is also observed in the monotonicity of rate-level responses and PSTH types. Since there is very little correlation with most of these response properties among neighboring neurons, it is not too surprising that there is no relationship between these properties and the distance separating the units. Also, because we have so few units with large BF differences, if there are some relationships they would be hard to detect using this small sample size.

Conclusions

The most highly correlated properties of neighboring neurons were the best-frequency and pure tone threshold. Bandwidths, rate-intensity profiles, and temporal discharge patterns showed much greater differences among neighboring neurons. The former involve measurements at low stimulus levels near the neurons' characteristic frequencies; the latter requires measurements either away from the CF or at higher levels. One possible explanation for this behavior may be that neighboring neurons receive similar primary inputs tuned to the same frequency; however, at higher levels, more inputs from other frequency channels may be recruited which could introduce more variability in the observed responses.

This simple model of inputs to ICC cells seems supported by recent studies. Snyder and Sinex (2002) reported on changes in multi-unit frequency tuning in the IC in response to focal lesions of the cochlea. They hypothesized that if neurons tuned to a particular frequency in the IC only receive inputs that are similarly tuned, then lesioning these frequencies at the cochlea should destroy frequency tuning of individual neurons in that frequency region of the IC. They report that focal lesions in the cochlea affect the tuning of individual neurons across a wide region of the IC, and the effects are seen only in a change in the tuning curves around the range of frequencies affected by the cochlear lesion.

Malmierca et al. (2005) support this hypothesis with anatomical data. They look at the organization of axons from the cochlear nucleus in the IC. They observe inputs with large synaptic boutons and inputs with smaller boutons. The larger boutons are

narrowly focused suggesting that these may be the primary inputs defining the CF of the units; however, the smaller boutons which are not as well focused and span a wider range than the lamina defined by the larger boutons, may contribute off-frequency inputs to neighboring laminae.

As we have discussed above, the strong correlation in Characteristic Phase may indicate that at least at some locations in the ICC, the ITD-sensitivity of neighboring neurons arises from inputs from a common or similar source. Specifically, the correlation in characteristic phase may reflect the segregation of inputs from the MSO and LSO. In spite of this strong correlation, we see little or no common response of mean-IPD or Characteristic Delay. This is consistent with previous reports which were unable to find a map of ITD in the ICC.

We have presented here responses of neighboring neurons to simple, pure-tone stimuli. We found that the responses can become different and complicated at moderate to high sound levels and away from the CF region of neurons. Since most sounds encountered in daily tasks are not near threshold levels, neighboring neurons may respond quite differently in real world listening tasks. It remains to be seen how neighboring neurons with seemingly different response properties would respond to more complex stimuli and specific detection and processing tasks.

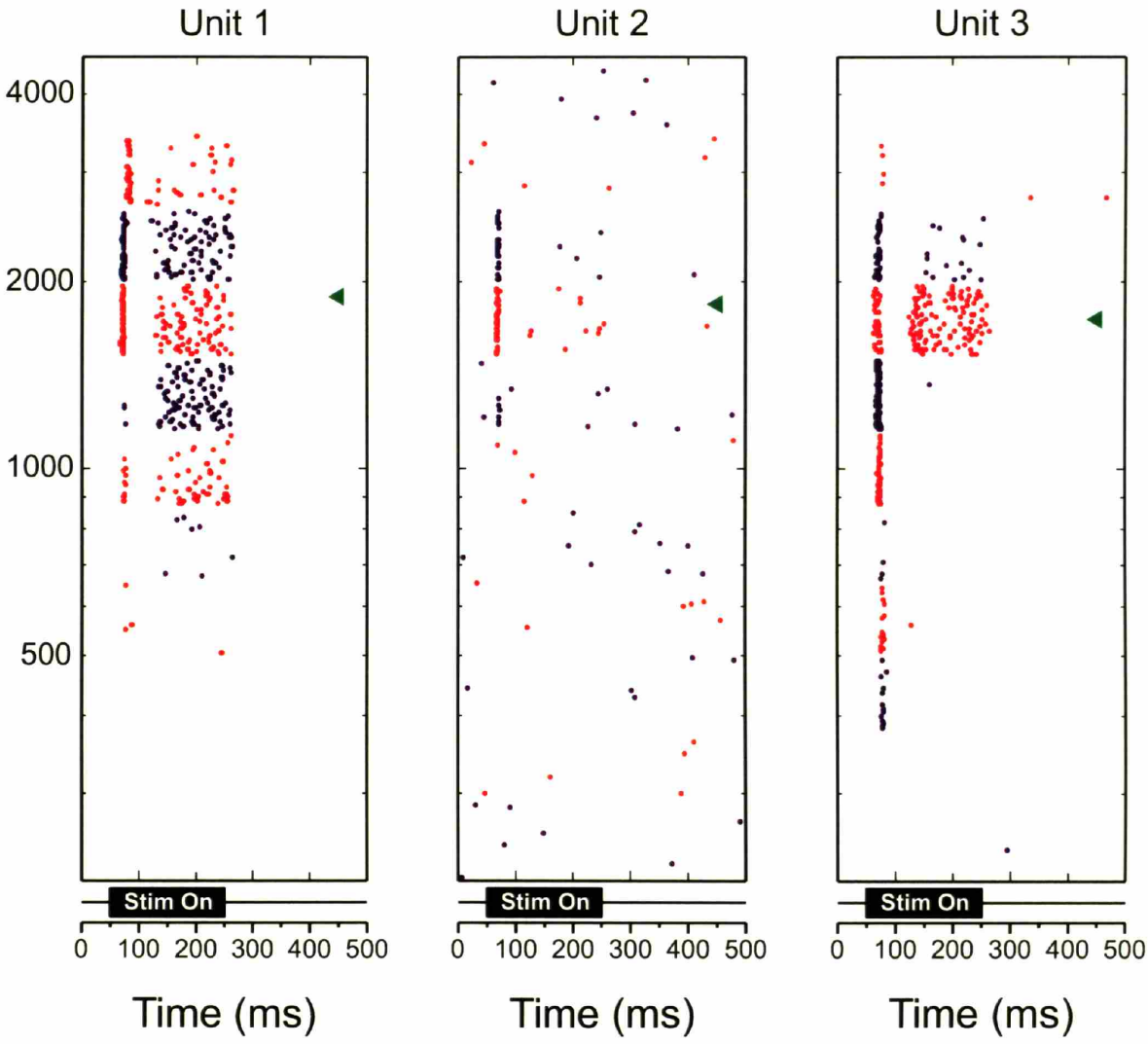

Figure 1. Dot raster responses of three simultaneously recorded single-units. Each panel shows the dot raster for each of the three units in response to a pure tone stimulus (XdB) of varying frequency. The alternating blue and red bands indicate fifty trials at a fixed frequency. The stimulus is on from 50-250ms as indicated below each raster plot. The green triangles indicate the computed Best Frequencies for each unit (1892 Hz, 1840 Hz, and 1741Hz respectively)

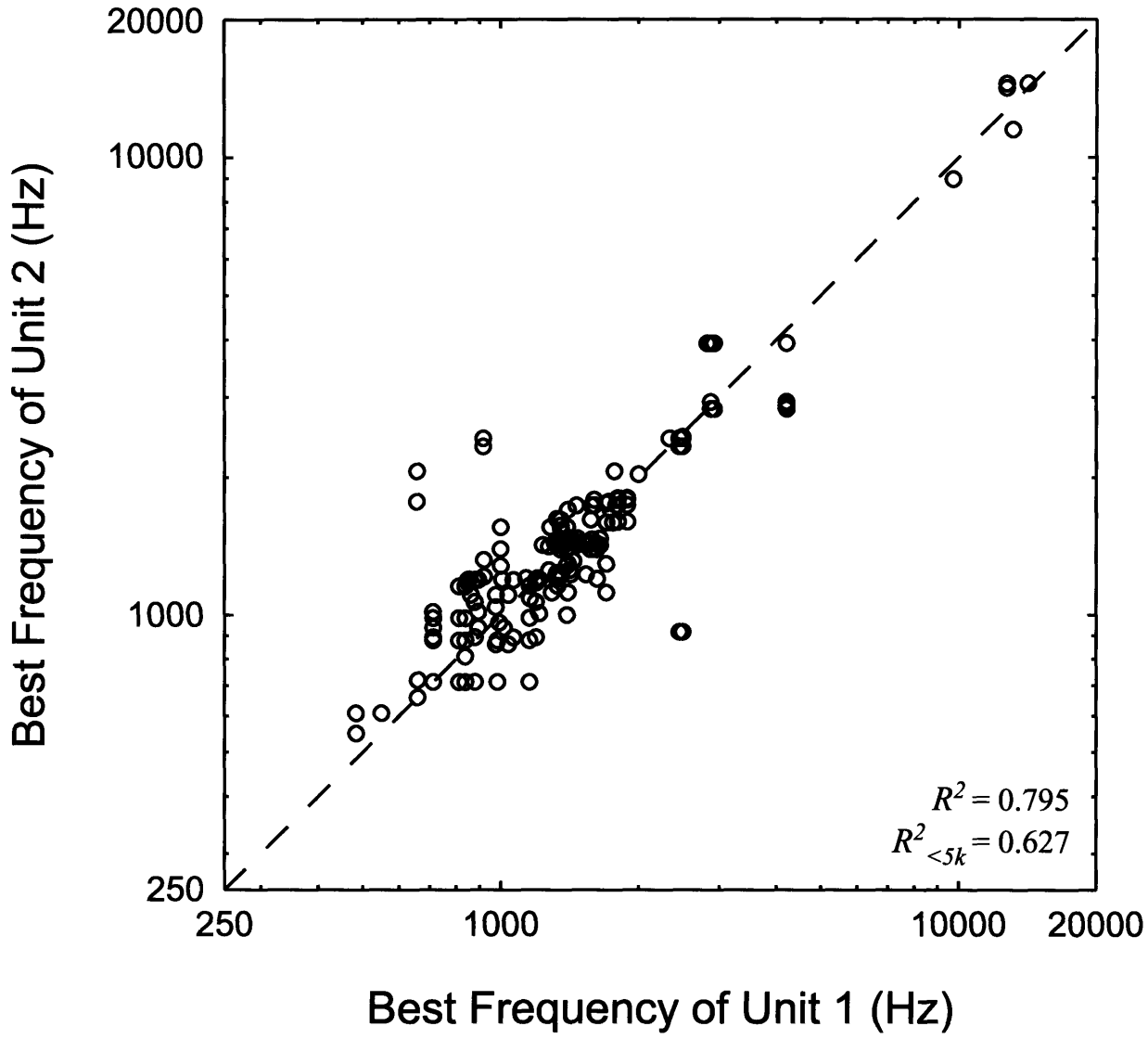

Figure 2. Each point represents the best frequency of the first unit vs. the best frequency of the second unit for every neighboring neuron pair. There is no significance to which unit is unit 1 and which is unit 2. ρ=0.89.

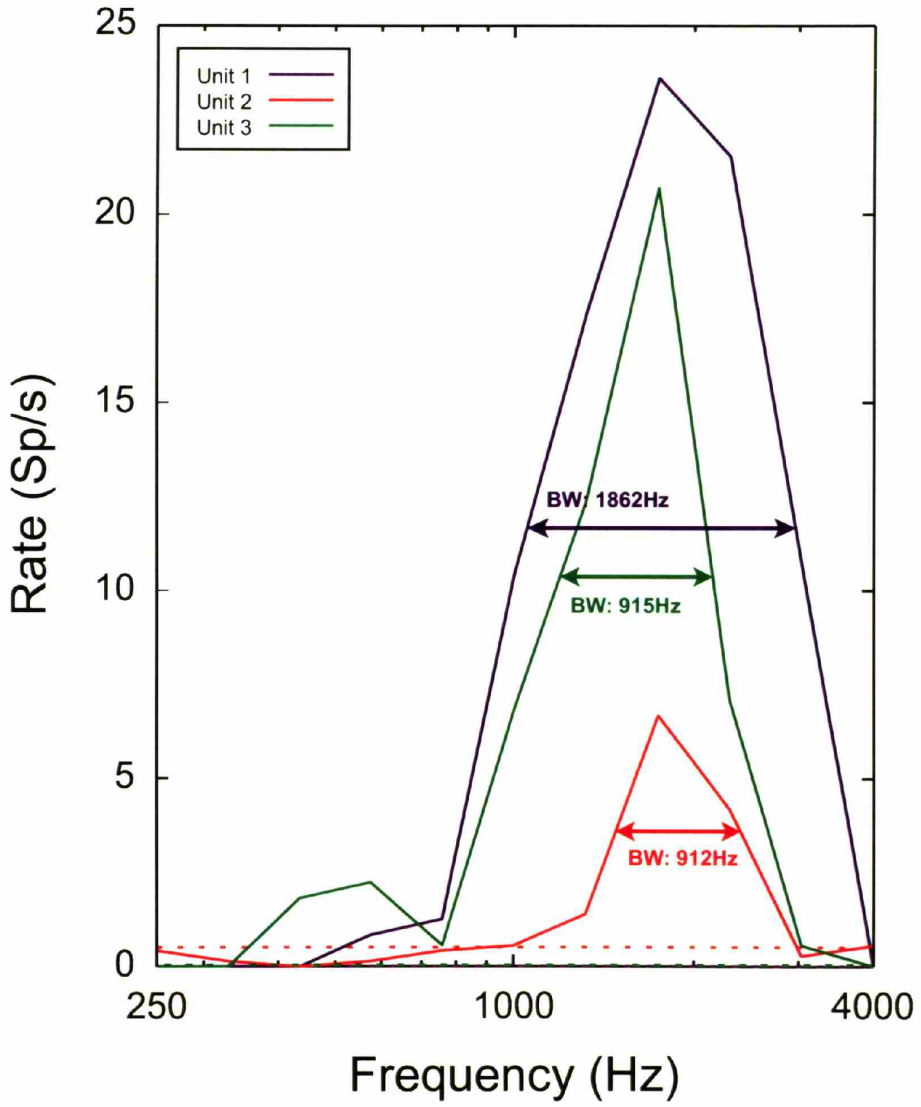

Figure 3. Rate-frequency curves for the three dot rasters from figure 1. The solid lines represent the rate during the stimulus on periods; the corresponding dashed lines represent the rate during the stimulus off periods. The horizontal lines indicate the place where the half-bandwidth is measured. The half-bandwidths are 1862 Hz, 915 Hz, and 912 Hz respectively.

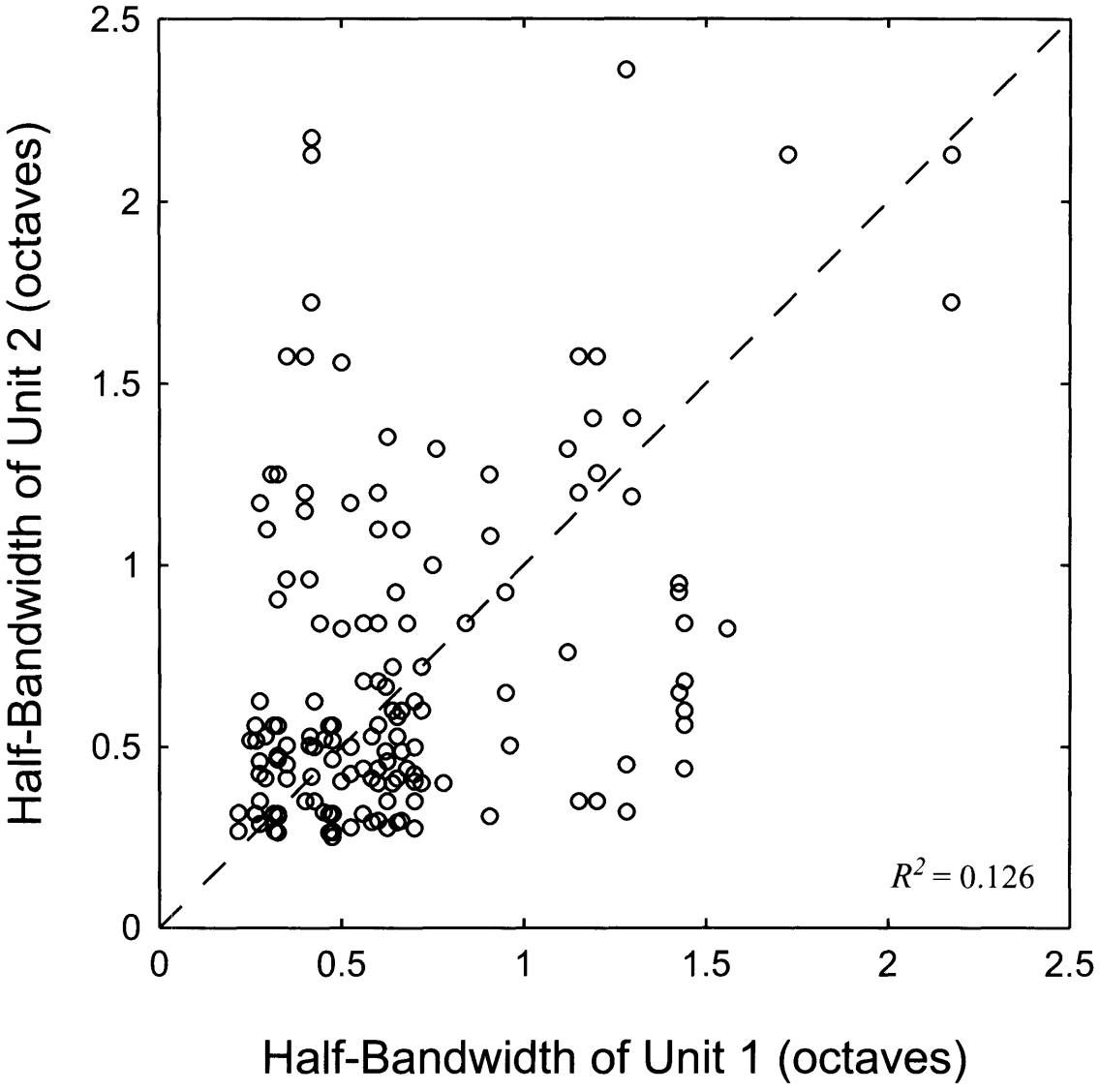

Figure 4. Comparison between half-bandwidth of neighboring neuron pairs. There is no significance to which unit is chosen as unit 1 or unit 2. ρ=0.355.

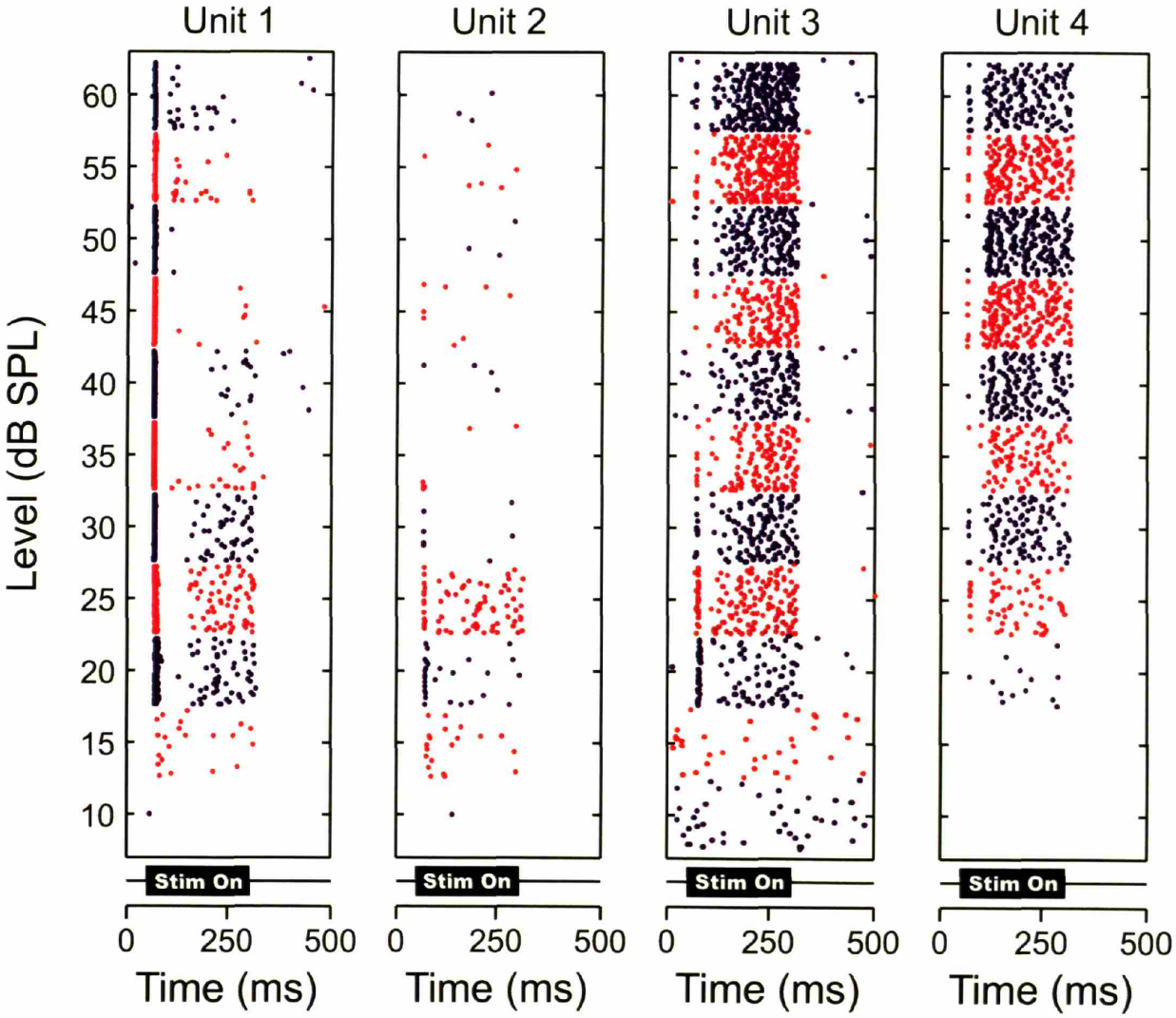

Figure 5. Dot raster responses of four simultaneously recorded single-units. Each panel shows the dot raster for each of the four units in response to a pure tone stimulus (1kHz) of varying level. The alternating blue and red bands indicate fifty trials at a fixed level. The stimulus is on from 50-300ms as indicated below each raster plot. All four units show similar thresholds. Units 1 and 2 have non-monotonic dependency.

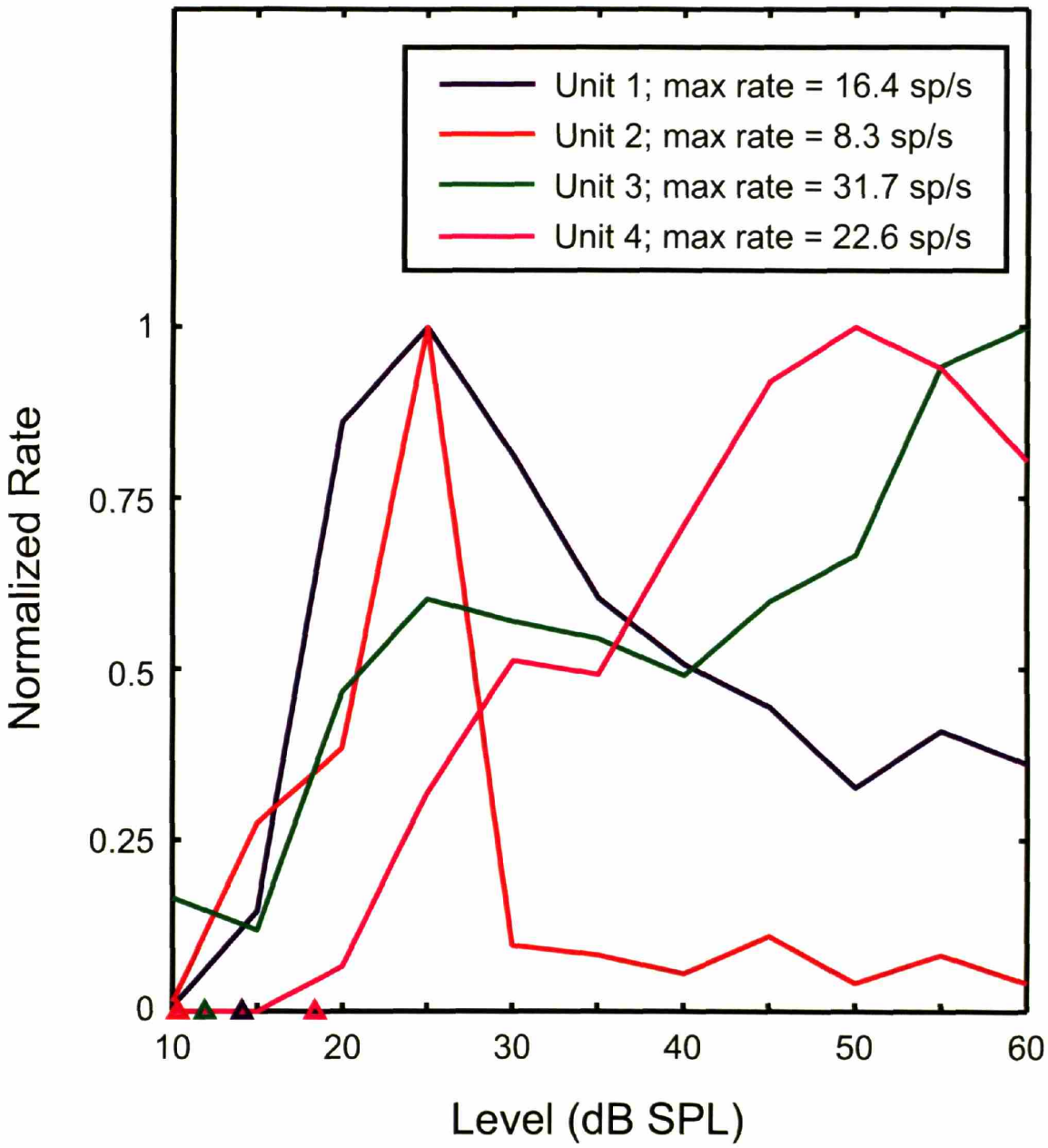

Figure 6. Rate-level curves for four simultaneously recorded neighboring neurons. All the curves have been normalized to a maxmium rate of 1. The stimulus frequency was 1000Hz. The triangles on the x-axis indicate the computed thresholds. The range of thresholds spans less than 10dB. These four units exhibit a mix of non-monotonic and monotonic rate-level dependencies.

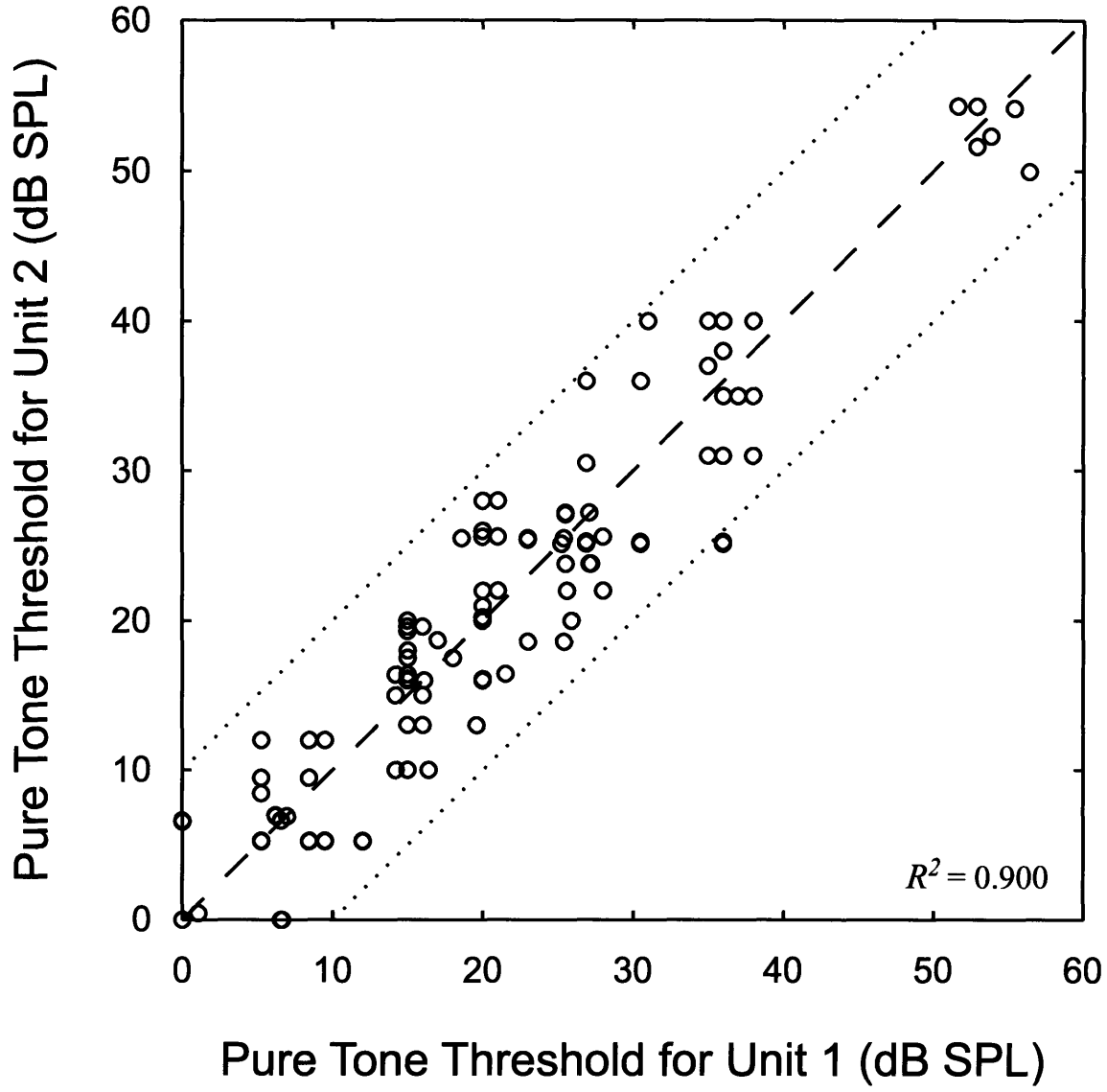

Figure 7. Comparison of pure tone thresholds at the best frequency for neighboring neuron pairs. 106/108 pairs have thresholds wthing 10dB of each other. ρ=0.949. There is not significance to which unit is unit 1 or unit 2.

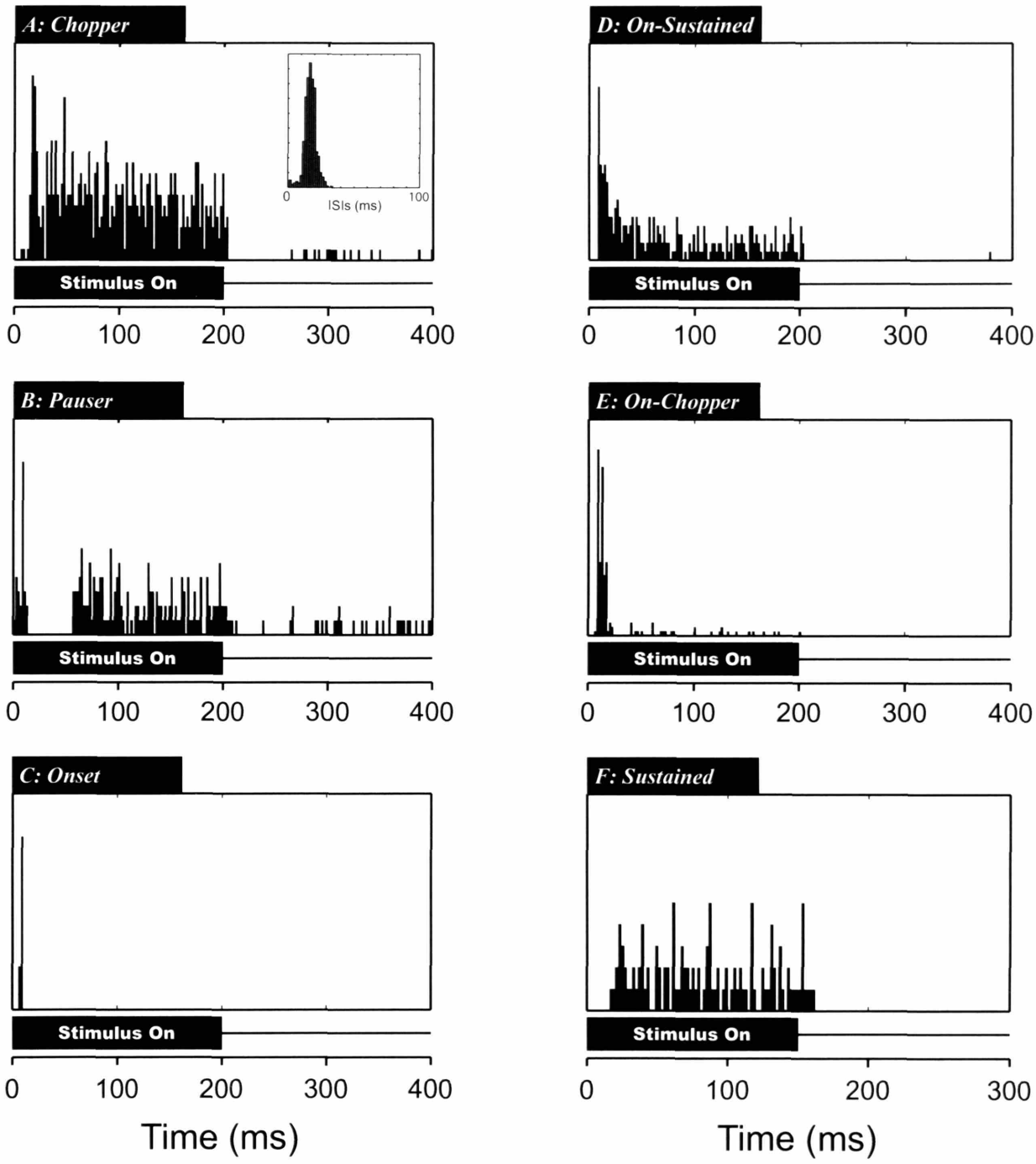

Figure 8. Examples of different PSTH types. *A)* Chopper - sustained firind with multiple peaks and/or low CV; *B*) Pauser - characterized by large onset peak followed by period of little or no activity then sustained firing; *C*) Onset - large onset peak followed by little or no activity; *D*) On-Sustained - large onset peak that settles into sustained firing; *E*) On-Chopper - large onset peak with little or no sustained activity, onset response has two or more peaks; *F*) Sustained - no significant onset peak but sustained activity throughout stimulus

	Onset	Chopper	Onset-Chopper	Pauser	Onset-Sust	Sust.	Other
Onset	24						
Chopper	5	0					
Onset-Chopper	1	1	0				
Pauser	51	10	4	31			
Onset-Sust	1	3	0	8	6		
Sust.	9	3	0	9	9	3	
Other	4	0	0	2	0	0	1

Table 2. Matrix of distribution of PSTH pairs.

PSTH Type	LeBeau et al. (1996)	Current study
Pauser	23% (16/70)	42% (55/130)
Onset	21% (15/70)	32% (41/130)
On-Sustained	20% (14/70)	8% (10/130)
Sustained	19% (13/70)	8% (11/130)
Chopper	9% (6/70)	6% (8/130)
Other	6% (4/70)	3% (4/130)
On-Chopper	3% (2/70)	1% (1/130)

Table 1 – This table shows the distribution of different single-unit temporal discharge patterns reported by Le Beau et al. (1996) compared with our results.

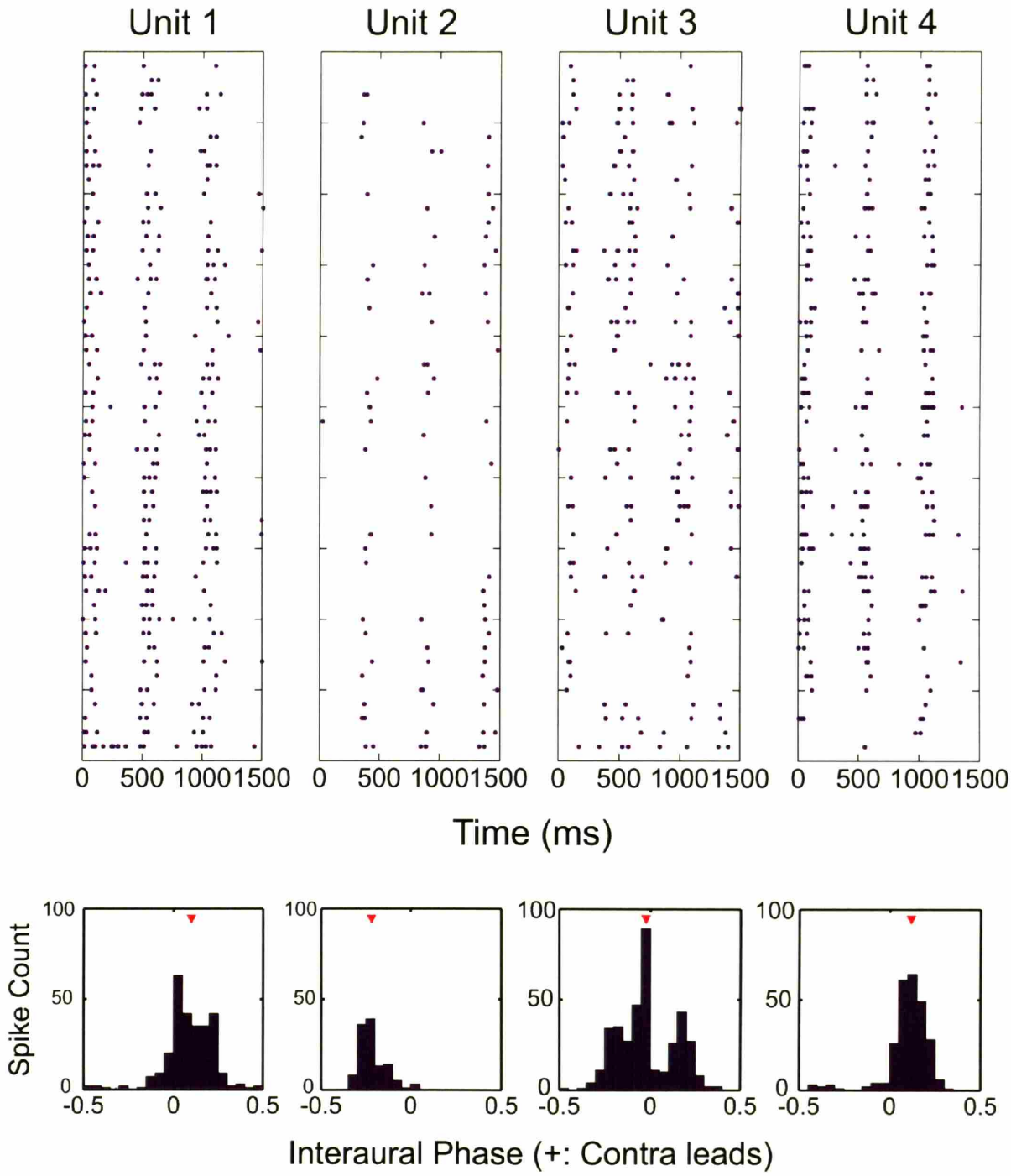

Figure 9. The top four plots show dot rasters for four simultaneously recorded neighboring neurons in response to a binaural beat stimulus (915Hz, XdB). The beat period is 500ms. The four lower plots show period histograms for each of these units computed over the beat period. The red triangles indicate the mean interaural phase.

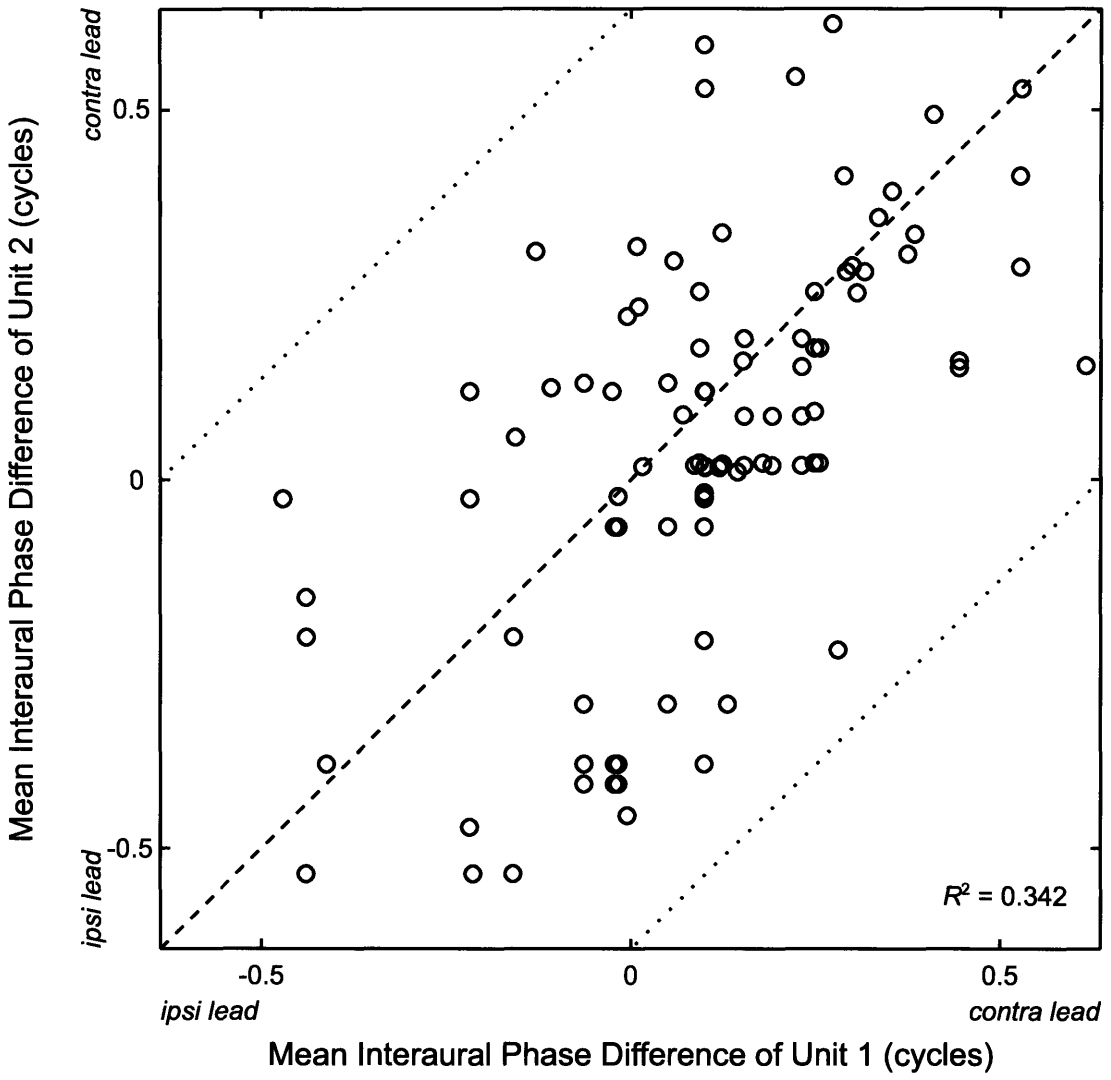

Figure 10. Comparison of mean interaural phase difference for neighboring neuron pairs. X-axis is unit 1 and y-axis is unit 2. There is no significance to which unit is chosen as unit 1 or unit 2. All IPDs measured using binaural beats near the multi-unit CF. Correlation coefficient ρ=0.585. Dashed line indicates unity line. Dotted lines indicate IPD difference of 1/2-cycle.

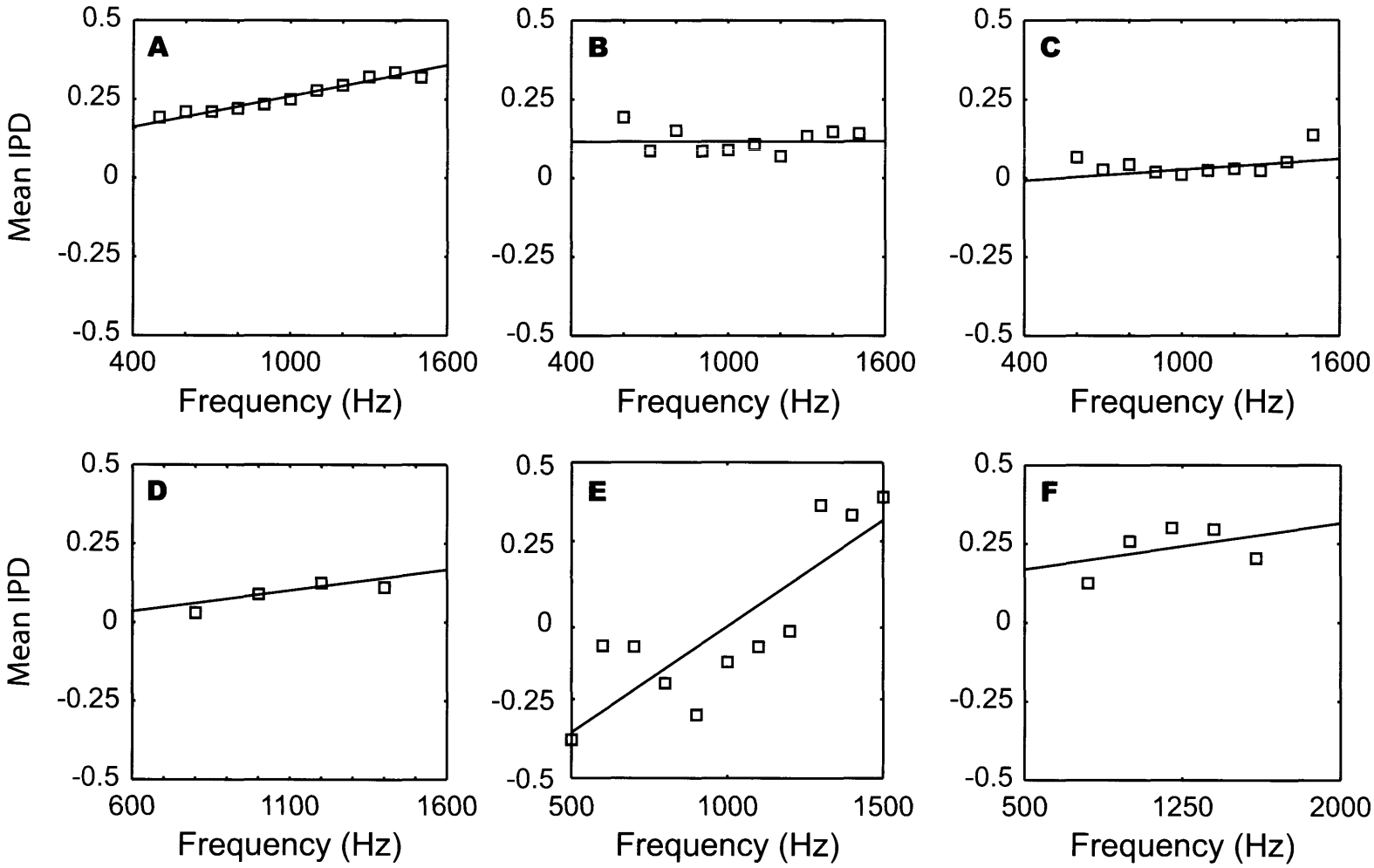

Figure 11. Weighted regression lines fit to phase-frequency data for six single-units. (A-D) These four units pass our linearity test. In general, the lines are good fits, though in a couple of cases, there is some definite variance away from the fit line. (E-F) These two units do not pass our linearity test and are not included in our discussion of CD and CP

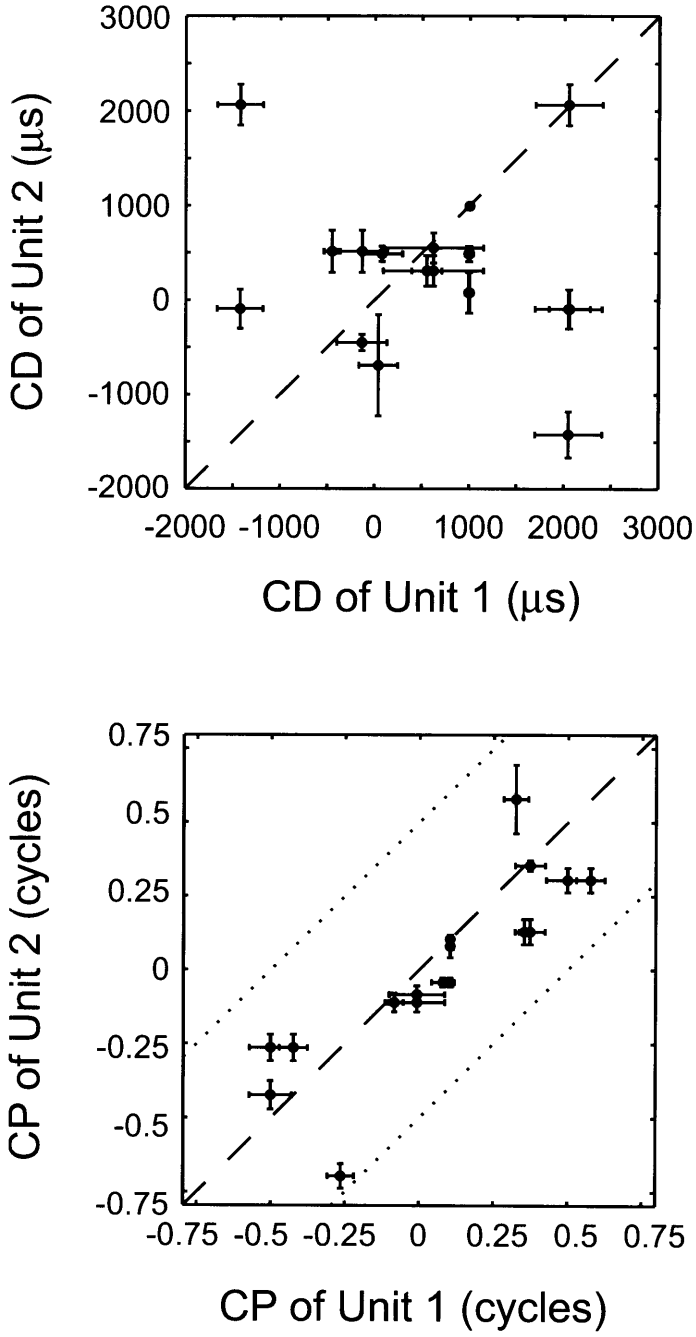

Figure 12 - Comparisons of Characteristic Delay and Characteristic Phase between neighboring neurons. Characteristic Delay scatter plot shows no strong relationship (ρ=-0.19); however, the Characteristic Phases are highly correlated (ρ=0.84, $p < 0.05$).

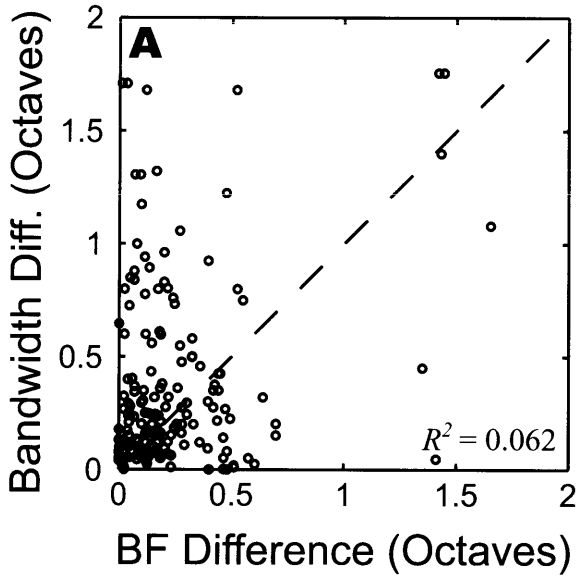

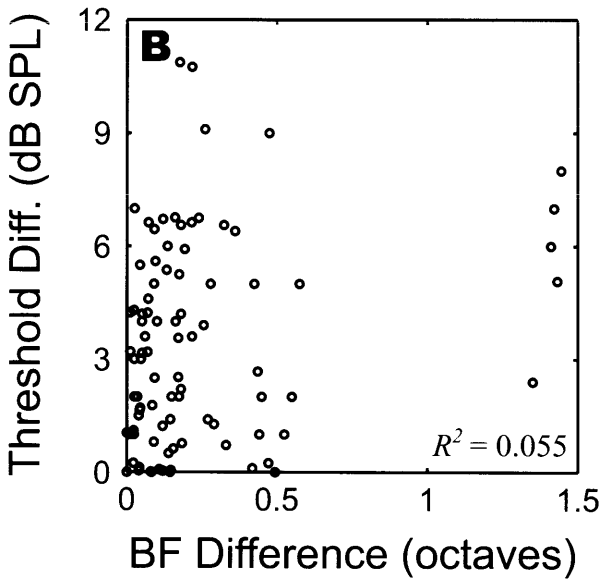

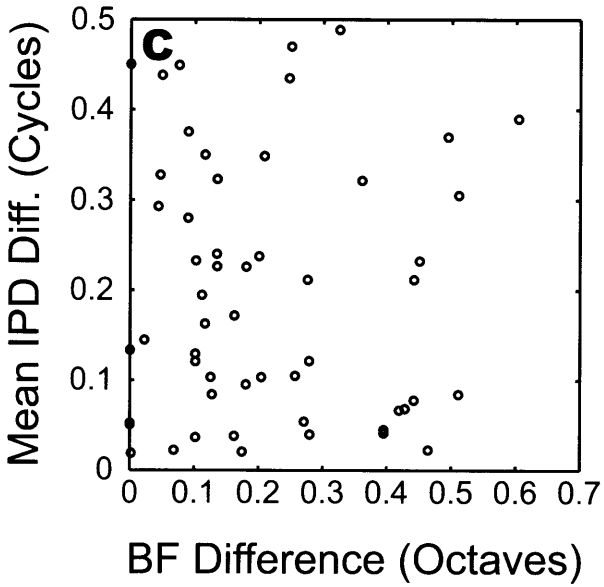

Figure 13. Comparison of BF differences between pairs with differences in other response properties. **A**) Comparison with bandwidth differences. Shows no relationship. Largest BF differences still show large scatter in bandwidth differences. **B**) Comparison with threshold differences. Shows no relationship. Again, largest BF differences still show scatter in threshold differences. **C**) Comparison with mean-IPD differences. No observable relationship.

Chapter 3: Comparing Single- and Multi-Unit Responses in the Inferior Colliculus

Introduction

In recent years, increases in computing power, greater data storage and handling capacity, and improvements in micro-electrode technology have allowed single-unit electrophysiologists to routinely record simultaneous responses of many individual neurons (Schmidt, 1999). Though these technologies have been largely developed and used by researchers working in visual (Maynard et al., 1997), motor (Riehle et al., 1997; Maynard et al., 1999; Chapin, 2004), and somatosensory (Nicolelis et al., 1995) cortices and the hippocampus (Wilson and McNaughton, 1993), auditory researchers are also adopting these techniques (Blake et al., 2002; Snyder and Sinex, 2002). As we have seen in chapters 1 and 2, one of these techniques, the tetrode, can be used effectively in the auditory brainstem to expand our understanding of local organization of the physiological responses.

Of the methods currently available for simultaneous multi-unit recording, many rely on large multi-electrode arrays with recording sites fixed relative to each other (Moxon, 1999; Schmidt, 1999). If the recording sites exhibit impedances similar to those used in single electrode, single-unit recordings, a given site needs to be very close to the cell body in order to record the extracellular action potentials (Robinson, 1968). Because these arrays typically do not allow independent positioning of individual electrodes,

positioning all or even a few of the electrodes close enough for clear, isolated, single-unit recordings is virtually impossible.

Because of these limitations, the site impedances used are generally lower than those used for single-unit recording. The lowered impedance serves to effectively increase the spatial 'range' from which the site will capture action potential activity (Robinson, 1968). While this increases the chances that many of the electrodes will record action potentials, it also increases the likelihood that these recordings will contain multi-unit data; that is, the recorded action potentials may originate from multiple neural sources.

Because of the likelihood of obtaining multi-unit recordings, many labs have turned to spike sorting algorithms to identify individual neurons' contribution to the observed multi-unit records (Oghalai et al., 1994; Ohberg et al., 1996; Lewicki, 1998; Moxon, 1999; Shoham et al., 2003). As we have shown in chapter 1, using microwire electrodes with low impedance, the chance of error in single channel spike sorting can be quite high, meaning that even after implementing spike sorting algorithms, the records obtained are likely to arise from multiple neurons.

For some studies of ensemble responses, the coarse observation of multi-unit responses provides enough information. For example, implementing brain-machine interfaces in the motor cortex have proven quite successful in providing an adequate view of the ensemble response to implement fine motor control of artificial devices (Chapin, 2004; Shoham et al., 2005). However, in many studies, multi-unit responses cannot answer the questions being addressed. For example, our work previously reported in chapter two has exploited some of these new technologies to characterize local response

characteristics. These single-unit characterizations may not be useful if the data used were from multi-unit records.

To understand the usefulness of multi-unit recordings in interpreting both single-unit responses as well as ensemble responses, here we directly investigate the relationship between single-unit recordings and multi-unit recordings. Since these relationships are partly dictated by local anatomy and the organization of physiological responses, it is necessary to address this question on a site specific basis.

In this study, we examine the relationship between multi-unit recordings and single-unit responses in the auditory midbrain. As we have seen in chapter 2, neighboring neurons in the inferior colliculus show a complex pattern of differences and similarities in their responses to pure tones. We have hypothesized that some of these differences may arise through variability in synaptic inputs while others may arise from differences in the membrane channel properties. Here, we investigate how these differences may affect the multi-unit response properties which presumably reflect a summation of the activity from many neurons near the recording site.

We use tetrodes to record the responses to pure tones in the central nucleus of the inferior colliculus (ICC). We then compare the well-isolated single-unit response obtained from using spike sorting on our tetrode recordings with the multi-unit data recorded from single channels of the tetrode.

Methods

Animal Preparation

The data presented here were collected from the inferior colliculi of fifteen anesthetized adult cats. The surgical methods were previously described in chapter 1. To assess the general health of the auditory neural pathway, we monitored the click-evoked Auditory Brainstem Response (ABR) as described in chapter 1.

Data Acquisition

All recordings from the IC were made with tetrodes as described in chapter 1. As we mentioned in chapter 2, because we were interested in characterizing the sensitivity to interaural timing differences, we typically positioned our electrode in low-frequency regions of the ICC.

Stimuli

Acoustic stimuli used for quantitative analyses consisted of pure tones presented either binaurally or monaurally. The stimuli were digitally generated and delivered via closed acoustic assemblies as described in chapter 1. The stimuli used for different response characterizations were described in detail in chapter 2.

Experimental procedure

The experimental procedure used was identical to the procedure described in chapter 2.

Data Analysis

SINGLE-UNIT RESPONSES

The single-unit responses presented in this study arise from the tetrode recordings and spike sorting already described in chapter 2. Briefly, from a given recording site, we record the raw waveforms from all four tetrode channels in response to our different stimuli. Off-line, the signals are bandpass filtered (300-3000Hz) and 60-Hz noise is removed from the raw data. We apply the spike detection algorithm described in chapter 1 and identify the times of all detected neural events. For every neural event time, a 0.75 ms sample of the waveforms from each channel is collected. Using the collected waveforms from each channel, we sort the data based on the Principal Component weights for each waveform. Events generated from an individual neuron cluster together in our Principal Component space, and are separated to define the spike times for each single-unit in our recording.

MULTI-UNIT RESPONSES

To measure multi-unit responses, we implemented an algorithm similar to that used by (Harris et al., 1997). Briefly, beginning with the raw waveform from a single tetrode channel, we first bandpass filter the signal (300-3000Hz) and then high pass filter the signal with cutoff at 1kHz. The high pass filtered signal feeds into a Schmitt trigger and the output of the Schmitt trigger defines the multi-unit event times. The level of the Schmitt trigger is selected to give an output spike rate of approximately 100 sp/s when no stimulus is present.

We chose this particular measure of multi-unit activity because it is not easily biased by the single-units in the recording. Measures such as the rms of the waveform can be highly skewed by the presence of large action potentials from one unit. Also, the high spontaneous rate criterion for determining the amplitude threshold leads to a very high multi-unit rate which is not very susceptible to being influenced by any single-unit in the recording. We need to keep in mind thought that with the low thresholds we use, our multi-unit responses could reflect post-synaptic, sub-threshold activity as well as action potential activity.

Because we are applying the multi-unit measures to our tetrode recordings, at each recording site, we measure multi-unit responses on each of the four recording channels. For the various characterizations we compare between single and multi-unit recordings, we measure the characteristic for all four multi-unit responses and average the results.

The response characterizations for best frequency, bandwidth, threshold, rate-level monotonicity, and interaural time difference sensitivity were described previously in chapter 2. To obtain the multi-unit response characteristics, we computed the relevant parameter for the multi-unit responses from each of the four tetrode channels and then used the mean value as our multi-unit characteristic. Because we empirically observed that the multi-unit response is nearly identical across all four channels, taking the mean across all four channels is similar to choosing any one of the four channels individually.

Results

The data reported here were collected from 77 recording sites in 15 different animals. Because we were interested in units that exhibited binaural sensitivity to interaural phase disparities, the majority of the sites were located in the low-frequency regions of the central nucleus of the inferior colliculus.

Frequency Tuning

Figure 1 shows rate-frequency curves for a single-unit and the four multi-unit responses from each of the four tetrode channels at one site. The top panel, panel A, shows the single-unit response; panel B shows the four multi-unit curves. The solid lines represent the spike rates measured over the stimulus duration while the dashed lines

represent the spontaneous rate. Within a small scaling factor, the multi-unit rate-frequency curves from each of the four tetrode channels. Additionally, the best-frequencies (BFs) for the four multi-unit curves are similar to the BF for the single-unit. The tuning widths are similar for the multi-units and are broader than for the single-unit.

The triangles above the curves indicate the measured BFs for each curve. To characterize the multi-unit BF, we average the four measured BFs from the four multi-unit rate-frequency curves. For this particular recording site, the single-unit has a BF of 920Hz. By comparison, the multi-unit curves have BFs of 847, 847, 758, and 801 Hz, which gives an average BF across the four channels of 813Hz. Horizontal lines indicate the location at which the half-bandwidths are measured. For the single-unit, the half-bandwidth is 0.92 octaves. The multi-unit half-bandwidth measure, obtained by averaging the half-bandwidths of each of the four multi-unit curves is 1.69 octaves confirming a broader tuning for the multi-unit rate-frequency curves.

Of the 77 recording sites in this study, we have measured rate-frequency curves at 67 sites. Of these 67 recordings, we ignore 13 measurements because they were measured at levels more then 15dB above the multi-unit threshold. Therefore, we present frequency tuning information for 54 recording sites. For each of these sites, we measure the BFs and half-bandwidths for both the single-unit and multi-unit responses and compare the responses.

Figures 2 and 3 compare the BFs and half-bandwidths between the multi- and single-unit responses measured levels within 15dB of threshold. Figure 2 shows a scatter plot of the best isolated single-unit BFs plotted against the multi-unit BFs from each recording site. There is a strong correlation between the BF of single-units and multi-unit

recordings. Quantitatively, 48% (26/54) of the single-unit and multi-unit BFs lie within 0.1 octave of each other, and 74% (40/54) of the single-unit and multi-unit BFs lie within ¼-octave of each other. Only two sites exhibited a difference in BF greater than ½-octave. The median difference in BF was 0.10 octaves and the maximum BF difference was 1.06 octaves. The correlation coefficient between the single-unit and multi-unit BFs is 0.971[1]. If we compute the correlation without the six sites with BFs above 3kHz, we obtain a correlation coefficient of 0.914 which corresponds to an $R^2 = 0.835$.

Figure 3 shows the corresponding scatter plot for the half-bandwidths of the multi-unit responses plotted against the best-isolated single-unit responses. Compared with the best-frequency relationship seen in figure 2, this plot shows greater scatter indicating that the tuning width of the single-units are not as well reflected in the multi-unit responses as the best-frequency. Most of the data points (87%; 46/53) lie above the identity line indicating that, in general, the bandwidths measured from the multi-unit responses are typically larger than those of the single-units. Quantitatively, we observe differences in the half-bandwidth greater than 1.5 octaves; the median bandwidth difference observed is 0.43 octaves. Though there is greater scatter from the identity line than observed for the best-frequency measures, there is a definite relationship between the single-unit bandwidths and the bandwidth observed from the multi-unit responses (ρ=0.647, $p < 0.0001$).

The previous results suggest that multi-unit rate responses approximately reflect the single-unit frequency tuning. However, these results only consider responses measured within 15dB SPL of the pure tone threshold at CF. Our previous results from

[1] The correlation is computed using the logarithm of the best-frequencies to reflect variation seen in the log-log plot of single-unit BF vs. multi-unit BF.

chapter 2 as well as results from Snyder and Sinex (2002) suggest that ICC neurons may receive inputs from a wide range of frequencies at higher levels. Therefore, higher levels may introduce greater complexity to the relationship between single-unit and multi-unit responses. We repeated the analysis above for levels about 20-30dB SPL above the levels used in Figures 2 and 3.

We have 32 recording sites from which we measured rate-frequency curves at multiple levels. These results comparing BF and half-bandwidth are displayed in figure 4. Panel A of figure 4 shows the comparison of BFs between the single- and multi-unit responses. Compared against the near threshold measurements shown in figure 2, we see a greater deviation away from the identity line at these higher levels, though the multi-unit BFs still accurately predict the single-unit BFs at many recording sites particularly for higher BFs. However, only 56% (18/32) of the sites show single-unit and multi-unit BFs within ¼-octave of each other as compared with 74% at lower levels. The median BF difference is 0.17 octaves with the largest observed difference at almost 1.2 octaves. The correlation coefficient between the single-unit and multi-unit BFs at these higher levels is 0.85. If we ignore the site with BF around 14kHz, the correlation coefficient drops to 0.671 compared with a correlation coefficient of 0.914 at lower levels. This difference is not significant at the 0.005 significance level ($p=0.012$, *t*-test for correlation).

Panel B of figure 4 shows a scatter plot comparing the single-unit and multi-unit half-bandwidths at higher levels. Compared with the same measure at low levels shown in figure 3, we do not see a large difference in the overall relationship between single- and multi-unit responses. Clearly, the bandwidths measured from both single and multi-unit responses at the higher levels are generally larger than those seen at lower levels. In

most cases, the multi-unit responses still show larger bandwidths than the single-unit responses. The largest difference in bandwidth remains slightly larger than 1.5 octaves and the median bandwidth difference is now around ½-octave. The correlation coefficient between the single-unit and multi-unit bandwidth is 0.657. This is similar to the correlation coefficient near threshold.

Rate-Level Functions

At 59 of the 77 recording sites, we measured rate-level functions. At fifteen of the sites, the multi-unit thresholds were lower than the lowest measured intensity. For the remaining 44 sites, we investigated the relationship between the threshold of the multi-unit responses and the threshold of the best isolated single-unit at each recording site.

Figure 5 shows a scatter plot of multi-unit thresholds vs. single-unit thresholds. This plot reveals consistently higher thresholds for single-units; only 3 of the 44 sites had single-unit thresholds lower than the multi-unit thresholds. Of these three sites, the greatest threshold difference was less than 2dB. Overall, the correlation coefficient was 0.915 suggesting that the threshold of the multi-unit response reflects quite closely the threshold of the single-units.

The red dashed line in figure 5 shows a regression line fit to the data points. The regression line has slope, $m = 0.96 \pm 0.13$, and intercept, $b = 7.04 \pm 3.00$ (limits are 95% confidence intervals). The slope is very close to 1 suggesting that in general, the multi-unit threshold directly reflects the single-unit threshold with a slight offset. That offset is described by the intercept and appears to be approximately 5dB.

We also looked at the shape of the rate-intensity curves at 49 recording sites. In particular, we looked at monotonicity of the rate-intensity curves. Looking only at the best-isolated single-unit at each site, 65% (32/49) show a monotonic response whereas the remaining 35% (17/49) are non-monotonic. At every recording site, the multi-unit rate-intensity curves are monotonic; however, some of the multi-unit rate-intensity curves saturate while other do not. Applying the criteria described in the Methods section, we count the combinations of monotonic or non-monotonic single-unit responses compared with whether the multi-unit responses saturate. Table 1 shows the distribution of combinations across all 49 sites.

The results in table 1 indicate that where single-unit rate-intensity curves are monotonic, the multi-unit rate-intensity curves are less likely to saturate; whereas when the best isolated single-unit exhibits a non-monotonic rate-intensity curve, the multi-unit rate-intensity curve is more likely to saturate. Applying a standard χ^2 test, we see that the observed correlation is statistically significant ($p < 0.005$).

	Multi-Unit Saturated	Multi-Unit Non-saturated
Single-Unit Monotonic	10	22
Single-Unit Non-monotonic	14	3

Table 1 – Combinations of monotonicity of single-unit rate-intensity curves and saturation of multi-unit rate-intensity curves. The contingency table reveals significant correlation between single-unit monotonicity and whether multi-unit rate-intensity curves saturate ($p<0.005$)

Interaural Phase Sensitivity

We also investigated the interaural phase sensitivity in multi-unit responses. This provides an opportunity to investigate how single-unit representations are related to multi-unit representations for a response variable that does not have a well defined map in the ICC. While the tonotopic map is well described, no obvious map of interaural phase sensitivity has been reported. If small patches of neurons with similar best-ITDs exist, we might expect that common best-ITD to be reflected in the multi-unit response; however, in chapter 2, we have shown that neighboring neuron pairs can exhibit very different ITD tuning in response to pure tones. Therefore, it is unclear whether a multi-unit response would show clear and well defined IPD tuning.

To investigate the IPD tuning, we used binaural beat stimuli. (Yin and Kuwada, 1983) demonstrated that mean IPDs computed from binaural beat responses are interchangeable with mean IPDs computed from rate-ITD response curves. Because we can measure responses to binaural beats much faster than presentating multiple stimuli with varying interaural time delays, the data presented here are all responses to binaural beat stimuli.

We measured the single- and multi-unit responses at 31 recording sites to binaural beat stimuli (2-Hz period) at frequencies near the CF of the local region. Figure 6 shows period histograms of the response to binaural beats computed over the beat period for both single- (top row) and multi-unit (bottom row) responses for three different sites (Single-Unit BFs: 892Hz, 1403Hz, and 1210Hz). First note that all the histograms show preference for a preferred range of interaural phases. In panels A/B and panels E/F, this

range is similar between the single and multi unit responses; at the site represented by panels C/D, both units clearly prefer contralateral leading phase; however, the peak IPD is different between the single- and multi-unit responses.

Computing the vector average and obtaining a mean-IPD for each response in figure 6, we find that the single-units in panels A, C, and E have mean-IPDs of -0.045, 0.158, and 0.135 cycles respectively; the corresponding multi-unit responses from panels B, D, and F have mean-IPDs of -0.013, 0.393, and 0.153 respectively.

We plot the multi-unit measure against the single-unit measure in figure 7 for our 31 sites. For both single- and multi-unit responses, the mean-IPDs were almost entirely positive (contra lead); only six single-unit responses and one multi-unit response had negative mean-IPD. The one multi-unit response with a negative mean-IPD did not correspond to any of the six sites where we measured a negative mean-IPD from the single-unit response. Qualitatively, there appears to be a loose correlation between the single- and multi-unit IPD sensitivities. Quantitatively, we observe single-unit mean-IPDs spanning a range of 0.915 cycles. In contrast, the largest difference between single- and multi-unit measures of mean-IPD is 0.5 cycels while the median observed difference is 0.12 cycles. The correlation coefficient between the single-unit and multi-unit mean-IPDs is 0.681. From sampling 100,000 data sets of 31 randomly drawn pairs of phases, we estimate the 95% confidence interval for IPD as [0.46,0.72] which contains the correlation coefficient ρ=0.681.

Typically the mean-IPDs computed from the multi-unit responses are closer to zero delay than those computed from the single-unit responses; that is, most of the points in figure 7 lie above the identity line. This difference may result from significant multi-

unit response during the negative phase response of the binaural beat stimulus. This activity would pull the mean-IPD for a unit with a positive mean-IPD closer to zero. For example, the main lobes of the multi-unit and single-unit period histograms shown in figure 6 are quite similar in shape and position; however, the spike activity during the negative phase of the beat stimulus results in a mean-IPD for the multi-unit response that is lower than the single-unit mean-IPD by 0.05 cycles.

In some cases, the extra spike activity during the negative phases is not enough to explain the differences between the single-unit and multi-unit IPD sensitivity. Figure 8 gives two examples where there seems to be a real difference in the mean-IPDs that does not arise from our analysis methods. For the first site, panels A and B show the single-unit and multi-unit responses respectively. This indicates the most striking example where the single-unit mean-IPD is shifted by almost exactly 0.5 cycles relative to the multi-unit mean-IPD. Panels C and D again show the single- and multi-unit responses respectively for a less obvious case. Here the mean-IPDs differ by only 0.09 cycles, however, looking at the period histograms, the peak in IPD sensitivity is defined more clearly in the single-unit case and the peaks of the two histograms do not lineup well.

These examples and the summary plot of figure 7 suggest that, while in general, multi-unit responses provide a reasonable estimate of single-unit IPD sensitivity (accounts for 46% of the variance), there are clear examples where multi-unit responses exhibit well defined beat sensitivity that differs strongly from the response of at least one single-unit in the vicinity of the recording site.

At 11 of the 31 sites where we recorded binaural beat sensitive responses, we measured binaural beats at multiple frequencies. We considered the phase-frequency

relationship and investigated whether the responses showed a linear relationship between mean-IPD and frequency indicated a characteristic delay mechanism involved in generating the IPD sensitivity. To determine linearity, we followed the procedure outline in (Yin and Kuwada, 1983). Of the 11 sites, five showed a non-linear phase-frequency relationship for both the single-unit and multi-unit responses; one site exhibited a linear phase-frequency relationship for the multi-unit response but the single-unit response did not satisfy our criterion for linearity; the remaining five sites had linear single-unit responses with non-linear multi-unit responses.

Discussion

We were interested in investigating the relationship between single-unit and multi-unit measures in the auditory midbrain. This question has increasing implications as multi-electrode arrays replace traditional single-electrode, single-unit electrophysiology. These newer devices rely on fixed spaced arrays and frequently encounter multi-unit data on many of the recording sites. To adequately interpret these results, we need to understand the relationship between single-unit responses which contribute to the multi-unit response and the more global multi-unit measures.

We looked at three basic response characteristics of ICC principal neurons: frequency tuning, rate-intensity profiles, and IPD sensitivity. Frequency tuning and rate-intensity profiles have been used widely throughout the auditory system to characterize single-unit responses. These characterizations are useful because they define some of the most basic properties of the channels through which acoustic information is transmitted.

IPD sensitivity is a well studied property of ICC neurons, but there are no reports of clear maps of ITD tuning in the ICC. Because there is little evidence correlating ITD sensitivity with anatomical arrangements, we wanted to investigate how the multi-unit and single-unit responses may be related.

Frequency tuning

Because the central nucleus of the IC is tonotopically organized, we expect the multi-unit response to capture well the best-frequency characteristic of the single-unit responses. However, whether the specific shape of the tuning as reflected by the bandwidth will be captured by the multi-unit response is less obvious. Also, at moderate to high sound levels, as more inputs tuned to frequencies far from CF may be recruited we may expect more heterogeneity in the responses locally, and this may create a great disparity between single-unit and multi-unit responses.

We have seen that the multi-unit response captures the BF of the single-unit extremely well. Even when we measured the BF at higher stimulus levels, we see clear evidence of correlation between the BF of the multi-unit responses and the BF of the single-unit responses. However, the overall correlation did drop to ρ=0.671 from ρ=0.914. This may suggest that shifts in single-unit BF with SPL do not parallel the shift in the multi-unit response. Because many neurons contribute to the multi-unit response, the multi-unit response may not be sensitive to what may be small variations in the response of a single neuron.

We also considered the half-bandwidth as a measure of the width of the tuning and an indication of whether the multi-unit responses also predict the shape of the tuning. It is clear from figures 3 and 5 that, in general, the multi-unit responses do not capture this specific shape of the single-unit frequency tuning. Though there is a coarse correlation suggesting that the multi-unit response reflects whether the single-unit tuning is broad or narrow in a gross sense, it does not always reliably reflect the tuning of the single-units.

This inability to capture the tuning characteristics of single-units may reflect a heterogeneity in single-unit bandwidths in the local regions contributing to the multi-unit responses.

IPD sensitivity

Our results regarding the interaural phase sensitivity suggest that the multi-unit responses do not always predict the single-unit response well. In some cases, the differences are small and may arise from the specific methods we use to compute multi-unit responses. However, in some of the cases, the multi-unit response exhibits clear tuning to a single dominant interaural phase that differs strongly and noticeably from the mean-IPD of a single-unit.

In chapter 2, we saw that neighboring single-units can display great disparity in their phase sensitivity. If we had a completely heterogeneous mixture of units with different phase sensitivities that contribute to the multi-unit responses, we might expect that the multi-unit response would be broad and poorly tuned rather than displaying the

clear tuning we have seen in so many cases. It is possible that the multi-unit responses reflect not only spiking activity, but also sub-threshold post-synaptic potentials. Under this hypothesis, the majority of inputs innervating the cells in a local region may have a common IPD sensitivity; however, within any individual cell, the actual tuning to IPD may be shaped by other secondary inputs which contribute minimally to the multi-unit response, but generate action potentials in certain cells. Also inhibitory inputs that modulate ITD tuning may have very little effect on the multi-unit activity.

Comparison with other single-units

All the data presented so far has only considered the best separated single-unit from each recording site. However, at many of the sites, we have multiple single-units which could be used for comparison. It is possible that our choice of using the unit that is most easily separable may bias the sample towards cells with large extracellular potentials.

Figure 10 shows comparisons of multi-unit BF against the single-unit BFs that provides the best correlation and worst correlation with the multi-unit responses. If we ignore the data points at BFs above 3kHz, the best correlation we can achieve is ρ=0.98 and the worst correlation is ρ=0.594. Applying Fisher's z-test we compare the previous results using the best isolated single-unit with these results. This reveals that the differences in correlation between the best isolated single-unit and the best correlated responses are statistically significant ($p < 0.005$ for both comparisons).

We repeated the analysis for bandwidth, threshold, and IPD sensitivity. For these characteristics, we observe no statistically significant change in correlation when we select the best correlated units or the worst correlated unit. These are also the features that showed no large correlations with the best isolated single units. The lack of correlation with any of these populations is consistent with our assumption that the best isolated unit does not bias our results by only looking at a particular population of neurons.

Conclusions

These results demonstrate clear examples of cases in which the multi-unit response not only fails to capture the single-unit response but in the case of interaural phase sensitivity appears simply as a differently tuned single-unit. These examples suggest great caution must be used in interpreting single-channel multi-unit data.

The technologies most likely to lead to the increased use of multi-unit data are the large microelectrode arrays. These arrays have been developed and are mostly being used in the motor and somatosensory cortices and the hippocampus. In these regions, researchers are interested in looking at ensemble dynamics, and in the motor cortex increasingly interest is growing in using the output of these arrays to control prostheses. For these applications, the coarse representation given by multi-unit responses may provide enough information to approach these problems. However, as we begin to apply these technologies to studying neural coding mechanisms, we need to be cautious when interpreting multi-unit data.

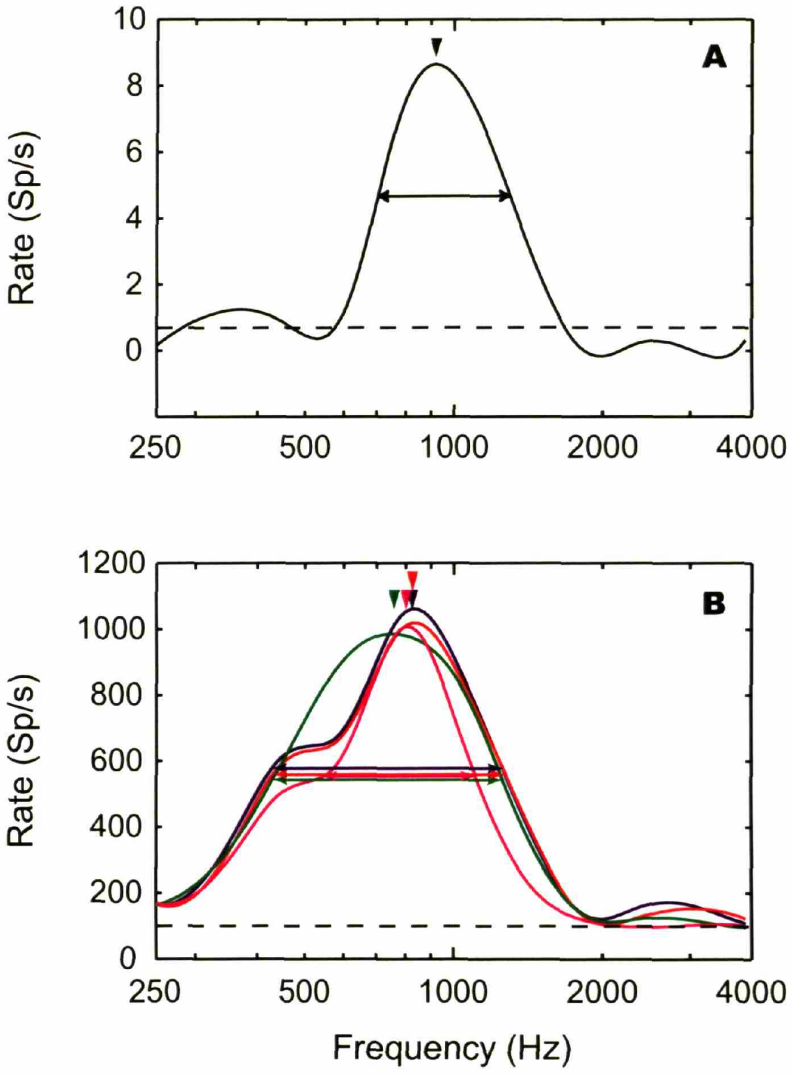

Figure 1 - Single and multi-unit rate-frequency responses. (A) Single-unit rate-frequency response measured at 40dB SPL (12dB above multi-unit threshold). The dashed line indicates the measured spontaneous rate for the unit. The triangle above the curve indicates the measured BF for the unit; the BF is 920 Hz. The horizontal line indicates the half-bandwidth of the rate-frequency curve; the half-bandwidth for this unit is 0.92 octaves. (B) Multi-unit rate-frequency responses for the four multi-unit responses from the four tetrode channels. The dashed line indicates a spontaneous rate of 100 sp/s. The triangles and horizontal lines indicate the BF and half-bandwidth for each of the four curves. The mean BF and half-bandwidth for the multi-unit responses are 813 Hz and 1.69 octaves respectively.

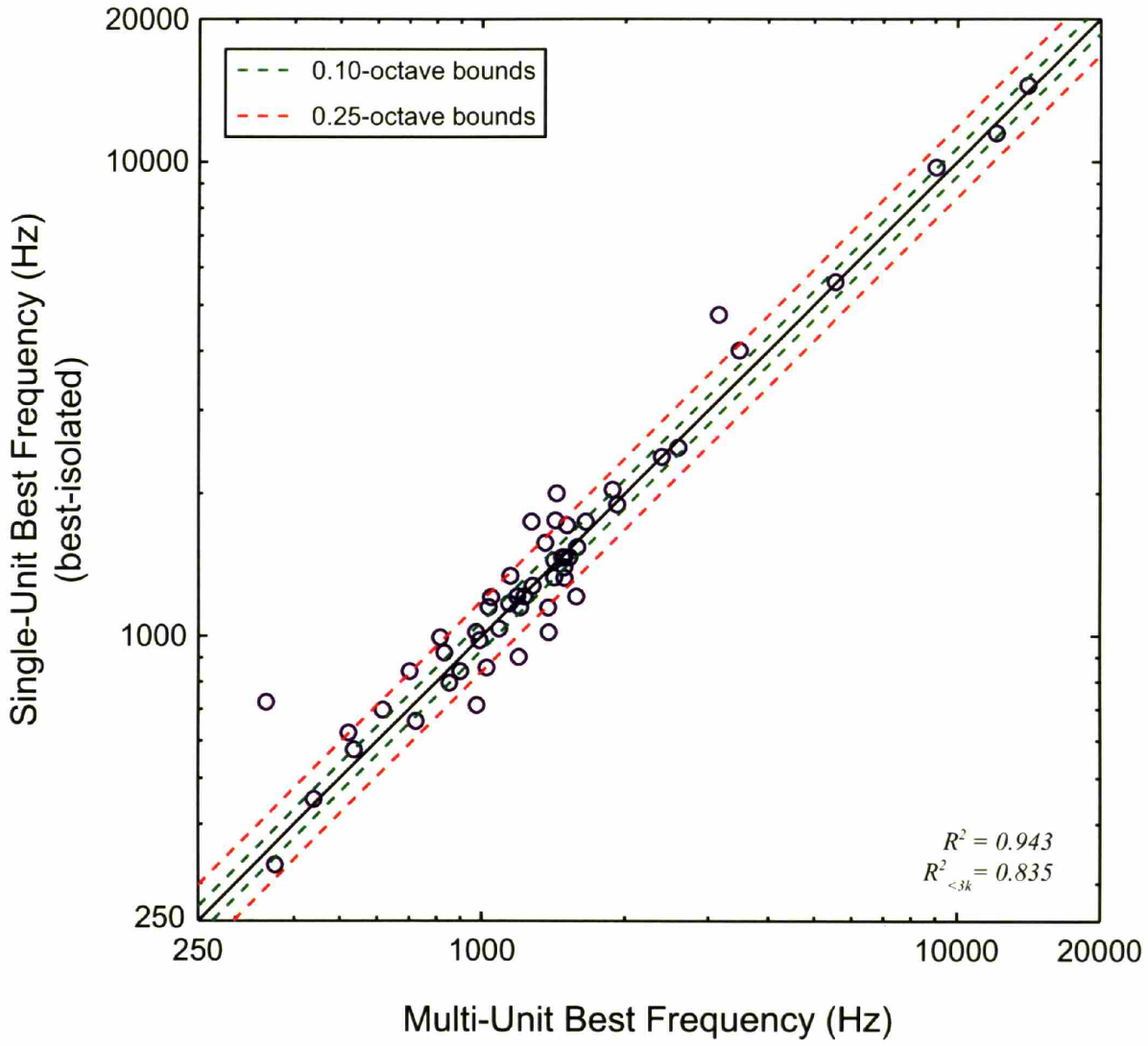

Figure 2 - Comparison of best frequencies of multi-unit responses and best isolated single-unit near threshold. This plot shows the multi-unit best frequency responses plotted against the best isolated single-unit responses. The dashed green lines indicate boundaries of 0.1 octave difference; the dashed red lines indicate boundaried 1/4-octave difference. The relationship exhibits a correlation coefficient of ρ=0.971 or R^2 = 0.943. Note because of deliberate sampling in low-CF regions of the ICC, we have an over-representation of best frequencies between 500-2000Hz. To minimize the effects of the high-BF units on our correlation, we also computed the correlation without sites exhibiting BFs over 3kHz. The resulting correlation coefficient and R^2 are 0.914 and 0.835 respectively.

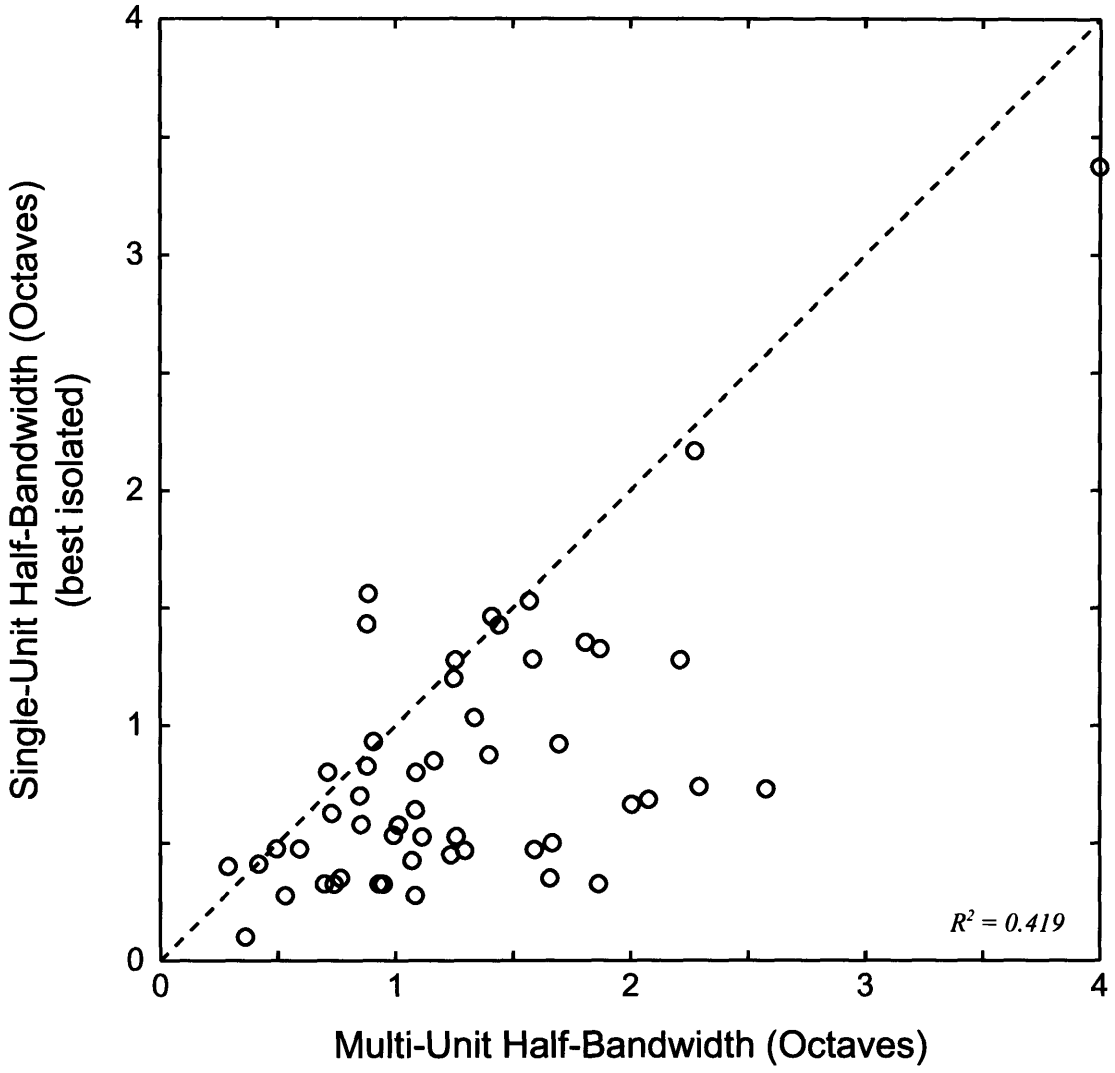

Figure 3 - Comparison of half-bandwidths of multi-unit response with the best isolated single-unit near threshold. This plot shows the multi-unit half-bandwidths plotted against the best isolated single-unit half-bandwidths. The relationship exhibits a correlation coefficient of $\rho=0.647$ or $R^2 = 0.419$. The dashed line is the identity line.

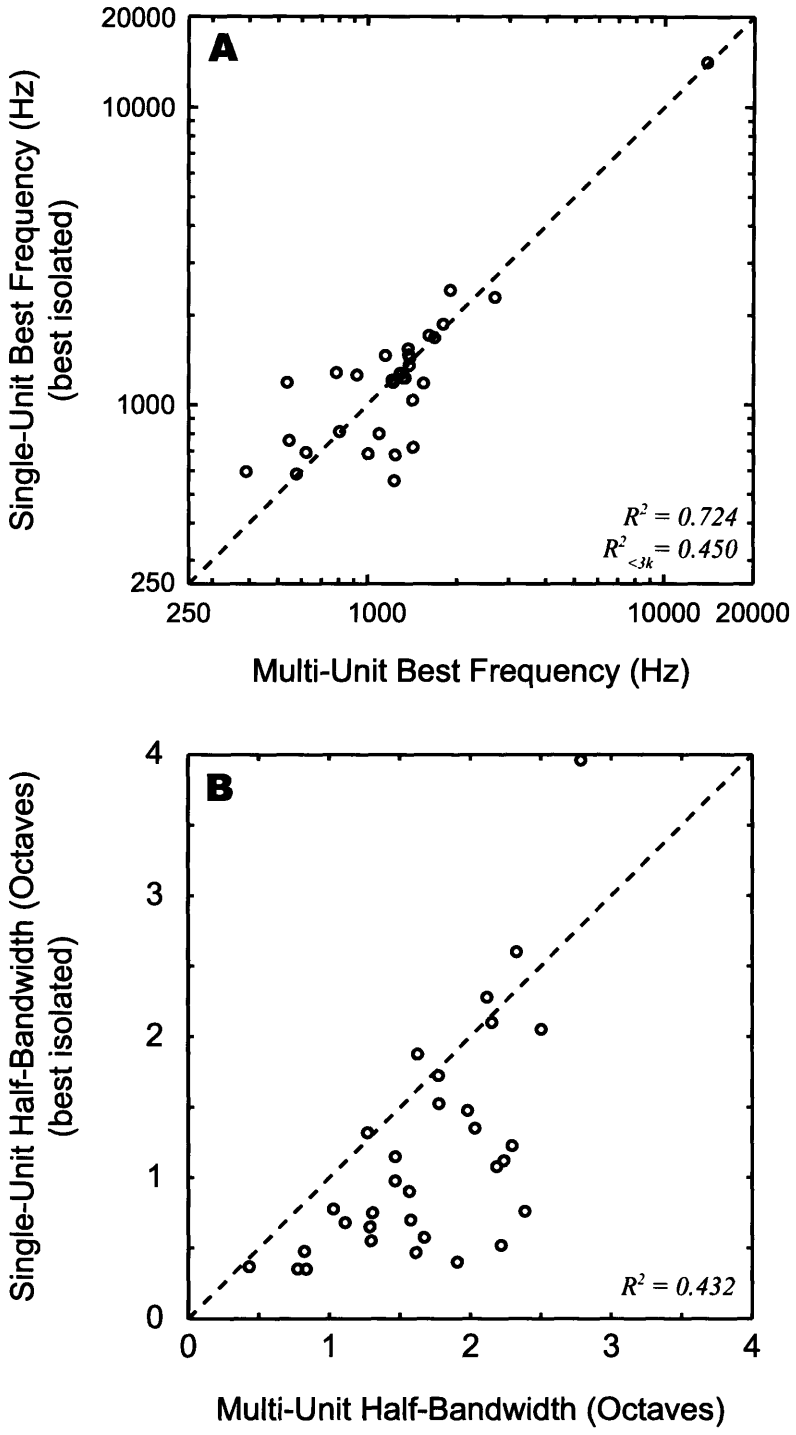

Figure 4 - Comparisons of best frequencies and half-bandwidths measured at 20-30dB above threshold. (A) Comparison of best-isolated single-unit and multi-unit best frequencies. At these higher levels, ignoring the one high BF site, the correlation coefficient is ρ=0.671. (B) Comparison of best-isolated single-unit and multi-unit half-bandwidths. The correlation coefficient is ρ=0.657.

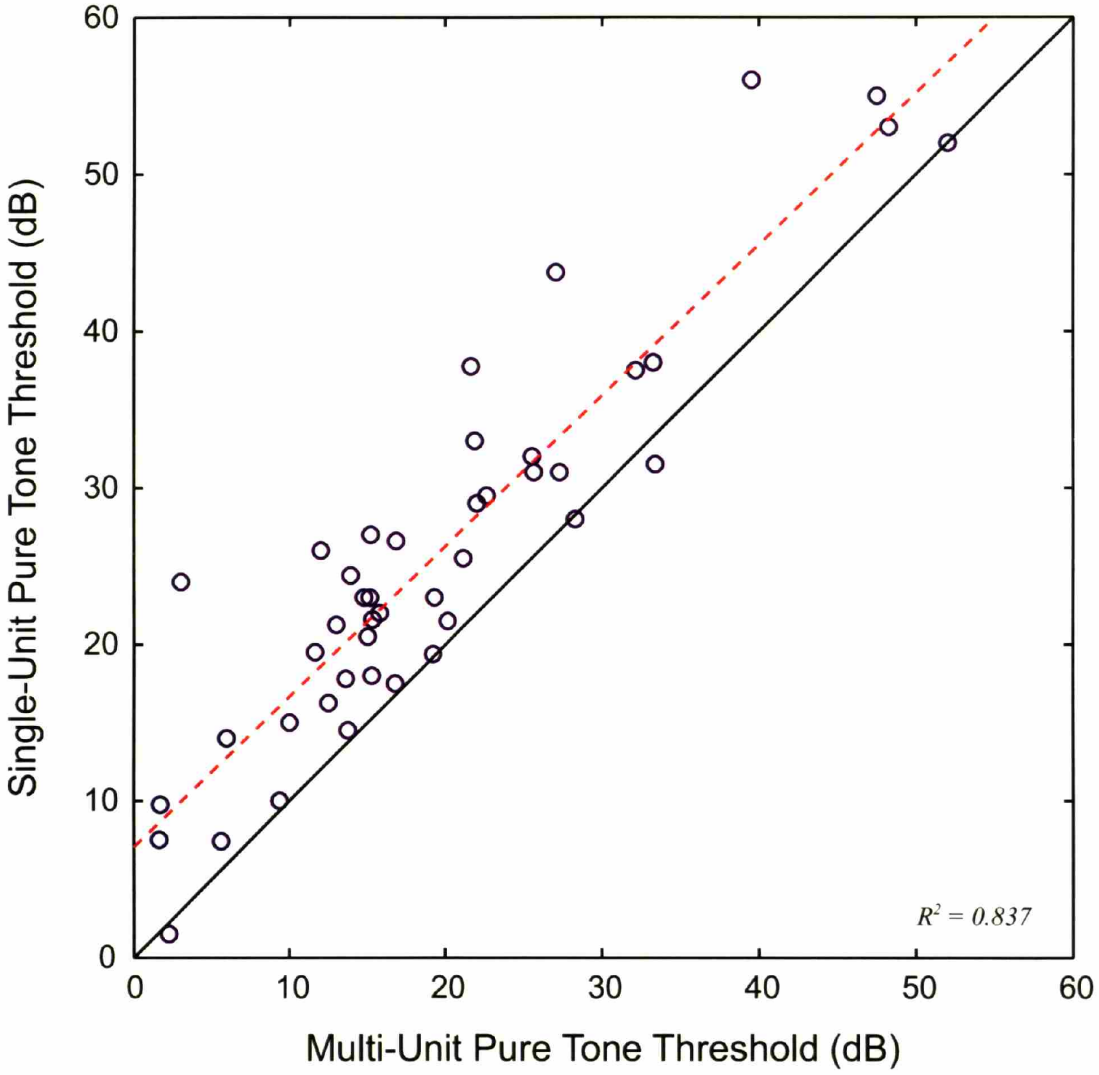

Figure 5 - Comparison of pure tone threshold between multi-unit responses and the best-isolated single-unit responses. The dashed red line shows a regression line fit to the data points. This line has slope m = 0.96 ± 0.13 and intercept b = 7.04 ± 3.00 (limits are 95% confidence intervals). This suggests that the multi-unit thresholds reflect the single-unit thresholds with a simple offset given by the intercept of the regression line. The correlation coefficient is ρ=0.915.

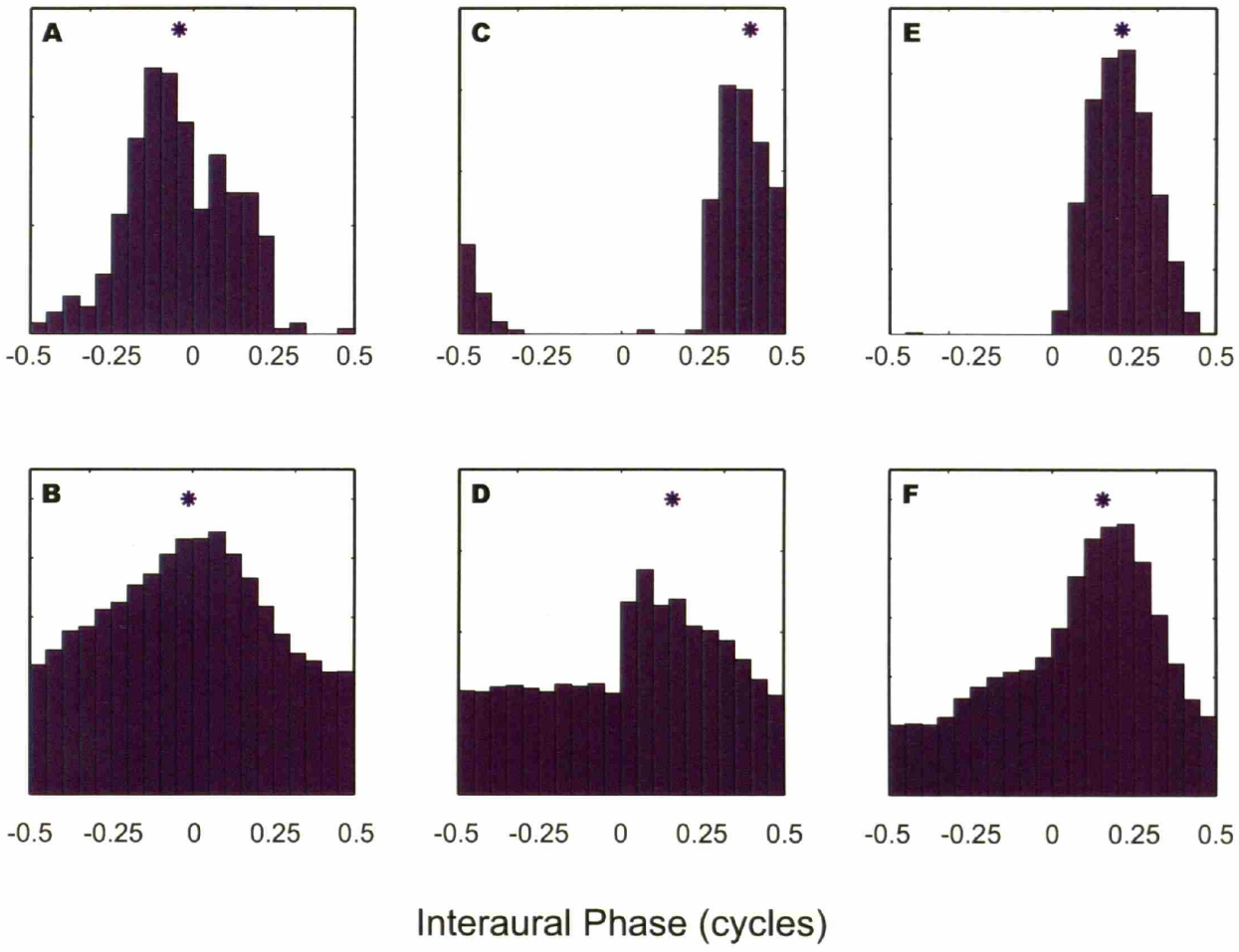

Figure 6 - Period histograms for single-units and corresponding multi-unit responses. (A-B) panel A gives the single-unit response and panel B shows the multi-unit response. (C-D) Another example of period histograms for single- and multi-unit responses. Note difference in mean-IPD. (E-F) Third example period histogram. Not that the aterisks in each plot show the mean-IPDs.

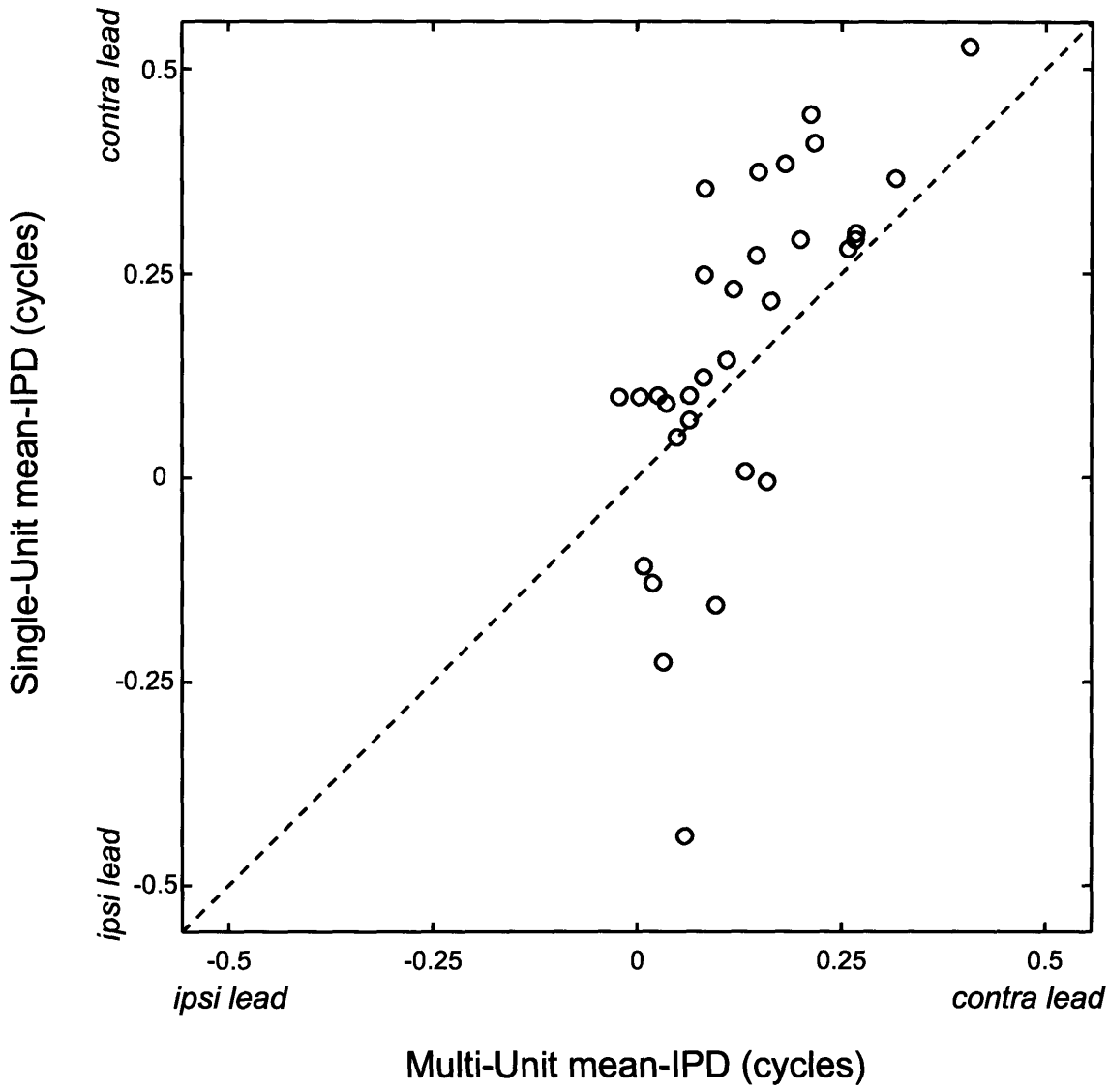

Figure 7 - Comparison of mean-IPD between multi-unit responses and single-unit responses. All the single-unit responses are the most separable unit from each recording site. Correlation coefficint is ρ=0.681.

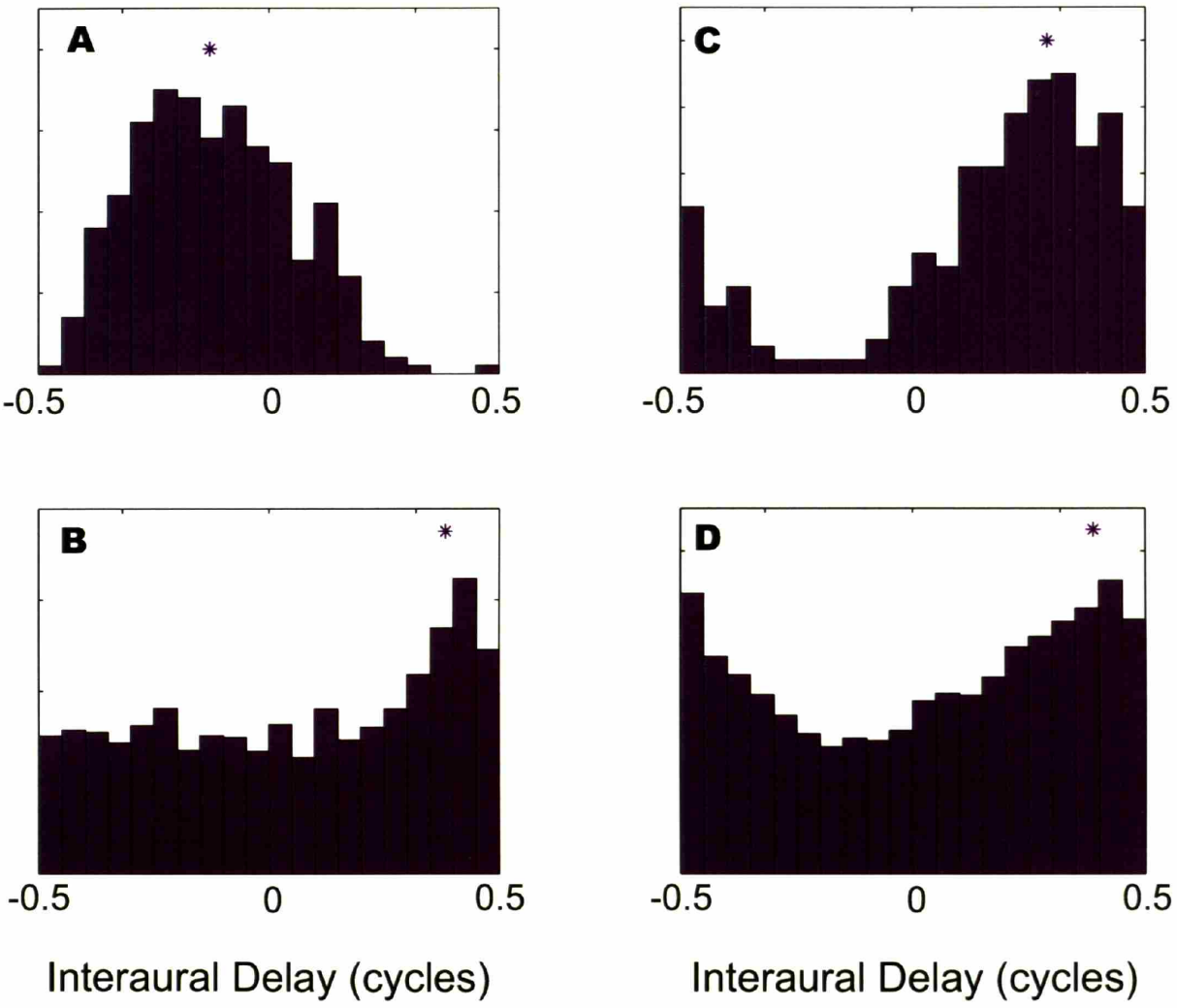

Figure 8 - Plots A and B show period histograms for single-unit (A) and multi-unit (B) binaural beat respones. Plots C and D show another example of single-unit (C) and multi-unit (D) binaural beat respones. Asterisks show the mean-IPD for each histogram. Note the differences in mean IPD between multi- and single-unit responses for these examples.

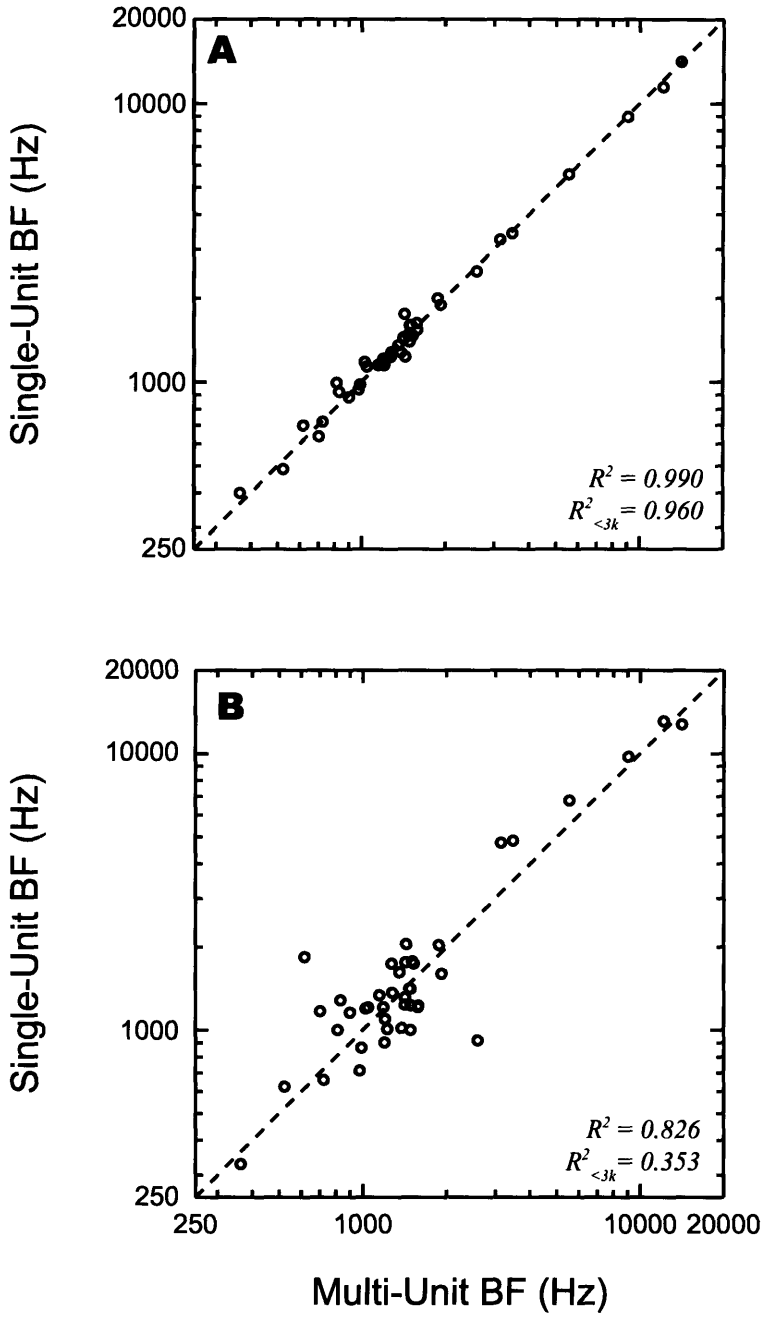

Figure 9 - Plots of multi-unit BFs vs single-unit BFs for single-units that yield the best and worst correlation. (A) - The best possible correlation between single-unit and multi-unit responses; (B) - The worst possible correlation between single-unit and multi-unit responses

CONCLUSIONS

We used tetrodes to separate single-unit contributions to multi-unit recordings. In Chapter 1 we showed that tetrodes significantly improve spike sorting compared with using single-channel recordings. These results suggest that in the inferior colliculus (IC), the additional spatial information added by the tetrodes provides information that is critical for achieving successful spike sorting. In Chapter2, we used tetrodes to record responses of neighboring units in the central nucleus of the inferior colliculus (ICC). We characterized these responses and identified similarities and differences in the response properties of neighboring neurons. We showed that neighboring neurons can show large differences in a number of response properties, though at low levels and near the best frequencies, we see some strong similarities. Lastly, in Chapter 3 we investigated how well unsorted multi-unit activity at a particular recording site captures the response properties of single-units recorded from the same site. We found that the multi-unit responses typically provide

Based on our experience with using tetrodes in the inferior colliculus, we believe that tetrodes offer a powerful tool for studying local organization of single-unit responses throughout the CNS. The architecture of the ICC, and specifically, hypotheses about the existence of functional zones (Oliver and Shneiderman, 1991) make it a logical site to investigate the response properties of neighboring neurons. However, within the auditory brainstem itself, there are other potential applications for tetrodes. In the MSO, where there are very few recordings, studying the responses of neighboring neurons to varying interaural timing differences (ITD) may help us understand whether the proposed Jeffress

model of coincidence detectors with delay lines is a good model of ITD coding in the MSO. In the ventral cochlear nucleus where there appears to be segregation of anatomical cell types as well as physiological cell types, understanding similarities and differences among neighboring neuron responses may help us understand what type of information processing is performed in different regions.

While our results from chapter 1 validate tetrodes as a useful tool for studying responses of local single-units, our results also show that applying spike sorting techniques to single-channel, multi-unit activity can introduce a high error rate in classifying single units. Other possible methods for recording from single-units that are close together would likely attempt to isolate single-units on individual electrodes. As we have discussed, these methods while possible would probably be very hard to implement. In particular, isolating and holding single-units on independently controlled electrodes would require long holding times for each single-unit; using large fixed arrays of high impedance electrodes would be limited by the likelihood of isolating a single-unit on more than one channel when there is no independent control of each electrode position. Additionally, since both approaches use multiple electrodes, trying to position them in the same region of the IC would lead to significant tissue damage. These considerations suggest that using multi-unit activity to acquire the responses of neurons that are close together offers a much more practical and reliable method. Our results also suggest that the spatial information available on tetrodes is extremely important for achieving good isolation of single-units.

While the tetrode offers a new view into neural responses, it also has some tradeoffs. Foremost is the potential problem of overlapping spike waveforms. This may

not be a large problem in higher neural centers where single-units spike rates are moderate, and particularly if stimuli are represented in the average rate of responses; however, this can pose a large obstacle for investigating neural representations that rely on fine timing of action potentials. In particular, if two neighboring neurons have similar fine timing structure, the likelihood of overlapped spikes is large and could lead to many misclassified or unclassified spikes.

In spite of some of this tradeoff, tetrodes proved useful in investigating local neural responses in the ICC. In particular, we found some response properties were very similar among neighboring neurons while others were seemingly unrelated. The average rate response to pure tones of neighboring neurons showed greatest similarity at low levels near the best frequency with greater differences when stimulated with off-BF frequencies and levels well above threshold. We have hypothesized that this may suggest that the tonotopic arrangement of the ICC reflects organization of primary inputs arranged by their frequency tuning that are similar among neighboring neurons with secondary inputs tuned to a much wider range of frequencies that are more variable among neighboring neurons. As we have mentioned in Chapter 2, this hypothesis is supported by both physiological (Snyder and Sinex, 2002) and anatomical data (Malmierca et al., 2005). Since most natural stimuli contain a wide range of frequencies and usually exist well above the threshold levels of single-units, these secondary inputs are likely to have a large influence on the responses of single-units. While we have reported the responses of ICC neurons to pure tone stimulation, work with more complex stimuli is needed to understand what role off-BF inputs play in the response properties of neighboring ICC neurons.

Further complicating our understanding of ICC responses is the apparently random arrangement of PSTH response types. These response patterns may reflect patterns from lower nuclei or they may reflect processing in the IC itself. If the response patterns reflect patterns from inputs, then this would suggest a very heterogeneous mix of inputs from lower nuclei converging on a small area in the IC. If, however, the PSTH responses we observe reflect the membrane properties of individual neurons, then this suggests that the different cell types as defined by membrane channel properties (Sivaramakrishnan and Oliver, 2001) are randomly distributed. Under either hypothesis, the significance of the randomness of PSTH types remains difficult to determine since we don't have a very good understanding of the relevance of different PSTH types in information coding.

Our investigation of ITD sensitivity shows no strong organization of either mean-IPD at BF or Characteristic Delays. However, we find that the Characteristic Phase appears to be reasonably well correlated. As we discussed in chapter 2, the correlation of CP may reflect segregation of different inputs. It is believed that ITD-sensitive units with CP of around 0 or 1 reflect peak-like responses which are believed to reflect response types in the Medial Superior Olive (MSO) whereas CPs around 0.5 reflect trough-like responses and reflect response types in the Lateral Superior Olive (LSO) (McAlpine et al., 1998). The correlation of CP then may reflect segregation of inputs from MSO and LSO. However, our results regarding mean-IPD and CD suggest that within these regions, responses are not obviously organized by best-IPD.

All these results together paint a rather complicated picture of the physiological organization of the ICC. However, further work with tetrodes may help improve our

understanding of the complexities of this arrangement. Our work has focused on primarly characterizing pure tone responses. While this provides a good foundation for further exploration, some additional characterization using spectrally complex stimuli and amplitude modulated stimuli would naturally extend our work and make it more relevant to natural stimuli.

Also, as tetrodes have allowed us to look at local populations, other improvements in single-unit recording and large multi-electrode arrays would allow us to perform similar characterizations for widely separated neurons. Understanding how the relationships among neighboring neurons differ from the relationships among widely separated neurons could help improve our understanding of the organization of responses. New large electrode arrays and devices for independently moving single electrodes can help achieve these goals. However, our results suggest that some caution must be taken to ensure that only single-units are recorded.

We have shown in chapter 1 that attempts to sort multiple spike waveforms from single channels introduces large sorting errors, including the classification of multi-unit clusters as single-unit responses. Care needs to be taken to avoid these problems, for we have also shown that multi-unit responses can deviate significantly from single-unit responses depending on the response property we are studying.

In conclusion, having characterized the responses to pure tones, we believe that future work should employ tetrodes in studies of neural coding previously done using with single-unit recordings. Because of the complexity of organization seen in our responses to pure tones, it seems that *if* there are organizational principles reflected in the responses of neighboring neurons, they may seen in responses to complex stimuli.

Therefore, as investigators explore the coding of different acoustic and psychophysical parameters, using tetrodes offer added dimensions along which to study neural coding.

REFERENCES

Abeles, M. and M. H. Goldstein (1977). "Multispike train analysis." Proceedings of the IEEE **65**(5): 762-773.

Adams, J. C. (1979). "Ascending projections to the inferior colliculus." J Comp Neurol **183**(3): 519-38.

Blake, D. T., F. Strata, A. K. Churchland and M. M. Merzenich (2002). "Neural correlates of instrumental learning in primary auditory cortex." Proc Natl Acad Sci U S A **99**(15): 10114-9.

Brunso-Bechtold, J. K., G. C. Thompson and R. B. Masterton (1981). "HRP study of the organization of auditory afferents ascending to central nucleus of inferior colliculus in cat." J Comp Neurol **197**(4): 705-22.

Chapin, J. K. (2004). "Using multi-neuron population recordings for neural prosthetics." Nat Neurosci **7**(5): 452-5.

Drake, K. L., K. D. Wise, J. Farraye, D. J. Anderson and S. L. BeMent (1988). "Performance of planar multisite microprobes in recording extracellular single-unit intracortical activity." IEEE Trans Biomed Eng **35**(9): 719-32.

Fisher, N. I. (1993). Statistical analysis of circular data. Cambridge [England] ; New York, NY, USA, Cambridge University Press.

Goldberg, J. M. and P. B. Brown (1969). "Response of binaural neurons of dog superior olivary complex to dichotic tonal stimuli: some physiological mechanisms of sound localization." J Neurophysiol **32**(4): 613-36.

Gray, C. M., P. E. Maldonado, M. Wilson and B. McNaughton (1995). "Tetrodes markedly improve the reliability and yield of multiple single- unit isolation from multi-unit recordings in cat striate cortex." J Neurosci Methods **63**(1-2): 43-54.

Harris, D. M., R. V. Shannon, R. Snyder and E. Carney (1997). "Multi-unit mapping of acoustic stimuli in gerbil inferior colliculus." Hear Res **108**(1-2): 145-56.

Henkel, C. K. and K. M. Spangler (1983). "Organization of the efferent projections of the medial superior olivary nucleus in the cat as revealed by HRP and autoradiographic tracing methods." J Comp Neurol **221**(4): 416-28.

Hulata, E., R. Segev and E. Ben-Jacob (2002). "A method for spike sorting and detection based on wavelet packets and Shannon's mutual information." J Neurosci Methods **117**(1): 1-12.

Kandel, E. R., J. H. Schwartz and T. M. Jessell (2000). Principles of neural science. New York, McGraw-Hill, Health Professions Division.

Kiang, N. Y. and E. C. Moxon (1974). "Tails of tuning curves of auditory-nerve fibers." J Acoust Soc Am **55**(3): 620-30.

Kuwada, S., T. R. Stanford and R. Batra (1987). "Interaural phase-sensitive units in the inferior colliculus of the unanesthetized rabbit: effects of changing frequency." J Neurophysiol **57**(5): 1338-60.

Langner, G. and C. E. Schreiner (1987). Topology of functional parameters in the inferior colliculus of the cat. New Frontiers in Brain Research. N. Elsner and O. Creutzfeldt. Stuttgart, Thieme: 122.

Le Beau, F. E., A. Rees and M. S. Malmierca (1996). "Contribution of GABA- and glycine-mediated inhibition to the monaural temporal response properties of neurons in the inferior colliculus." J Neurophysiol **75**(2): 902-19.

Lewicki, M. S. (1998). "A review of methods for spike sorting: the detection and classification of neural action potentials." Network **9**(4): R53-78.

Litovsky, R. Y. and B. Delgutte (2002). "Neural correlates of the precedence effect in the inferior colliculus: effect of localization cues." J Neurophysiol **87**(2): 976-94.

Malmierca, M. S., R. L. Saint Marie, M. A. Merchan and D. L. Oliver (2005). "Laminar inputs from dorsal cochlear nucleus and ventral cochlear nucleus to the central nucleus of the inferior colliculus: two patterns of convergence." Neuroscience **136**(3): 883-94.

Maynard, E. M., N. G. Hatsopoulos, C. L. Ojakangas, B. D. Acuna, J. N. Sanes, R. A. Normann and J. P. Donoghue (1999). "Neuronal interactions improve cortical population coding of movement direction." J Neurosci **19**(18): 8083-93.

Maynard, E. M., C. T. Nordhausen and R. A. Normann (1997). "The Utah intracortical Electrode Array: a recording structure for potential brain-computer interfaces." Electroencephalogr Clin Neurophysiol **102**(3): 228-39.

McAlpine, D., D. Jiang, T. M. Shackleton and A. R. Palmer (1998). "Convergent input from brainstem coincidence detectors onto delay-sensitive neurons in the inferior colliculus." J Neurosci **18**(15): 6026-39.

Merzenich, M. M. and M. D. Reid (1974). "Representation of the cochlea within the inferior colliculus of the cat." Brain Res **77**(3): 397-415.

Moore, G. P., J. P. Segundo, D. H. Perkel and H. Levitan (1970). "Statistical signs of synaptic interaction in neurons." Biophys J **10**(9): 876-900.

Morest, D. K. and D. L. Oliver (1984). "The neuronal architecture of the inferior colliculus in the cat: defining the functional anatomy of the auditory midbrain." J Comp Neurol **222**(2): 209-36.

Moxon, K. A. (1999). Multichannel Electrode Design: Considerations for Different Applications. Methods for neural ensemble recordings. M. A. L. Nicolelis. Boca Raton, CRC Press: 25-46.

Nicolelis, M. A., L. A. Baccala, R. C. Lin and J. K. Chapin (1995). "Sensorimotor encoding by synchronous neural ensemble activity at multiple levels of the somatosensory system." Science **268**(5215): 1353-8.

Nicolelis, M. A. L. (1999). Methods for neural ensemble recordings. Boca Raton, CRC Press.

Nunez, P. (1981). Electric fields in biological tissue. Electric Fields of the Brain. P. Nunez. Oxford, Oxford University Press: 75-139.

Oghalai, J. S., W. N. Street and W. S. Rhode (1994). "A neural network-based spike discriminator." J Neurosci Methods **54**(1): 9-22.

Ohberg, F., H. Johansson, M. Bergenheim, J. Pedersen and M. Djupsjobacka (1996). "A neural network approach to real-time spike discrimination during simultaneous recording from several multi-unit nerve filaments." J Neurosci Methods **64**(2): 181-7.

Oliver, D. L., G. E. Beckius, D. C. Bishop and S. Kuwada (1997). "Simultaneous anterograde labeling of axonal layers from lateral superior olive and dorsal cochlear nucleus in the inferior colliculus of cat." J Comp Neurol **382**(2): 215-29.

Oliver, D. L. and D. K. Morest (1984). "The central nucleus of the inferior colliculus in the cat." J Comp Neurol **222**(2): 237-64.

Oliver, D. L. and A. Shneiderman (1991). The Anatomy of the Inferior Colliculus: A Cellular Basis for Integration of Monaural and Binaural Information. Neurobiology of Hearing: The Central Auditory System. R. A. Altschuler. New York, Raven Press, Ltd.: 195-222.

Oliver, D. L. and A. Shneiderman (1991). The anatomy of the inferior colliculus: a cellular basis for integration of monaural and binaural information. Neurobiology of Hearing: Central Auditory System. R. A. Altschuler, R. P. Bobbin, B. M. Clopton and D. W. Hoffman. New York, Raven: 195-222.

Peruzzi, D., S. Sivaramakrishnan and D. L. Oliver (2000). "Identification of cell types in brain slices of the inferior colliculus." Neuroscience **101**(2): 403-16.

Quiroga, R. Q., Z. Nadasdy and Y. Ben-Shaul (2004). "Unsupervised spike detection and sorting with wavelets and superparamagnetic clustering." Neural Comput **16**(8): 1661-87.

Riehle, A., S. Grun, M. Diesmann and A. Aertsen (1997). "Spike synchronization and rate modulation differentially involved in motor cortical function." Science **278**(5345): 1950-3.

Robinson, D. A. (1968). "The electrical properties of metal microelectrodes." Proc IEEE **56**(6): 1065-1071.

Rockel, A. J. and E. G. Jones (1973). "The neuronal organization of the inferior colliculus of the adult cat. I. The central nucleus." J Comp Neurol **147**(1): 11-60.

Schmidt, E. M. (1999). Electrodes for Many Single Neuron Recordings. Methods for neural ensemble recordings. M. A. L. Nicolelis. Boca Raton, CRC Press: 1-24.

Schreiner, C. E. and G. Langner (1988). "Periodicity coding in the inferior colliculus of the cat. II. Topographical organization." J Neurophysiol **60**(6): 1823-40.

Shneiderman, A. and C. K. Henkel (1987). "Banding of lateral superior olivary nucleus afferents in the inferior colliculus: a possible substrate for sensory integration." J Comp Neurol **266**(4): 519-34.

Shoham, S., M. R. Fellows and R. A. Normann (2003). "Robust, automatic spike sorting using mixtures of multivariate t-distributions." J Neurosci Methods **127**(2): 111-22.

Shoham, S., L. M. Paninski, M. R. Fellows, N. G. Hatsopoulos, J. P. Donoghue and R. A. Normann (2005). "Statistical encoding model for a primary motor cortical brain-machine interface." IEEE Trans Biomed Eng **52**(7): 1312-22.

Sivaramakrishnan, S. and D. L. Oliver (2001). "Distinct K currents result in physiologically distinct cell types in the inferior colliculus of the rat." J Neurosci **21**(8): 2861-77.

Snyder, R. L. and D. G. Sinex (2002). "Immediate changes in tuning of inferior colliculus neurons following acute lesions of cat spiral ganglion." J Neurophysiol **87**(1): 434-52.

Stiebler, I. (1986). "Tone-threshold mapping in the inferior colliculus of the house mouse." Neurosci Lett **65**(3): 336-40.

Takahashi, S., Y. Anzai and Y. Sakurai (2003). "A new approach to spike sorting for multi-neuronal activities recorded with a tetrode--how ICA can be practical." Neurosci Res **46**(3): 265-72.

Wilson, M. A. and B. L. McNaughton (1993). "Dynamics of the hippocampal ensemble code for space." Science **261**(5124): 1055-8.

Yin, T. C. and S. Kuwada (1983). "Binaural interaction in low-frequency neurons in inferior colliculus of the cat. III. Effects of changing frequency." J Neurophysiol **50**(4): 1020-42.

Young, E. D., J. M. Robert and W. P. Shofner (1988). "Regularity and latency of units in ventral cochlear nucleus: implications for unit classification and generation of response properties." J Neurophysiol **60**(1): 1-29.